UNIVERSIDADE FEDERAL DO PARANÁ - UFPR

GIULIA HERBST

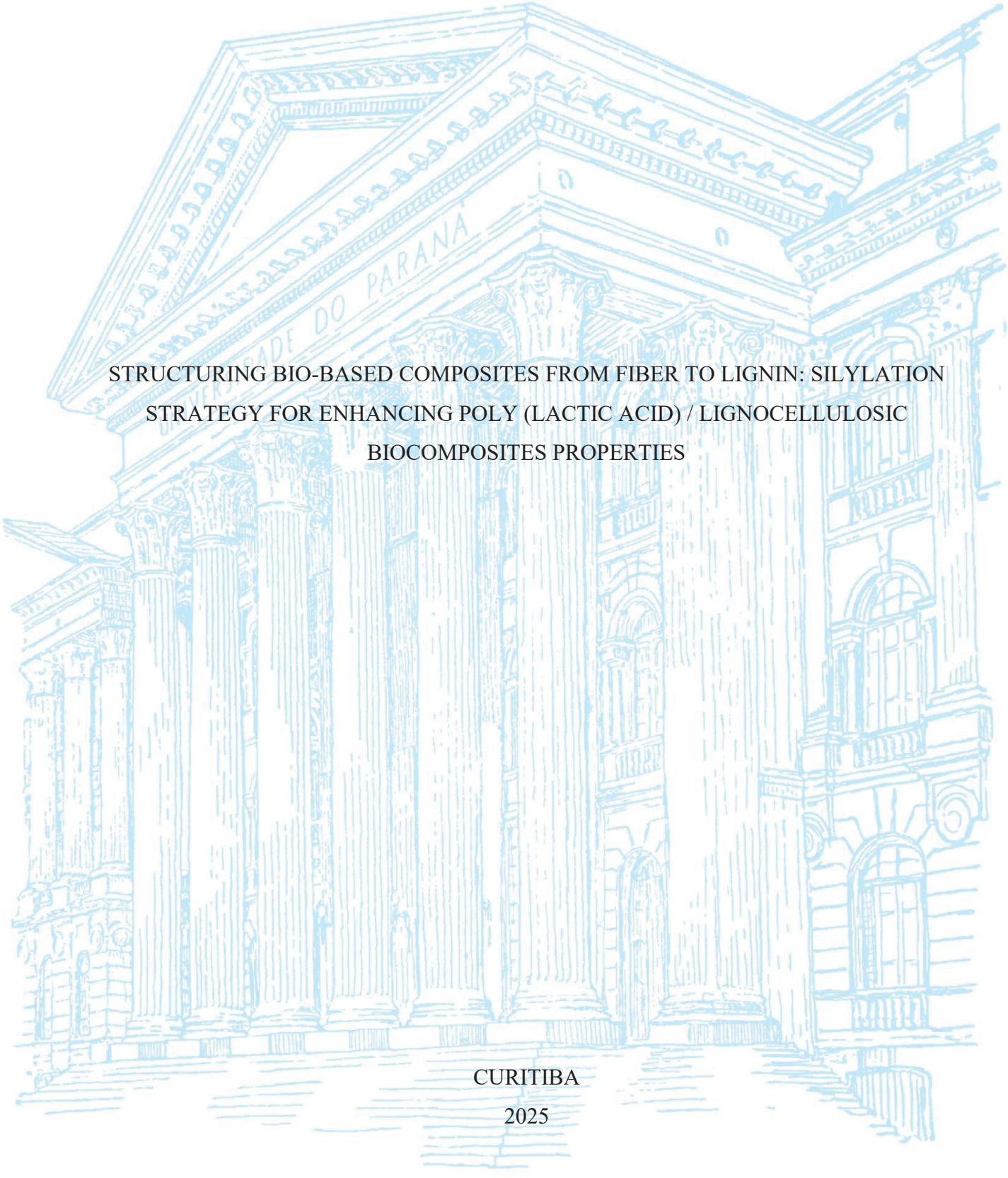

STRUCTURING BIO-BASED COMPOSITES FROM FIBER TO LIGNIN: SILYLATION STRATEGY FOR ENHANCING POLY (LACTIC ACID) / LIGNOCELLULOSIC BIOCOMPOSITES PROPERTIES

CURITIBA

2025

GIULIA HERBST

STRUCTURING BIO-BASED COMPOSITES FROM FIBER TO LIGNIN: SILYLATION STRATEGY FOR ENHANCING POLY (LACTIC ACID) / LIGNOCELLULOSIC BIOCOMPOSITES PROPERTIES

Tese de doutorado apresentada ao Programa de Pós-Graduação em Engenharia Química – PPGEQ, do Setor de Tecnologia, da Universidade Federal do Paraná, como requisito para a obtenção do título de Doutor(a) em Engenharia Química.

Orientador: Prof. Dr. Marcos Lúcio Corazza.
Coorientador: Prof. Dr. Luiz Pereira Ramos
Coorientador: Prof. Dr. Marc Delgado Aguilar

CURITIBA

2025

DADOS INTERNACIONAIS DE CATALOGAÇÃO NA PUBLICAÇÃO (CIP)
UNIVERSIDADE FEDERAL DO PARANÁ
SISTEMA DE BIBLIOTECAS – BIBLIOTECA DE CIÊNCIA E TECNOLOGIA

Herbst, Giulia
Structuring bio-based composites from fiber to lignin: silylation strategy for enhancing poly (lactic acid) / lignocellulosic biocomposites properties / Giulia Herbst. – Curitiba, 2025.
1 recurso on-line : PDF.

Tese (Doutorado) - Universidade Federal do Paraná, Setor de Tecnologia, Programa de Pós-Graduação em Engenharia Química.

Orientador: Marcos Lúcio Corazza
Coorientadores: Luiz Pereira Ramos; Marc Delgado Aguilar

1. Biocompósitos. 2. Ácido polilático. 3. Fibras lignocelulósicas. I. Universidade Federal do Paraná. II. Programa de Pós-Graduação em Engenharia Química. III. Corazza, Marcos Lúcio. IV. Ramos, Luiz Pereira. V. Aguilar, Marc Delgado. VI. Título.

Bibliotecário: Elias Barbosa da Silva CRB-9/1894

TERMO DE APROVAÇÃO

Os membros da Banca Examinadora designada pelo Colegiado do Programa de Pós-Graduação ENGENHARIA QUÍMICA da Universidade Federal do Paraná foram convocados para realizar a arguição da tese de Doutorado de **GIULIA HERBST**, intitulada: **STRUCTURING BIO-BASED COMPOSITES FROM FIBER TO LIGNIN: SILYLATION STRATEGY FOR ENHANCING POLY (LACTIC ACID) / LIGNOCELLULOSIC BIOCOMPOSITES PROPERTIES**, sob orientação do Prof. Dr. MARCOS LÚCIO CORAZZA, que após terem inquirido a aluna e realizada a avaliação do trabalho, são de parecer pela sua APROVAÇÃO no rito de defesa.
A outorga do título de doutora está sujeita à homologação pelo colegiado, ao atendimento de todas as indicações e correções solicitadas pela banca e ao pleno atendimento das demandas regimentais do Programa de Pós-Graduação.

CURITIBA, 08 de Dezembro de 2025.

Assinatura Eletrônica
08/12/2025 14:52:20.0
MARCOS LÚCIO CORAZZA
Presidente da Banca Examinadora

Assinatura Eletrônica
08/12/2025 15:13:26.0
ALEXANDRE FERREIRA SANTOS
Avaliador Interno (UNIVERSIDADE FEDERAL DO PARANÁ)

Assinatura Eletrônica
08/12/2025 17:22:40.0
MARCO DI LUCCIO
Avaliador Externo (UNIVERSIDADE FEDERAL DE SANTA CATARINA)

Assinatura Eletrônica
08/12/2025 12:19:52.0
PEDRO HENRIQUE GONZALEZ DE CADEMARTORI
Avaliador Externo (UNIVERSIDADE FEDERAL DO PARANá - DEPARTAMENTO DE ENGENHARIA E TECNOLOGIA FLORESTAL)

ACKNOWLEDGMENTS

I am profoundly grateful to my family, who have always been there for me and supported me in every decision, especially my parents, Amarildo and Cleonice, for encouraging me to pursue this path, and to my sisters, Luana and Thais, for their companionship and affection.

I would like to express my sincerest gratitude to Prof. Dr. Marcos Lúcio Corazza for allowing me to learn, work, and grow as a researcher under his guidance and support since my Master's degree, which has enabled me to pursue doctoral research.

I would like to express my gratitude to Prof. Dr. Luiz Pereira Ramos for all the guidance on my doctoral thesis, invaluable input, constructive feedback, and support through an exchange scholarship.

I am extremely grateful to Prof. Dr. Marc Delgado Aguilar for welcoming me during two research stays at Universitat de Girona. His support allowed me to pursue my research in biocomposites, making this thesis possible. This work reflects the interest and inspiration that his insightful contributions instilled in me.

I would like to thank Prof. Dr Luis R. S. Kanda, Prof. Dr Quim Tarrés, Dra. Gabriela A. Bastida, who were essential to my journey through growing as a researcher under their guidance and support.

I would also like to thank my research mates from both UFPR and UdG universities, LACTA and LEPAMAP research groups, for turning me into the researcher that I am today.

I would like to thank the "Conselho Nacional de Desenvolvimento Cientifico e Tecnológico" (CNPq, Brasil) for supporting me with a scholarship granted through the MAI/DAI Program, with the support of ERT Earth Renewable Technologies do Brasil Ltd. Also, financial support of the "Coordenação de Aperfeiçoamento de Pessoal de Nível Superior" (CAPES, Brazil) for a first stay SWE scholarship at the Universitat de Girona.

RESUMO

A transição para uma economia sustentável exige materiais que não apenas substituam opções baseadas em combustíveis fósseis, mas também ofereçam desempenho competitivo e maior circularidade. Biopolímeros e reforços lignocelulósicos fornecem uma alternativa sustentável, reduzindo a dependência de recursos fósseis e permitindo o uso de materiais renováveis. Nesse contexto, as biorrefinarias são essenciais para converter biomassa em materiais funcionais, auxiliando na substituição gradual de derivados de petróleo. No entanto, desenvolver biocompósitos de alto desempenho continua sendo desafiador devido à baixa compatibilidade entre matrizes poliméricas hidrofóbicas e biomassa hidrofílica. Ajustar as interações interfaciais é, portanto, fundamental para garantir resistência mecânica, durabilidade e desempenho a longo prazo. Este estudo explora as relações estrutura–propriedade em biocompósitos de poliácido láctico (PLA) reforçados com polpa de madeira moída (SGW) e frações de lignina, enfocando como modificação química por sililação e branqueamento das fibras afeta a adesão interfacial. Fibras de SGW (20 e 30 % em massa) foram sililadas com (3-glicidiloxipropil)trimetoxisilano (GPS) em proporções entre 3 e 10 % para melhorar a ligação matriz-fibra. Testes reológicos mostraram que fibras não branqueadas, com maior teor de lignina e razão de aspecto, promoveram melhor estruturação e a maior resistência à tração (14 % e 27 % para 20 e 30 % SGW, respectivamente). O melhor reforço ocorreu com 30 % SGW modificado com 5–7 % GPS, produzindo propriedades termomecânicas semelhantes às de compósitos comerciais de polipropileno. Após o branqueamento, a morfologia das fibras mudou, aumentando finos e reduzindo comprimento, o que enfraqueceu a rede e o módulo de armazenamento, embora tenha melhorado a fluidez. Uma estratégia complementar de compatibilização foi avaliada em filmes de PLA-lignina com ligninas de madeira macia (LS) e dura (LH) modificadas com 1–5 % de GPS. As ligninas sililadas aumentaram a viscosidade do PLA, evidenciando ligação interfacial mais eficiente, enquanto LS promoveu maior nucleação que LH. As propriedades mecânicas melhoraram mais em filmes de LH com 1 % de GPS. Todos os filmes forneceram forte bloqueio de UV, ampliando seu potencial para embalagens. Os resultados destacam que a engenharia interfacial via sililação com GPS é essencial para otimizar a compatibilidade entre biomassa e polímero. Ao ajustar a estrutura química de fibras naturais de fontes renováveis e aprimorar a química interfacial, é possível produzir biocompósitos que unem sustentabilidade e desempenho comparável ao de plásticos convencionais.

Palavras-chave: biocompósitos, ácido polilático, interface, acoplamento de silano, fibras lignocelulósicas

ABSTRACT

The transition toward a bio-based economy demands materials that not only replace fossil-based options but also offer competitive performance and better circularity. Biopolymers and lignocellulosic reinforcements provide a sustainable alternative, decreasing reliance on fossil resources and enabling renewable material use. In this context, biorefineries are crucial for converting biomass into functional materials, assisting the gradual replacement of petroleum derivatives. However, developing high-performance biocomposites remains difficult due to the poor compatibility between hydrophobic polymer matrices and polar biomass. Therefore, adjusting interfacial interactions is key to maintaining mechanical strength, durability, and long-term material performance. This study explores structure-property relationships in poly (lactic acid) (PLA) based biocomposites reinforced with stone groundwood (SGW) pulp and lignin fractions, focusing on how chemical modification, silylation, and fiber bleaching affect interfacial adhesion. First, SGW fibers (20 and 30 wt.%) were silylated with concentrations of 3–10 wt.% of (3-glycidyloxypropyl)trimethoxysilane (GPS) to improve matrix–fiber bonding. Rheological tests showed that unbleached fibers, which retain higher lignin content and aspect ratio, promoted better melt structuring and achieved the highest increases in tensile strength (14% and 27% for 20 and 30 wt% SGW, respectively). The best reinforcement was found with 30 wt% SGW modified with 5 and 7 wt.% GPS, producing thermo-mechanical properties similar to those of commercial polypropylene composites. After progressive bleaching, the fiber morphology changed by increasing fines and reducing fiber length, which weakened fiber networking and storage modulus, even though it improved flowability. A complementary compatibilization strategy was assessed for PLA–lignin films using softwood (LS) and hardwood (LH) lignins modified with 1–5 wt% GPS. Silylated lignins increased PLA viscosity, demonstrating more effective interfacial bonding, while LS showed higher nucleating effects than LH. Mechanical properties were most improved for LH films containing GPS at 1 wt%. All PLA-lignin films provided strong UV-blocking capability, expanding potential application in packaging. Overall, the results showed that interfacial engineering through GPS-based silylation is a key strategy for optimizing biomass–polymer compatibility. By altering the chemical structure of bio-based fillers, improving interfacial chemistry, it is possible to produce biocomposites that combine sustainability with performance similar to conventional plastics.

Keywords: biocomposites, polylactic acid, interface, silane coupling, lignocellulosic fibers

LIST OF FIGURES

LIST OF TABLES

LIST OF ABBREVIATIONS OR ACRONYMS

3D - three-dimensional

ASTM - American Society for Testing and Materials

CAGR - compound annual growth rate

DSC - Differential scanning calorimetry

FDM - fused deposition modeling

FTIR - Fourier-transform infrared spectroscopy

GPS - 3-glycidyloxypropyl trimethoxysilane

ISO - International Organization for Standardization

LA - lactic acid

LCF - lignocellulosic fibers

MFI - melt flow index

NF - natural fibers

PCL - poly(ε-caprolactone)

PDLA - poly (D-lactic acid)

PDLA - poly (DL-lactic acid)

PEG - poly (ethylene glycol)

PET - poly (ethylene terephthalate)

PGA - poly (glycolic acid)

PGW - pressure groundwood

PLA - poly (lactic acid)

PLGA - poly (lactic-co-glycolic acid)

PLLA - poly (L-lactic acid)

PP - polypropylene

PS - polystyrene

RMP - refiner mechanical pulping

SGW - stone groundwood

TAPPI - Technical Association of the Pulp and Paper Industry

TCP - tricalcium phosphate

TGA - Thermogravimetric analysis

TMP - thermomechanical pulping

UV - ultraviolet

LIST OF SYMBOLS AND VARIABLES

T_g - glass transition

T_m - melting temperature

MPa - megapascal

GPa - giga pascal

wt - weight fraction

ρ - density

Xc - degree of crystallinity

x - fraction

σ - contribution

fc - coupling factor

χ_1 - fiber orientation factor

χ_2 - interface factor

FTSF - fiber tensile strength factor

G' - storage modulus

G'' - loss modulus

η^* - complex viscosity

tan (δ) - loss factor

E - Young's modulus

IFSS or τ - interfacial shear stress

T_i -initial temperature

T_{max} - maximum degradation temperature

T_f - final degradation temperature

TGA_R - residue from thermogravimetric analysis

T_{cc} - cold-crystallization temperatures

T_c - crystallization temperature

ΔH - enthalpy

TABLE OF CONTENTS

CHAPTER 1 – INTRODUCTION

1.1 INTRODUCTION

Environmental pollution and climate change represent major global challenges driven by the extensive use of fossil-based resources, leading to increased greenhouse gas emissions and the accumulation of waste in natural ecosystems (Afshar et al., 2024; Buhaug et al., 2023; Islam et al., 2024). In response to the growing environmental challenges, significant progress has been made toward the transition to a biobased economy (Wilde; Hermans, 2024). This emerging economy, founded on the innovative and cost-efficient utilization of biomass to produce biobased products and bioenergy (De Jong; Jungmeier, 2015).

In this context, biorefineries have gained importance as sustainable technological systems designed to convert renewable biomass into fuels, chemicals, and materials, offering the potential to substitute approximately 30% of global fossil fuel use with bio-based alternatives in the coming years (Sulis et al., 2025; Wu; Restrepo-Flórez; Vasco-Correa, 2024). Among the biorefinery products, biopolymers and biocomposites are key innovations toward the development of sustainable materials derived from renewable biological sources, minimizing waste generation, and promoting the efficient use of renewable resources without compromising material performance (Chang; Mohanty; Misra, 2020; Gupta et al., 2022).

Poly (lactic acid) (PLA) has attracted particular attention as one of the most commercially available and environmentally friendly biopolymers. Derived from renewable feedstocks such as corn or sugarcane, PLA is used in diverse sectors, including high-performance automotive and aerospace components, as well as in medical implants, drug delivery systems, and consumer goods such as packaging and 3D printing materials (Bhong et al., 2023; Ranakoti et al., 2023; Trivedi; Gupta; Singh, 2023). Despite its many advantages, PLA also has limitations, including moderate mechanical strength, brittleness, low thermal stability, and moisture sensitivity, which can restrict its applications (Bikiaris et al., 2023). To overcome these drawbacks, research has focused on developing PLA-based biocomposites in which lignocellulosic fractions derived from natural fibers (NF) are incorporated into the polymer matrix to improve performance (Trivedi; Gupta; Singh, 2023). In recent years, these materials become potential alternatives to conventional petroleum-based composites, particularly polypropylene (PP)-based systems, which dominate the market of short fiber

reinforced composites due to their low cost, ease of processing, and balanced mechanical performance (Unterweger; Brüggemann; Fürst, 2014).

The use of NF, and their isolated structural components (cellulose, hemicellulose, and lignin) derived from agricultural residues, papermaking by-products, or food industry waste, represents an effective strategy for upcycling biomass, contributing to waste valorization and sustainability (Santos et al., 2024b). However, achieving satisfactory compatibility in PLA-NF-based systems remains challenging due to differences in polarity, crystallization behavior, and thermal stability, resulting in poor interfacial compatibility between hydrophilic NF and the hydrophobic PLA matrix. This incompatibility reduces interfacial bonding and stress transfer, limiting mechanical performance, durability, and upscale (Gholampour; Ozbakkaloglu, 2020).

Improving the interfacial adhesion between PLA and the lignocellulosic reinforcement is a key step toward obtaining composites with enhanced performance. A well-designed interface not only ensures more efficient stress transfer and durability but also contributes to sustainability by reducing waste generation and extending the useful lifetime of materials (Santos et al., 2024a). To address this challenge, lignocellulose surface modification treatments have been proposed to enhance the interfacial adhesion of PLA biocomposites (Shaker; Ali; Militky, 2023). Chemical treatments can expose cellulose microfibrils, increasing surface roughness and interfacial area, which enhances adhesion with the polymeric matrix, and also affect the lignin fraction polarity or introduce reactive groups that improve interfacial bonding (Mariana et al., 2021; Prome et al., 2025; Tazwar; Antora; Rahman, 2025).

Beyond surface treatments, the use of silane coupling agents through silylation reactions is widely recognized as one of the most effective methods to strengthen fiber–polymer interfacial interactions (Karthik et al., 2024). In this process, silane molecules are hydrolyzed to form silanol groups, which can chemically bond with hydroxyl groups present on the fiber surface, and their organofunctional groups interact with the polymer matrix (Chen et al., 2021). This dual reactivity promotes improved interfacial adhesion, leading to enhanced mechanical performance, reduced moisture absorption, and increased durability of biocomposites (Karthik et al., 2024). However, the effectiveness of silylation on lignocellulosic reinforcements depends on fiber composition, especially lignin levels and hydroxyl group availability (Chen et al., 2021). Although these advances have been made, most studies focus either on cellulose-rich fibers or isolated lignin, but do not consider the different lignin types, and the effect of lignin content on fiber. In this way, research on the combined effects of lignin content, chemical modification, and coupling agent effectiveness in PLA composites remains limited.

Achieving optimal interfacial adhesion between the hydrophobic PLA and the hydrophilic lignocellulosic components remains a critical scientific and technological challenge (Hasan; Rabbi; Maruf Billah, 2022). In this way, this work is justified by the need to establish relationships among structure, composition, and interfacial properties in PLA/lignocellulosic, providing a basis for comparing their performance with conventional PP-based composites. Addressing the combined effects of lignin content, chemical modification, and coupling agent effectiveness in PLA composites by providing understanding and targeted enhancement of the fiber–matrix interface is therefore crucial to unlock the full potential of these biocomposites as viable alternatives to petroleum-based materials, supporting global sustainability efforts, reducing environmental pollution, and promoting the circular bioeconomy.

1.2 OBJECTIVES

1.2.1 OBJECTIVE

To evaluate the influence of silylation of chemically untreated lignocellulosic fibers, bleached fibers, and lignin on the interfacial adhesion and overall properties of PLA-based composites.

1.2.2 SPECIFIC OBJECTIVES

a. To investigate the effect of silylation on the surface characteristics of the whole fraction of lignocellulosic fibers and assess its impact on the interfacial interactions and mechanical performance of PLA composites, by injection molding of specimens.

b. To analyze how different bleaching stages combined with silylation modify the chemical structure and interfacial adhesion of lignocellulosic fibers in PLA composites, by injection molding of specimens.

c. To develop PLA–lignin biocomposites with silylated soft and hardwood lignin and evaluate the influence of this modification on their dispersion on both lignin types, interfacial bonding, and functional properties by hot-press film production.

1.3 THESIS OUTLINE

This section illustrates the action diagram of this research, as shown in **Figure 1.1**. Poly(lactic acid) (PLA) biocomposites incorporating pine stone groundwood (SGW) fibers, bleached SGW, and lignin from softwood and hardwood sources were developed. Silylation was applied to all formulations to enhance thermo-rheological behavior and mechanical performance, with results detailed in Chapters 3, 4, and 5.

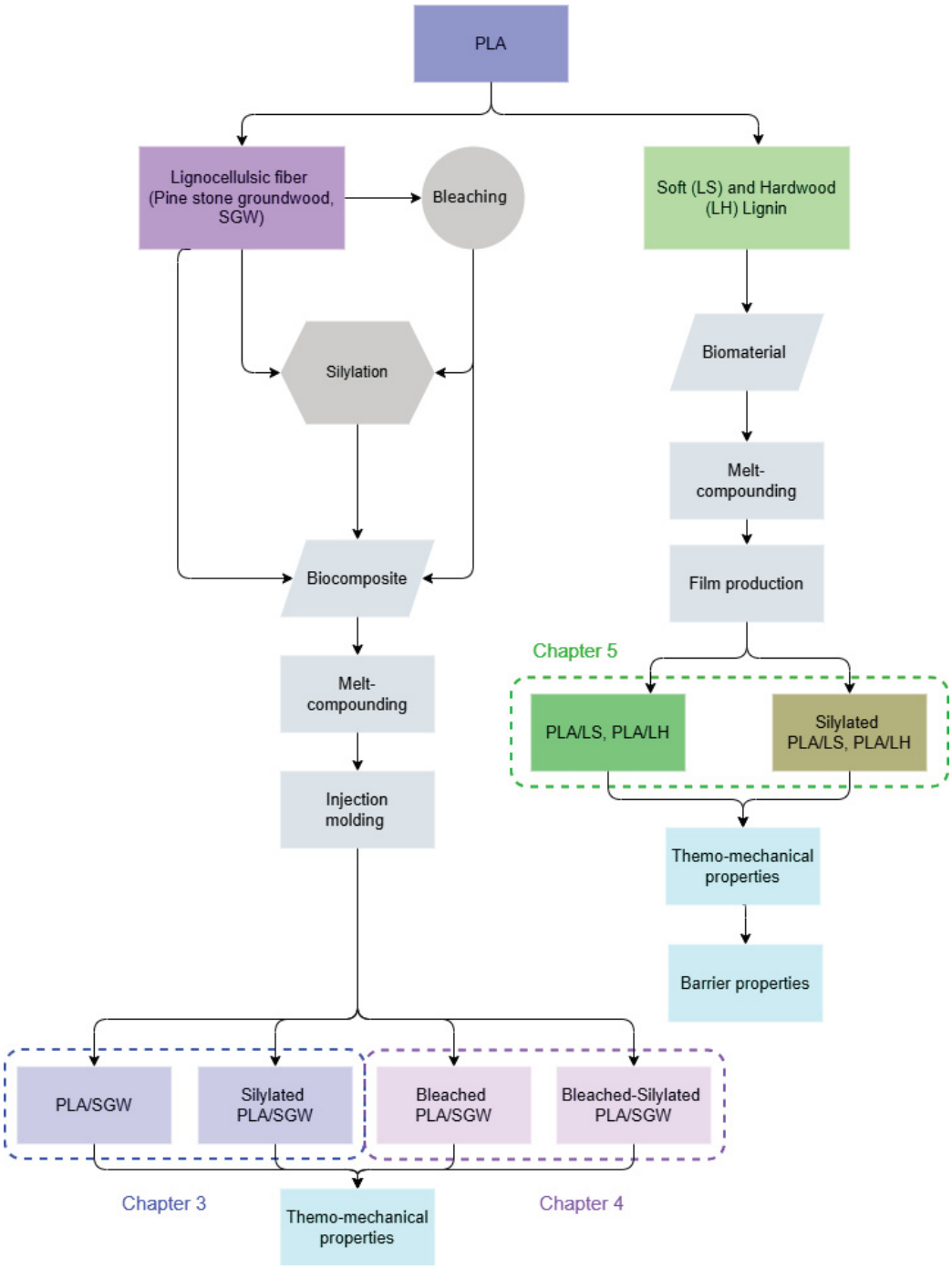

Figure 1. 1 Schematic action diagram of polylactic acid biocomposites.

CHAPTER 2 - LITERATURE REVIEW

2.1 BIOCOMPOSITES

Composite materials comprise a broad class of materials composed of physically and chemically different components with two or more constituents with distinct interfaces (Manu et al., 2022). An essential form of one dispersed phase as a reinforcement and/or a filler material to a continuous phase, determined as the matrix, which together forms a material with greater or different bulk properties from the isolated materials (Jayakumar; Saravanan; Philip, 2023). The matrix materials are classified as metal, ceramic, and polymer phase composites, and according to the reinforcement, are classified considering the material's shape as particles, laminates, and fibers (HSISSOU et al., 2021; JOSE et al., 2012).

Biocomposite materials are produced by combining at least one natural component to form a new material with enhanced performance compared to individual constituents (Rudin; Choi, 2013). Polymeric phase composites reinforced with natural plant-based fiber are the most studied class of biocomposites. Research and development of biocomposites have been steadily increasing due to their renewable nature (Christian, 2020).

Fully bio-based biocomposite materials, produced by biodegradable polymer matrices and renewable natural-based reinforcement, are eco-friendly materials and present a lower environmental footprint. Additionally, easily disposed of through composting and even recycled, they are potential candidates to replace oil-based non-renewable polymers (Andrew; Dhakal, 2022; Shanmugam et al., 2021).

The applications of polymeric biocomposites encompass the most distinct areas, from high-performance applications in the automotive and aerospace to biomaterials for pharmaceutics, and medical applications, mainly due to their inexpensiveness, biodegradable nature of some polymers and reinforcing fibers, renewability, and mechanical properties capable of replacing other compounds that use traditional synthetic reinforcements like glass or carbon fibers in high-performance applications (Andrew; Dhakal, 2022; Correa; Montalvo-Navarrete; Hidalgo-Salazar, 2019). Furthermore, for example, the substitution of fiberglass for natural fibers reduced the composite’s production energy cost by 80%, while the material cost was reduced by 5% (Shanmugam et al., 2021).

Besides biocomposites, which are usually referred to as natural fiber reinforced composites, they are also in pharmaceutics and medical devices as biomaterials produced with inorganic fillers. Due to biocomposite's non-toxicity, biodegradability, and biocompatibility, naturally derived biomaterials have long been used in numerous regenerative medical applications (Hashemi et al., 2024).

2.1.1 BIOCOMPOSITES MARKET

The demand for bio-based plastics and composites is expected to grow at a compound annual growth rate of 11.2% to 2030, while the production of materials from renewable feedstocks is projected to increase by 25% in 2030 (Gurunathan; Mohanty; Nayak, 2015). The global biocomposite consumption was estimated at $19.6 billion in 2020 and is projected to grow at a compound annual growth rate (CAGR) of 14.2% until 2025. In addition, the global synthetic fiber market, which was valued at $147.16 billion in 2019, is expected to experience a 5% CAGR by 2025. The decrease in demand for synthetic fibers in favor of natural fiber composite materials leads to increasing research in new biocomposites and the commercialization of finished products. (Shanmugam et al., 2021).

In the European market, over 30 compounding companies produced more than 100,000 tons of composite granulates with wood and natural fibers in 2018. Consumers and industry started requesting materials and products with a minimal environmental impact, lower carbon footprint, and with an end-of-life strategy for biocomposite products, aiming to reduce the use of fossil-based plastics (Partanen; Carus, 2019). Table 2.1 shows the market volume of biocomposite granulates in Europe for 2028.

Additionally, biomaterials, including neat and biocomposites, present a significant influence in the global medical device market, which is estimated to be USD 400 billion. The global biomaterials market is projected to reach USD 47.5 billion by 2025, up from USD 35.5 billion in 2020, with a compound annual growth rate (CAGR) of 6.0% at the time of the forecast (Oleksy; Dynarowicz; Aebisher, 2023).

Table 2. 1 Application areas and the potential for the market of biocomposites in Europe.

Biocomposites in Europe	Production tons p.a 2018	Production tons p.a 2028 (forecast)
Decking, fencing, and cladding, mainly extrusion molding.	200,00	220,000 – 250,000
Automotive, mainly compression molding, with high shares of natural fibers such as jute, kenaf, and hemp.	150,000	150,000
Technical applications, furniture, consumer goods, as well as rigid packaging, are mainly sourced from injection molding and 3D printing.	60,000	120,000 – 180,000
Total	410,000	490,000 – 580,000
Total figures include traded granulates for injection molding and extrusion	100,000	200,000 – 300,000

Source: Adapted from Partanen; Carus, (2019).

2.2 POLYMERIC BIODEGRADABLE MATRICES

Polymeric matrix composites are widely used in various industries, including electronics, biomedical, energy, and manufacturing, due to their good processability and ease of design and molding. As versatile composites, the polymeric matrix confers advantages such as high specific strength and high specific modulus, good fatigue resistance and high damage tolerance, and high multifunction properties that include high instantaneous temperature and ablation resistance (Chohan et al., 2022; Wang; Zheng; Zheng, 2011). Thermoplastics and thermosets are the most commonly used polymer types in advanced polymer composites. Thermoplastics are known for their ability to repeatedly melt and solidify, which allows for easy shaping and molding. They are also highly resistant to impact and can be recycled. On the other hand, thermosets have rigidity and strength; once they are formed, they cannot be reshaped or melted (Saba; Jawaid, 2018). Besides the type of polymeric matrix in terms of processability, the source of the polymer is also an important factor in composite assemblies.

The categorization of the polymeric matrices into renewable or non-renewable is determined by the source of the raw materials used in their production. Renewable matrices are derived from sustainable sources such as plants or biomass, while non-renewable matrices are

made from fossil fuels. In addition, one of the numerous advantages of using renewable sources of polymeric matrices is the faster biodegradation characteristic (Zhao et al., 2023). Renewable biodegradable matrices can rapidly undergo chain breakage after exposure to a specific biological medium and decompose into simpler substances (methane, carbon dioxide, inorganic compounds, biomass, and water). This property is intrinsically related to the synthesis of these materials by microbiological routes (Hasrc et al., 2001; Ray; Bousmina, 2006). Although biodegradability is a phenomenon associated with biopolymers from renewable sources, some polymers derived from fossil fuels also present this property, as illustrated in **Figure 2.1**.

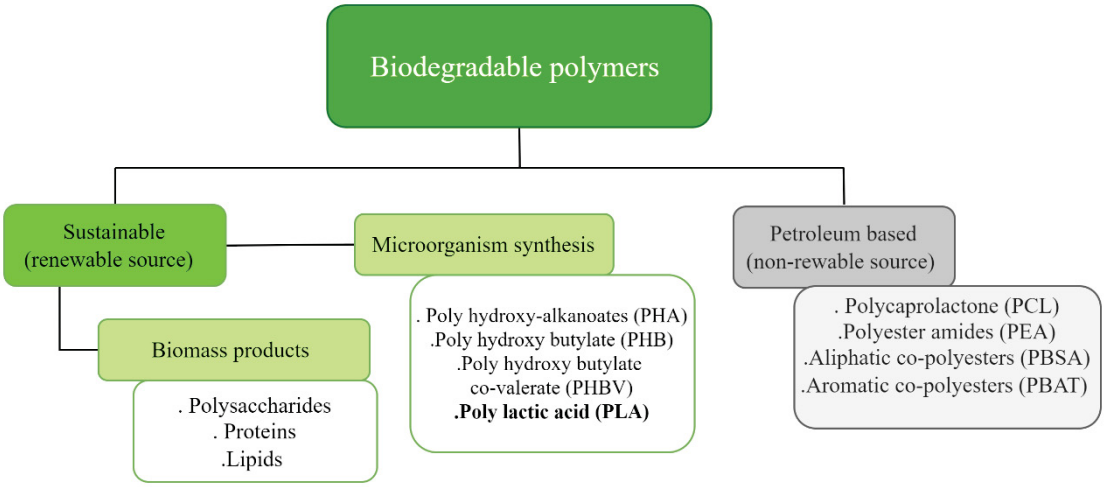

Source: Adapted from Averous; Boquillon, (2004).

Figure 2. 1 Classification of biodegradable polymers according to the polymer source.

Synthetic biodegradable matrices, such as aliphatic polyesters, are a class of biopolymers that present a hydrolyzable backbone polyester and are produced by conventional polymerization and synthesized from renewable materials, driven by biomass fermentation technologies (Zhang et al., 2021). Due to the large availability of raw materials, the development and adaptation of technologies raised the production of synthetic biodegradable polyesters on an industrial scale, leading to direct competition of these polymers with conventional plastics (Samir et al., 2022). Among the most synthesized polyesters are bio-based poly(lactic acid) (PLA), poly(glycolic acid) (PGA), poly (lactic-co-glycolic acid) (PLGA), and also oil-based poly(ε-caprolactone) (PCL), large used in biomedicine, as fundamental components for drug delivery systems, tissue engineering structures, and biomedical devices (Grøndahl; Jack; Goonasekera, 2017).

The most significant biodegradable aliphatic polyester synthesized monomers obtained from fully renewable sources, the poly (lactic acid) (PLA), has played a vital role in the manufacture of biocomposites (Rajeshkumar et al., 2021; Samir et al., 2022). PLA is a thermoplastic biodegradable polymer, and its unique characteristics as sustainability, biocompatibility, and compostability encourage its implementation in a large area of applications, from medical materials to high-performance biocomposites, in building and home furnishing to packaging and membranes (Li et al., 2023).

2.2.1 OVERVIEW OF POLY (LACTIC ACID)

Poly (lactic acid) (PLA), a biodegradable aliphatic polyester thermoplastic with good mechanical properties, processability, durability, and transparency, is one of the most rigid bioplastics commercially successfully applied to single-use items (Jem; Tan, 2020).

PLA presents three typical optical isomeric forms: the poly (L-lactic acid) (PLLA) and poly (D-lactic acid) (PDLA), which are optically active and crystallizable, and the racemic poly (DL-lactic acid) (PDLLA), an optically inactive and noncrystallizable form (Tsuji, 2013). The different forms of PLA derive from its building block, α-hydroxy acid, the lactic acid (LA) (2-hydroxy propionic acid), that exists in optically active D- or L-enantiomers, with identical physical and chemical properties; however, reactively differently (Jem; Pol; Vos, 2010). The L-isomer represents the major fraction of PLA produced by carbohydrate fermentation from renewable sources since the biological route is responsible for the synthesis of PLLA form with high optical purity, containing around 1-2% of the D-isomer (Lim; Auras; Rubino, 2008; Saeidlou et al., 2012).

The production of PLLA consists of the fermentation of first- or second-generation starch or glucose from renewable sources, such as corn, potatoes, beets, and sugarcane, to obtain the lactic acid monomer. The microorganism type, fermentation conditions, and the purification process determine the optical purity of LA and the process yield; these parameters are crucial to increase the molecular weight and ensure the optical purity during the PLA polymerization (Tsuji, 2013). Directed polycondensation of LA and ring-opening of the cyclic dimer of LA, the lactide form, are consolidated PLA polymerization methods. Both processes are based on the dehydration of lactic acid and condensed into oligomers, as demonstrated in **Figure 2.2**.

In terms of water removal during condensation of lactic acid, the ring-opening polymerization process is more efficient, since it performs at high temperature and under vacuum to remove moisture (Jem; Pol; Vos, 2010). The lactide is formed after catalytic depolymerization and purified with a distillation or crystallization process, ensuring the removal of residual moisture, lactic acid, and the meso-lactide (D,L-lactide) to further polymerize by a ring-opening reaction. The reaction occurs at temperatures above the lactide melting point and below the PLA degradation temperature until the resin is submitted to solidification and/or crystallization into pellets (Garlotta, 2002; Jem; Tan, 2020).

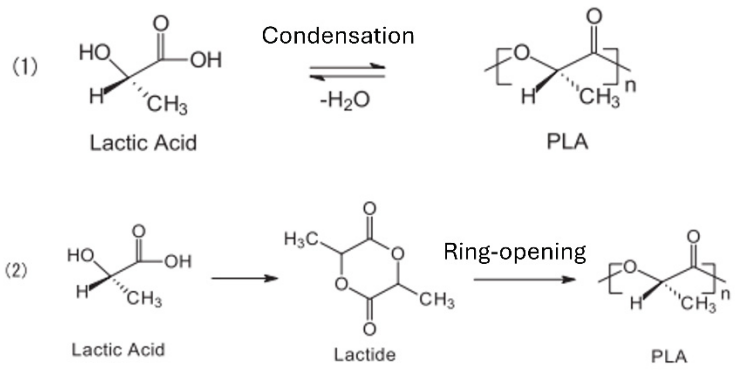

Source: Jem; Pol; Vos, (2010).

Figure 2. 2 PLA production processes, (1) direct polycondensation of lactic acid and (2) ring-opening polymerization of lactide.

In the polymerization process, molecular weight and crystallinity are adjustable properties that directly affect the mechanical response of PLA. The ring-opening polymerization of lactide monomers synthesizes high molecular weight polymer, usually greater than ~100,000 g/mole, and for specific applications, high-molecular-weight PLA with a narrow molecular weight distribution is achieved by modifying the initial polymer composition (Donate; Monzón; Alemán-Domínguez, 2020; Hamad et al., 2018). Also, the PLA quality has an intrinsic dependence on processing temperature, molecular weight, molecular orientation, crystallinity, and physical aging characteristics (Bergström; Hayman, 2016).

Semi-crystalline thermoplastics such as PLA present glass transition (T_g), and also melting temperature (T_m), both temperatures are affected by the molecular weight and the PLA optical purity (Lim; Auras; Rubino, 2008). The glass transition temperature determines PLA's chain mobility and its transition from glassy to rubbery, parameters related to rheological properties that affect the polymer manufacturing processability (Naser; Deiab; Darras, 2021).

Depending on the composition of the optically active form, PLA crystallizes in three forms (α, β and γ), and the crystal shapes influence the polymer melting temperature (Lim; Auras; Rubino, 2008). The more stable form, the α structure, presents a T_m of 185 °C and is obtained during PLA crystallization from melt or from solution, while the β structure presents a T_m of 175 °C, and the γ requires a specific crystallization process (Saeidlou et al., 2012; Tábi; Hajba; Kovács, 2016).

The rate of crystallinity reflects on the mechanical properties of the polymer, such as tensile strength, hardness, stiffness, and Young's modulus, and in its biodegradability (Boey; Lee; Tay, 2022). Furthermore, the PLA crystallinity affects the polymer's final applications, since high-end performance requires higher bulk microstructural and long-term properties, such as flame resistance, good weatherability, and durability, while medical devices require a higher degradation rate (Liu et al., 2020; Polak-Kraśna et al., 2021).

High-end performance application of PLA requires competitive mechanical properties, price, and better long-term properties related to a lower degradation rate in comparison to traditional polymers (Jem; Pol; Vos, 2010). As described in **Table 2.2**, PLA, a rigid polymer, exhibits mechanical properties comparable to polystyrene (PS) and poly (ethylene terephthalate) (PET), whereas polypropylene (PP) is more flexible with moderate stiffness and higher ductility, and PLA is stiff with higher stress at maximum load and exhibits lower impact strength (Cosate de Andrade et al., 2016; Peltola et al., 2014).

Table 2. 2 Characteristics comparison between PLA and traditional polymers.

Polymer	Density (g/mL)	T_g (°C)	T_m (°C)	Tensile strength (MPa)	Elongation (%)	Impact Izod (Jm^{-1})
PLA	1.24	56 - 60	140 – 175	53	3 - 6	12.8
PS	1.05	100	-	45	5	21
PET	1.39	69	255	57	70	59
PP	0.90	-20	175	31	200	53

Subtitle: T_g: glass transition temperatures, T_m: melting temperature, PS: polystyrene, PET: poly(ethylene terephthalate), PP: polypropylene.

Source: Adapted from Jem; Pol; Vos, (2010).

Although to meet the high-end performance application requirements, polymer compositing is an alternative consolidated method able to suppress PLA hydrolytic and thermal degradability and increase polymers' mechanical performance (Tsuji, 2013). Polypropylene

(PP) is one example of a reinforced polymer composite with short glass fibers enhancing its mechanical properties and achieving extraordinary levels in comparison with the neat polymer (Mutjé et al., 2006). However, compared with the traditional petroleum-based composites reinforced with synthetic fibers, which make the recycling process. PLA biocomposites reveal great benefits in renewability, biodegradability, compostability, low density, and additional properties such as biocompatibility, and use in medical device end-products (Rajeshkumar et al., 2021).

PLA is a thermoplastic material and is easily processed by traditional manufacturing methods, such as injection molding, extrusion, film extrusion, blow molding, thermoforming, fiber spinning, film forming, and additive manufacturing techniques such as three-dimensional printing, enabling PLA compositing (Farah; Anderson; Langer, 2016; Tümer; Erbil, 2021). **Table 2.3** presents some recent PLA biocomposites research for both high-performance applications, with different types of natural reinforcements.

Table 2. 3 PLA biocomposites applied in high-performance.

Reinforcement	Manufacture method	Achievements	Reference
Cellulase-treated wood fibers.	Twin-screw extruder, extrusion, and injection molding.	Increase in tensile and flexural strength and flexural modulus.	Wan et al., (2024)
Neat and chemically treated short bamboo fiber.	Injection molding.	Recyclability of the biocomposites	Rao; Debnath; Mahapatra, (2024)
Flax fiber and boron compounds.	Corotating twin-screw extrusion and injection molding.	Increase in the water absorption resistance after fiber alkali treatment, and Young's modulus and flexural modulus.	Avci et al., (2023)
Wood fibers non-, and alkali treated.	Corotating twin extruder and injection molding.	Increase in tensile and flexural strengths with the fiber content, no effect to the alkali treatment.	Cosse et al., (2023)
Untreated and bleached hemp fibers.	Melt-compounding by kinetic mixing, single-screw extrusion, and injection molding.	Yielding fully bio-sourced composites with enhanced stiffness.	Aguado et al., (2023)

Source: The author (2024).

Natural fibers and disposable minerals are employed as reinforcement and as fillers to improve PLA's thermal, water barrier, crystallization, mechanical, antimicrobial, and degradability properties, to produce fully biodegradable and compostable high-performance biocomposites (Rajeshkumar et al., 2021).

2.3 NATURAL FIBER REINFORCEMENT FOR BIOCOMPOSITES

Fibers as reinforcement provide the composite's matrix functional structural properties, such as high specific strength and stiffness, thermal stability, and acoustic insulation, while the matrix links the reinforcing fibers, conferring load transfer, chemical resistance of the structure, and the desired shape to the final product (Gurunathan; Mohanty; Nayak, 2015; Hasrc et al., 2001; Lotfi et al., 2021). According to their origin, fibers are classified as synthetic or natural, subdivided into synthetic organic and inorganic fibers, and natural animal, mineral, and plant-based lignocellulosic fibers (Rahman; Putra, 2018).

Natural fibers (NF) are plant-based fibers extracted from parts of plants such as leaves, stems, seeds, fruits, stalks, and grass/reeds. NFs are mainly composed of cellulose, hemicelluloses, lignin, pectin, and extractives. (John; Thomas, 2008; Lotfi et al., 2021). Cellulose is the main structural polysaccharide of plants' cell walls, formed by repeating β-(1,4)-bound D-glucopyranosyl units. The bonds create a highly arranged crystalline structure of cellulose, known as elementary fibrils, and the aggregation of these fibrils produces microfibrils, macrofibrils, or cellulosic fibers with high tensile strength, low density, and excellent reinforcing potential when incorporated into polymer matrices (Elfaleh et al., 2023a; Mokhena et al., 2021).

The framework of the lignocellulose cell wall is determined by the intra- and intermolecular bonds within the crystalline cellulose structure, surrounded by the hemicellulose and lignin amorphous fractions, as represented in **Figure 2.3** (Deng; Li; Chen, 2012). Hemicelluloses are copolymers composed of polysaccharide molecules, such as pentose and/or hexose sugars, mainly linked by β-(1, 4) glycosidic bonds (Kaur; Sharma, 2019). It is amorphous, more hydrophilic, and has lower thermal stability than cellulose, which limits its direct reinforcing ability in composite systems (Hosseinaei et al., 2012).

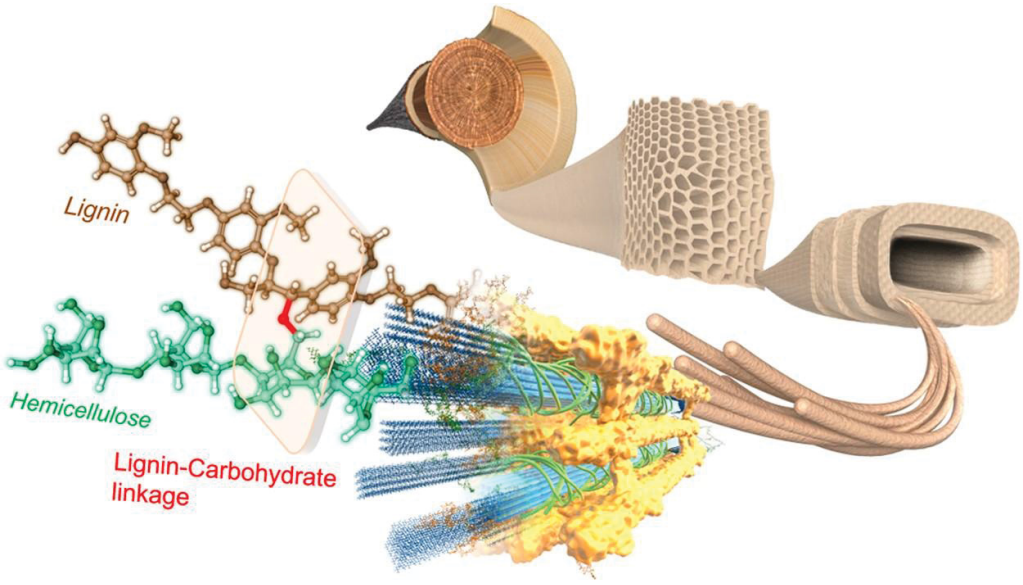

Source: Nishimura et al. (2018).

Figure 2. 3 Illustration of wood cell walls and their ultrastructure linking lignin and carbohydrate.

As the carbohydrate fraction, cellulose and hemicellulose influence not only the mechanical performance but also the barrier and functional properties of biocomposites. Cellulose primarily contributes to stiffness, strength, and structural reinforcement, while hemicellulose enhances flexibility, imparts oxygen barrier properties, and can act as a natural plasticizer in certain systems (Khouaja; Koubaa; Ben Daly, 2025; Lucena et al., 2025). However, their inherent hydrophilicity and sensitivity to thermal degradation remain challenges, particularly when processing hydrophobic or high-melting-point polymers (Cheng et al., 2025; Mohammed et al., 2023).

As the third major lignocellulosic component, lignin is a macromolecule formed by phenylpropanoid units combined according to the reactivity parameters of monomeric monolignols (Abolore; Jaiswal; Jaiswal, 2025). Both hemicelluloses and lignin fractions present amorphous structures that vary in composition among plant species, during the growing season, and in different parts of the plants (Chen, 2014).

The physical-chemical properties of lignocellulosic fibers (LCF) are closely linked to the performance of fiber-reinforced composites. Cellulose content enhances mechanical strength by increasing the fibers' tensile strength, while the microfibrillar angle determines the stiffness (John; Thomas, 2008). Lignin acts as a binding agent in fiber cells. However, high levels of non-cellulosic components, such as extractives, could decrease the bonding between the fiber and polymeric matrix (Bhat; Kumar; Mural, 2023; Vigneshwaran et al., 2020).

LCF over the conventional synthetic inorganic glass, aramid, and carbon fibers carry on similar tensile strength, and advantageous characteristics such as lower cost, lower density, no abrasion generated during the composite processing, renewability, recyclability, biodegradability, and fewer health risks involved in the fiber processing (Rahman; Putra, 2018). **Table 2.4** shows LCF characteristics, composition, and properties compared to synthetic fibers.

Regarding synthetic fiber compared to natural, it is expected that the lignocellulosic fibers could replace glass fiber in composites and migrate to the production of sustainable biocomposites from a biopolymer matrix (Ferreira; Cruz; Fangueiro, 2018). Although the lower density and good mechanical properties, as shown in **Table 2.4** for the most studied NFs, achieving optimal performance of fiber-reinforced composites depends on factors beyond the fiber structure and physicochemical properties (Kamarudin et al., 2022). The impurity content, moisture absorption, fiber orientation, and volume fraction of fiber concerning the matrix are inherent fiber characteristics that directly influence the interaction between the fiber and the matrix and play a crucial role in determining the mechanical properties of natural fiber-reinforced polymer composites (Mohammed et al., 2023).

Besides its high strength and modulus, cellulose's reactive surface, due to the availability of hydroxyl groups, also encourages its use as reinforcement for organic polymer composite materials (Hadjadj et al., 2016). However, the hydroxyl groups in lignocellulosic fibers determine the fiber's polarity and hydrophilic behavior. This results in moisture absorption, which leads to poor adhesion between the polar LCF and non-polar commercial thermoplastic polymers due to the contrasting hydrophobic characteristics of the matrix materials (Bhat; Kumar; Mural, 2023; Elfaleh et al., 2023b). Therefore, modifying the fibers' surface is the key to improving the fiber adherence to the matrix and reducing moisture absorption, conferring optimal stress transfer (Elfaleh et al., 2023b).

Despite natural fiber origin and chemical composition, fibers are also categorized by size and orientation, which are also characteristics that affect the fiber and polymer adhesion, as well as composite properties (Ahmad; Hamid; Osman, 2019). Depending upon their length and diameter, fibers are continuous (long) and discontinuous (short), and according to the orientation, fibers are unidirectional, multidirectional, or randomly oriented (Bhat; Kumar; Mural, 2023).

Table 2. 4 Properties comparison of natural and synthetic fibers.

Fiber type	Origin	Chemical composition (%)			Fiber length (mm)	Fiber diameter (mm)	Density (g/cm^3)	Tensile strength (MPa)	Young's modulus (GPa)	Elongation (%)
	Natural	**Cellulose**	**Hemicellulose**	**Lignin**						
Kenaf	Stem	45-57	8-13	22-25	1.4–11	4–36	1.4	223–930	14.5–53	1.5–2.7
Flax	Stem	64-72	18-21	2-3	10-65	5-38	1.4-1.5	343–2000	27.6–103	1.2–3.3
Bamboo	Stem	26-43	25-30	5-30	2-3	14-18	0.6-1.1	140–800	11–32	2.5–3.7
Abaca	Leaf	56-63	15-17	7-9	-	-	1.5	400–980	6.2–20	1–10
Jute	Stem	61-72	18-22	12-14	0.8-6	5-30	1.3-1.5	320–800	8–78	1–1.8
Sisal	Leaf	75-78	10-12	8-10	0.8-8	7-47	1.33-1.5	363–700	9–38	2–7
Banana	Leaf	63-83	17-21	5-7	0.1-4.2	12-30	1.35	500	12	1.5–9
Hemp	Stem	70-74	1-3	3-6	-	-	1.4-1.5	270–900	23.5–90	1–3.5
Softwood	Stem	40-44	25-28	25-29	-	-	0.3-0.60	45-111	3-15	4-5
	Synthetic									
E-Glass	inorganic	-	-	-			2.5	3500	72	2.5–3.4
Carbon	inorganic	-	-	-			1.7	4000	235	1.4–1.8
Aramid	inorganic	-	-	-			1.4	3100	63–67	3.3–3.7

Source: Adapted from Vigneshwaran et al., (2020), Lotfi et al., (2021) and Elfaleh et al., (2023).

Longer fibers usually absorb more energy before the fracture, resulting in improved mechanical properties of composites (Elfaleh et al., 2023b). Nonetheless, short fiber provides economic and manufacturing advantages over longer fiber-reinforced composites. Short fibers offer good processability in conventional extrusion and injection molding methods, and the final good composite properties are achieved as long as the aspect ratio (fiber length divided by its diameter) is high enough to support load transfer and ensure fiber orientation and distribution (Cruz-González et al., 2021; Watanabe, 2002).

To achieve high-performance composites reinforced with lignocellulosic fibers, surface properties, chemical composition, and configuration of the reinforcing fibers, including fiber orientation, length, and concentration, are the main factors that affect the interfacial adhesion and the mechanical properties (Ahmad; Hamid; Osman, 2019; Tseng; Chang; Hsu, 2017). Fiber orientation is given during the composite manufacturing process and is predicted by mechanical models from mechanical properties such as tensile strength (Flake C Campbell Jr, 2003). A good adhesion between fiber and matrix, usually achieved by the lignocellulosic fiber surface treatments, leads to the effective transfer of stresses through the interface, providing composite materials with superior properties (Elfaleh et al., 2023b; Hristov; Vlachopoulos, 2007).

2.3.2 STONE GROUNDWOOD FIBER AS REINFORCEMENT

Wood is a source of lignocellulosic fiber obtained from shrubs and trees, widely used in the manufacturing of pulp and paper products for the papermaking industry. As a heterogeneous, hygroscopic, and anisotropic material, wood fiber is classified as hardwood and softwood, which differ in lignocellulose fraction and fiber size (Elfaleh et al., 2023b; Khan; Srivastava; Gupta, 2020). Hardwood fibers come from deciduous trees, such as aspen and birch, while softwood fibers are mainly obtained from conifers (e.g., spruce and pine). Although hardwood has a more complex cellular structure and lower lignin content, softwood shows a more uniform cell structure and axial tracheid shape with no vessels or pores, which makes it generally preferred for composite applications due to its larger fiber aspect ratio (Chand; Fahim, 2008; Elfaleh et al., 2023b; Esteban et al., 2023).

In the papermaking industry, wood pulping is the fundamental process used to break down physically and/or chemically the wood structure into individual fibers. Pulping processes involve both grinding and refining and are categorized into chemical, semi-chemical,

thermomechanical, and mechanical pulping (Mboowa, 2024; Sandberg; Hill; Jackson, 2020). The mechanical pulping process defibrillates the fiber by mechanical friction under water or steam, with a total process yield of about 90–98%, with minimal loss of lignocellulosic fraction, high bulk, high stiffness, and low cost. Refiner mechanical pulping (RMP), thermomechanical pulping (TMP), pressure groundwood (PGW) pulping, and stone groundwood (SGW) pulping are the most used mechanical pulping processes (Bajpai, 2018).

In SGW pulping a debarked block of lengthwise wood is pressed against a rotating grindstone revolving at speeds of 1000 to 1200 rev/min. The friction generated in the grinding zone increases the media temperature and softens the wood, hence easing the fiber separation process (Mboowa, 2024). The relatively mild mechanical and thermal conditions employed during their production improve the performance of polymeric matrices. Different from TMP and RMP processes, which involve elevated temperatures and intense mechanical shearing that promote lignin softening and surface inactivation, SGW processing preserves fiber integrity and maintains lignin distributed along the fiber surface (Urdaneta et al., 2024). This results in improved interfacial compatibility with polymers. Additionally, the higher availability of accessible hydroxyl groups and the less condensed nature of lignin in SGW fibers favor its modification (López et al., 2013).

The direct wood fibrillation, as occurs in the SGW process, significantly increases fiber surface roughness by exposing cellulose microfibrils and cellulose-rich fine elements, thereby enhancing the pulp/fiber surface area, promoting hydrogen bonding among the fibers, and improving the fiber's reinforcing potential, as shown in **Figure 2.4** (Bianchi et al., 2019; Graupner et al., 2023).

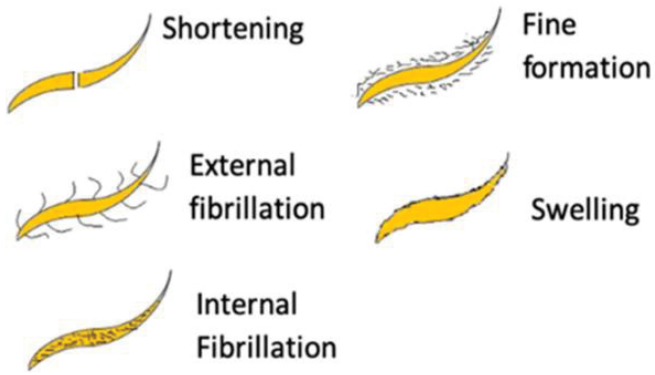

Source: Debnath et al., (2021).

Figure 2. 4 Changes in fiber properties during the fibrillation process.

SGW processing typically uses pine wood as raw material due to its widespread availability and low-cost pulp in the market, to produce newspaper sheets and packaging boards

(Julian et al., 2012). The chemical composition of pine wood before processing usually ranges from 40–46% of cellulose, 25–28% of hemicellulose, 27–29% of lignin, and 4-5% of extractives and ash, and its fiber normally presents a tensile strength from 12 to 27 MPa, and Young's modulus of 0.1–0.5 GPa (Khan; Srivastava; Gupta, 2020). Pine SGW is a high-fibrillated high-yield pulp (around 98.5 wt%), meaning that a high amount of cellulose micro-fibrils is available for hydrogen bonding, and its lignocellulosic fraction is unchanged after SGW pulping (López et al., 2011). However, as a lignocellulose fiber with hydrophilic and polar characteristics, enhancing the SGW surface to improve adhesion between polymer matrices and SGW is an alternative for composite production with high tensile strength.

SWG pulp was previously studied as fiber reinforcement for high-performance polypropylene composites by López et al., (2011) and Julian et al., (2012). Both studies evaluated the use of polypropylene functionalized with maleic anhydride (MAH-PP) as a surface compatibilizer for PP/SGW and observed an increase in composite tensile strength. Oliver-Ortega et al. (2016) evaluated tensile properties and micromechanical analysis of stone groundwood from pine softwood as reinforcement to polyamide composites, and further, Granda et al. (2016) compared the potential of wood fiber reinforcement for PLA composites using pine SGW, bleached kraft softwood, and fluff pulps. All previous research has observed an interesting increase in tensile strength in SGW-reinforced composites. However, the implementation of fiber surface treatment to enhance fiber dispersion and adhesion within the chosen matrix is gaining attention for study.

2.3.1 LIGNIN IN COMPOSITES

Lignin is the third most abundant component of lignocellulosic biomass, after cellulose and hemicellulose, accounting for 15–30% of plant dry mass. It is an amorphous, highly cross-linked polyphenolic macromolecule that provides rigidity, hydrophobicity, and resistance to microbial attack in plant cell walls (Kamdem Tamo et al., 2025). Lignin is an irregular, randomly cross-linked aromatic polyether composed of three main monolignols, *p*-hydroxyphenyl (H), guaiacyl (G), and syringyl (S), which originate from *p*-hydroxycinnamyl alcohols with varying degrees of methoxylation (Vanholme et al., 2019).

The monomeric composition of lignin varies among plant species. In conifers (softwoods), lignin is primarily composed of G units. Hardwoods, which include deciduous and broadleaf species, contain both G and S units. In contrast, grasses and other herbaceous plants

exhibit varying proportions of H, G, and S units (Mei et al., 2019; Suota et al., 2021b). These units are structurally bonded by β-O-4, β-5, β–β, and 5-5 linkages (Kamdem Tamo et al., 2025), as shown in **Figure 2.5**. Softwood lignins typically contain more guaiacyl units and are more resistant due to higher amounts of β-5′ and 5-5’ linkages. Conversely, hardwood lignins have a higher syringyl-to-guaiacyl ratio, making them less resistant and more accessible, which influences their polarity, branching, and reactivity (Li et al., 2025a; Rese et al., 2025; Suota et al., 2021b).

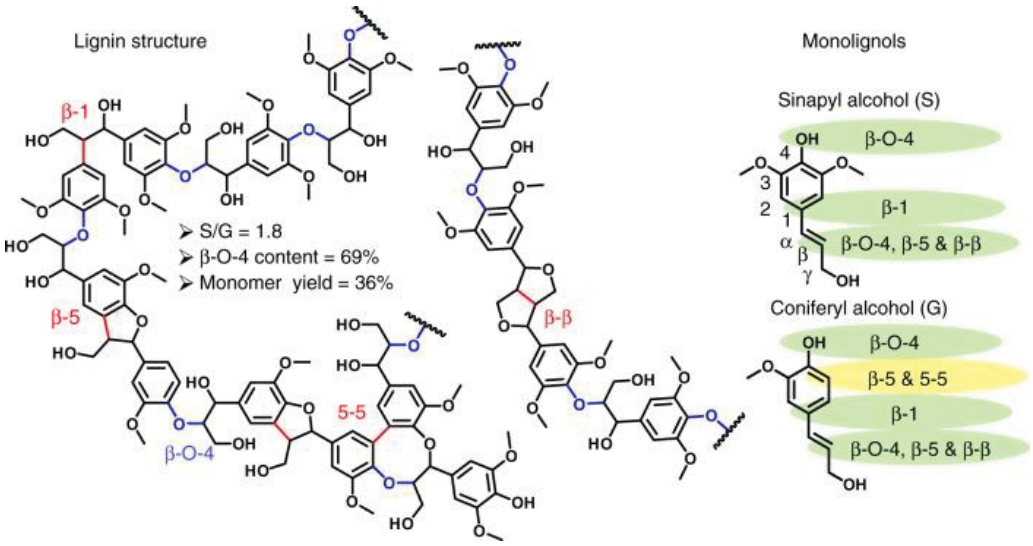

Source: Anderson et al., (2019)

Figure 2. 5 Overview of the main lignin monomers’ structure.

Its complex aromatic structure, lignin possesses unique properties compared to polysaccharide-based biopolymers, including intrinsic UV absorption, antioxidant activity, and high carbon content (Lin et al., 2021). These features have attracted growing interest in lignin as a functional additive or reinforcement in polymer biocomposites, particularly in the context of sustainable materials development and valorization of industrial byproducts from the pulp and paper or bioethanol industries (Jiju et al., 2025).

In polymer matrices, lignin has been investigated both as a filler and as a compatibilizer (Ridho et al., 2022). At low loadings, lignin can act as a multifunctional additive, imparting UV-blocking, antimicrobial, and antioxidant properties to films and composites. For biodegradable matrices such as polylactic acid (PLA), starch, or polyhydroxyalkanoates (PHAs), the incorporation of lignin has also been reported to enhance thermal stability by delaying degradation through radical scavenging mechanisms (Basbasan et al., 2022). However, due to its inherent brittleness and heterogeneous nature, lignin does not always

contribute directly to mechanical reinforcement (Kapuge Dona; Smith, 2025). Additionally, the particle size and origin of lignin, kraft, organosolv, or soda, have been shown to influence composite performance, with more purified or modified lignins generally offering better homogeneity and property improvements (Mansouri; Salvadó, 2006).

In addition to the lignin obtention process, the origin of lignin (grass, soft, and hardwood) plays a crucial role in compatibilization with polymeric matrices, particularly in terms of the syringyl (S) and guaiacyl (G) unit ratio, which strongly influences its interaction with polymeric matrices (Suota et al., 2021b). Syringyl units, characterized by two methoxy groups on the aromatic ring, exhibit a more linear and less condensed structure, which reduces intermolecular crosslinking and enhances molecular mobility. As a result, hardwood lignins generally show improved dispersion and interfacial interaction within polymer matrices (Johansson et al., 2023; Shu et al., 2021; Suota et al., 2021a). In contrast, guaiacyl-rich softwood lignins are characterized by a higher degree of condensation, leading to increased rigidity, stronger intermolecular interactions, and a more heterogeneous morphology when blended with thermoplastic polymers. These structural features tend to limit interfacial adhesion and promote phase separation in composites (Kapuge Dona; Smith, 2025; Park et al., 2019). Consequently, lignins with higher S/G ratios are often associated with better compatibility and dispersion in PLA-based systems, contributing to improved mechanical performance and more homogeneous composite structures (Anuar et al., 2023; Park et al., 2019).

In some cases, unmodified lignin leads to reduced tensile strength or elongation at break, mainly due to poor interfacial adhesion with hydrophobic polymer matrices and phase separation during processing. Zhu et al. (2015) reported a proportional decrease in the tensile strength of lignin PLLA composites as the untreated lignin load increased from 5 to 30 wt.%. Wang et al. (2020) also observed a decrease in tensile strength with lignin loads of 1, 3, and 5 wt.%. Recently, Ju et al. (2024) incorporated 10, 20, and 30% lignin, resulting in a reduction of the composites' tensile strength. Although after lignin modification or the use modifier to partially interact with the hydroxyl groups on the lignin, these researchers could improve the tensile strength of PLA-lignin composites at some loads.

To address compatibility challenges, various chemical modification strategies have been developed, including esterification, acetylation, and grafting with functional groups or coupling agents. Such modifications improve the dispersion of lignin within the polymer and promote stronger interfacial bonding (Santos et al., 2023; Thakur et al., 2014). Thus, lignin functionalization represents a key strategy to improve interfacial adhesion between lignin and

polymer phases. Chemical modifications introduce functional groups capable of reacting or interacting with the polymer matrix, reducing interfacial tension and enhancing load transfer efficiency. Such improvements not only strengthen mechanical properties but also expand the applicability of lignin as a renewable reinforcing component in polymer composites (Georgs et al., 2025). From a sustainability perspective, lignin-reinforced biocomposites offer significant potential as value-added applications for an abundant industrial byproduct (Oladzadabbasabadi et al., 2025).

2.4 FIBER SURFACE TREATMENT

Lignocellulosic fiber's amorphous regions, and the availability of hydroxyl and other polar groups, make the fiber surface susceptible to absorbing moisture, creating an unsuitable interfacial adhesion between fiber and polymer, leading to a decrease in the mechanical properties, loss of dimensional stability, and fiber biodegradation, reducing the potential application of natural fibers for reinforcing polymer composites (Ferreira; Cruz; Fangueiro, 2018).

In order to overcome the drawbacks related to the fiber surface, physical, biological or chemical fiber-modifying treatments are applied to provide an efficient hydrophobic barrier and optimize adhesion with the polymer matrix (Belgacem; Gandini, 2005; Elfaleh et al., 2023b). However, to preserve the fiber's mechanical strength, it is important to restrict surface modification treatments to the superficial hydroxyl groups; otherwise, aggressive surface modification generates surface adhesion bonding reduction and fiber degradation (Belgacem; Gandini, 2005; Martínez-Landeros et al., 2019).

Physical surface modification treatments separate natural fiber bundles into individual filaments by plasma, ultrasound, and UV light treatments (Ferreira; Cruz; Fangueiro, 2018). Biological treatments remove pectin, lignin, and hemicellulose components through enzymatic and bacterial activity to expose cellulose fiber and its hydroxyl groups (Naik; Allu; Purnima, 2024). While chemical surface modification treatments aim to covalently bond natural fibers' hydroxyl groups with specific chemical reagents, or by removing non-cellulosic components from the fiber surface. Chemical methods usually involve fiber treatment, such as alkali, silane coupling, maleated coupling, acetylation, permanganate, and peroxide (Ferreira; Cruz; Fangueiro, 2018; Khoathane; Sadiku; Agwuncha, 2015).

Usually, fiber surface treatment, as alkali treatment, involves the removal of the hemicellulose and lignin fraction, exposing cellulose molecules, increasing the number of possible reaction sites, and with that improving the adhesion of fibers to the polymeric matrix (Ferreira; Cruz; Fangueiro, 2018). However, several studies demonstrated that lignin, as cellulose, presents stabilization, compatibility, and reinforcement properties in composites. Lignin aromatic and cross-linked functional groups enable its application in polymeric matrices, improving the composite's wettability, mechanical, and fire-retardant properties. Besides that, lignin chemical structure also contains inter- and intramolecular hydrogen bonds, with possible reaction sites (Chihaoui et al., 2022; Ridho et al., 2022).

2.4.1 SILYLATION

In the interest of preserving the fiber lignocellulosic fraction, and the fibrillar structure as obtained in stone groundwood pulp, and using its hydroxyl-rich surfaces as a favorable strategy, chemical coupling mechanisms with molecular or macromolecular agents bearing one or several hydroxyl groups are implemented to establish covalent bonds at the interface between fiber and polymer (Belgacem; Gandini, 2005; Xie et al., 2010). This approach requires coupling bi-functional molecules, one capable of reacting with the fiber's superficial OH groups and the other capable of subsequent covalent bonding with the polymeric matrix (Abdelmouleh et al., 2004).

Silane coupling agents are a class of organosilicon compounds containing both organic and inorganic reactivity, mostly applied to improve the degree of cross-linking in the fiber/polymer interface (Pape, 2011). The inorganic part, under experimental conditions, condensates with the lignocellulosic hydroxyl groups, while its organofunctionality is coupled with the matrix (Belgacem; Gandini, 2005). Its generic chemical structure is represented as $R(4-n)Si(R'X)n$, where R represents an alkoxy, X represents an organofunctionality, R' is an alkyl bridge that connects the silicon atom to the organofunctionality, and n is equal to 1 or 2 (Xie et al., 2010). Normally, the structure contains three inorganic reactive alkoxy groups, methoxy or ethoxy groups, while the organofunctional groups are formed by amino, mercapto, glycidoxy, vinyl, or methacryloxy groups, as shown in Table 2.5 (Pape, 2011; Xie et al., 2010). Besides the silane inorganic groups presenting good interactions with natural fiber, each silane agent organic group presents relative affinity with a different polymeric matrix (Pape, 2011).

Table 2. 5 Silane coupling agent and its polymer type according to its organic group.

Organic group	Chemical Name	Indicated Polymer
Amine	Aminopropyltriethoxysilane	Acrylic, Nylon, Epoxy, Phenolics, PVC, Urethanes, Melamines, Nitrile Rubber
Diamine	Diaminopropyltrimethoxysilane	Acrylic, Nylon, Epoxy, Phenolics, PVC, Melamines, Urethanes, Nitrile Rubber
Methacrylate	3-Methacryloxypropyltrimethoxysilane	Unsaturated Polyesters, Acrylics, EVA, Polyolefin
Methyl	Methyltrimethoxysilane	Hydrophobing agent for mineral surfaces
Isobutyl	Isobutyltrimethoxysilane	Hydrophobing agent for mineral surfaces, Masonry water repellent
Epoxy	3-Glycidoxypropyltrimethoxysilane	Epoxy, PBT, Urethanes, Acrylics, Polysulfides

Source: Adapted from Pape, (2011).

To effectively utilize silane coupling agents for modifying the surface of lignocellulosic fibers, proper condensation of silanol groups with the hydroxy functions on the fiber surface must take place, as demonstrated in **Figure 2.6**, for a generic coupling agent structure. The first step of the reaction mechanism is the silane coupling agent alkoxy groups hydrolysis into silanol groups, reactive groups (Ferreira; Cruz; Fangueiro, 2018). Due to silanols' high reactivity, self-condensation occurs between their hydroxyl groups and forms oligomers. Once the silanol groups become attached to the hydroxyl groups on the surface of the fibers, adsorption takes place, and the silanol oligomers are physically adsorbed through secondary hydrogen bonding interactions. Chemical cross-linking is then achieved through hydrogen bonding between the silanols and the hydroxyl groups of the fibers, leading to the formation of covalent bonds after the release of water during the fiber drying process (Arslan; Dogan, 2018; Del Angel-Monroy et al., 2024).

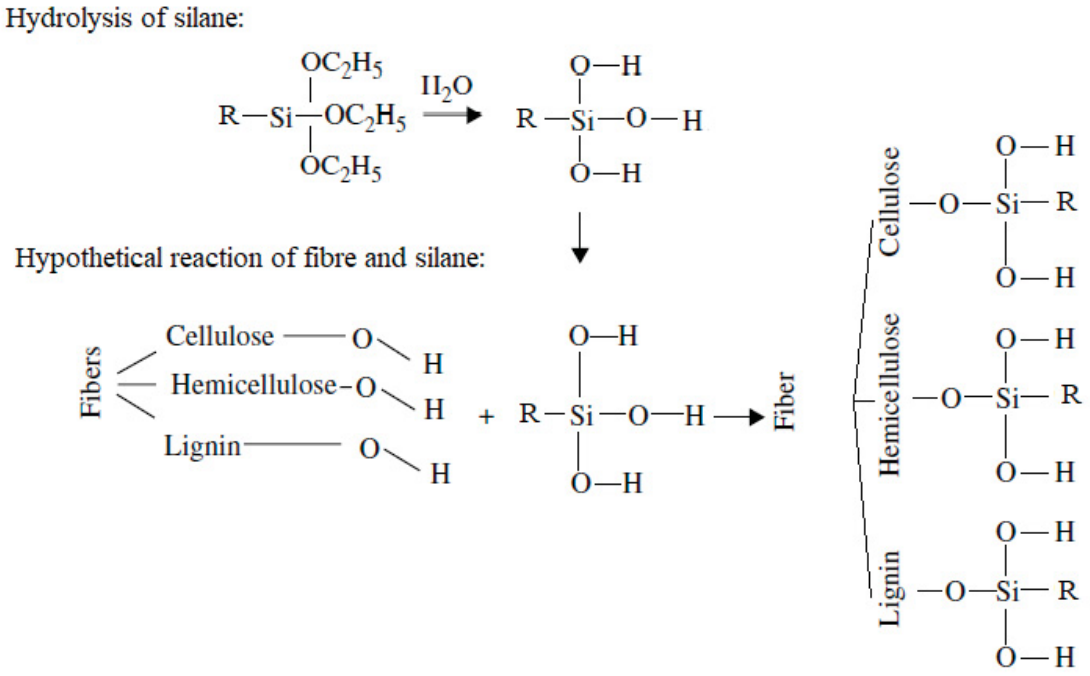

Source: Adapted from Sreekala et al. (2000).

Figure 2. 6 Generic reactions between the silane and the functional groups of natural fibers.

Hence, the complete fiber surface modification, the alkyl groups connect the silicon atom to the organofunctionality of the polymer functional groups, forming a siloxane bridge between the fiber and the polymer throughout heat during the composite melting-compound process, increasing the compatibility between polymer/fiber, leading to an increase in the interface strength of the polymer matrix (Ferreira; Cruz; Fangueiro, 2018).

Cabrera et al. (2020) studied the functionalization of nano-fibrillated cellulose fiber with two silane coupling agents, the 3-glycidyloxypropyl trimethoxysilane (GPS, named by some authors as KH-560) and 3-glycidyloxypropyl dimethylethoxysilane (GPMES) by a simple, direct, and environmentally friendly method, using 3 wt% of each silane and obtained successfully fiber functionalization through the condensation state of the grafted silanes network and elucidated the surrounding network to the cellulose surfaces, also observed improvement in fiber thermal properties.

Studies by Chen et al. (2021), tested the feasibility of four different silane coupling agents with amine, epoxy, and methacrylate organic groups, 3-aminopropyltrimethoxysilane (APS), γ-glycidoxypropyl-trimethoxysilane (KH-560), γ-methacryloxypropyltrimethoxysilane (KH-570), and γ-mercaptopropyltrimethoxysilane (KH-590), as molecular structure showed in **Figure 2.7**, used for constructing compatible interfaces between wheat straw/polylactic acid biocomposite. The authors tested all the coupling agents at a 2 wt% concentration, for a 30 wt%

of wheat straw fiber. However, the results indicate that KH-570-modified composite exhibited the best blending and tensile strength properties and best water resistance performance.

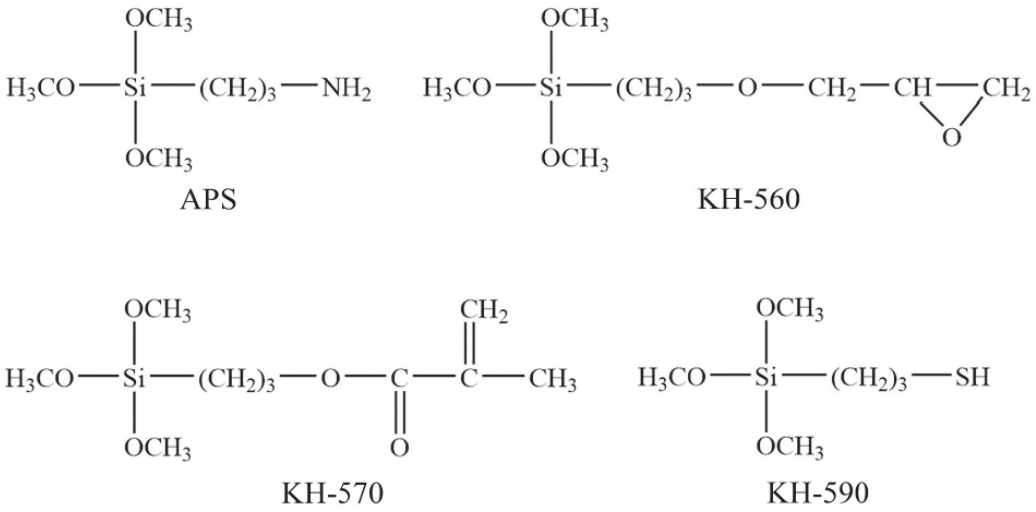

Source: Chen et al., (2021).

Figure 2. 7 Structures of amine, epoxy, and methacrylate silane coupling agents.

Yang et al., (2023) used three silane coupling agents, the amine APS (named by the authors as KH-550), epoxy KH-560, and methacrylate KH-570 with different molecular structures to modify the surface of waste corrugated paper fibers (WFs), using PLA as a matrix. The composite's microstructure, mechanical, thermal decomposition, and crystallization properties were evaluated. As a result, the composites treated with 4 wt% of KH-560 were able to improve mechanical properties, 115% higher than that of the pure PLA matrix for tensile strength, after comparison with both silanes at concentrations of 0, 2, 4, 6, and 8 wt%, at a 25 wt% of waste corrugated paper fibers.

Interesting results regarding the interface compatibility and mechanical properties of PLA/lignin composites coupled with γ-glycidoxypropyl-trimethoxysilane (GSP) were reported by Zhu et al. (2015) and Wang et al. (2020). The authors observed a smooth surface on the fractured composites treated with 2 wt.% and 5 wt.% silanes at 10 wt.% lignin, suggesting sufficient bonding between PLA/lignin and well-dispersed lignin particles, with increases in tensile strength and Young's modulus, although a decrease in elongation at break.

Considering the achievements of the silane γ-glycidoxypropyl-trimethoxysilane (GPS) for lignocellulosic fiber surface-modifying treatment for PLA composites and its reported development of a monolayer or a tridimensional covalent network onto the fiber chains, and its easy hydrolysis in its silanetriol equivalent in a 2 wt% aqueous solution as a fast reaction (De

Buyl; Kretschmer, 2008) was selected as a coupling agent for PLA composites as the focus of this work.

The use of a coupling agent capable of interacting with the hydroxyl groups of the lignin fraction, aligned with the use of a high-fibrillated pulp, is the focus of the present work, in which lignin is the target fraction of compatibilization between the untreated SGW fiber and lignin fraction. Different from conventional approaches that primarily target cellulose-rich surfaces, this strategy intentionally exploits the lignin-rich surface of SGW fibers. The preserved lignin structure and its accessible hydroxyl functionalities enable effective chemical interaction with the coupling agent, thereby enhancing fiber–matrix adhesion without the need for extensive chemical pretreatment. This approach highlights the potential of lignin not as an inert component, but as an active compatibilization site in biopolymer composites, aiming for improvement of mechanical properties.

2.4.2 BLEACHING PROCESSES

Bleaching processes are commonly used to enhance the brightness, purity, and surface features of lignocellulosic fibers by removing residual lignin, extractives, and chromophoric groups (Li et al., 2025a). In the pulp and paper industry, bleaching has traditionally been employed to produce high-bright pulps. The type of bleaching treatment affects not only the fiber color but also mechanical performance, hydrophilicity, and interfacial adhesion with polymer matrices (Peltola et al., 2019).

Although bleaching is often discussed alongside delignification, the two processes serve distinct roles in the paper industry. Delignification typically refers to the bulk removal of lignin during pulping, whereas bleaching focuses on eliminating the residual lignin and colored compounds that remain after primary pulping (Hintz; Lawal, 2018; Terzopoulou; Vouvoudi; Achilias, 2025; Tocco et al., 2021). This distinction is particularly relevant for biocomposite applications, where retaining a controlled amount of lignin may be beneficial for balancing mechanical properties, hydrophobicity, and matrix compatibility (Fazeli et al., 2024). Partial lignin removal through bleaching, rather than complete delignification, allows for a more nuanced tailoring of the fiber-matrix interface (Delgado-Aguilar et al., 2017; Ma et al., 2022).

Bleaching of natural fibers is commonly carried out using oxidizing agents such as acidified sodium chlorite, hydrogen peroxide, alkaline peroxide, ozone, or hypochlorite,

depending on the desired balance between fiber purity and cellulose preservation (Hashem; Farag, 2025; Samanth; Subrahmanya Bhat, 2023).

Among available bleaching technologies, acidified sodium chlorite ($NaClO_2$) is widely used for the bleaching and selective delignification of lignocellulosic fibers. Under acidic conditions, $NaClO_2$ is converted to chloric acid ($HClO_2$), which subsequently generates chlorine dioxide (ClO_2), a highly reactive oxidizing species that breaks down lignin into soluble fragments that can be washed away, leading to permanent fiber whitening (Guo et al., 2023; Kabir et al., 2012; Yue et al., 2015). In addition to lignin removal, ClO_2 also reacts with hydrophilic hydroxyl groups in hemicelluloses and other polar surface constituents, reducing the overall moisture affinity of the fibers and increasing their hydrophobicity (Samanth; Subrahmanya Bhat, 2023; Yue et al., 2015). Although a slight reduction in the degree of polymerization of cellulose may occur due to mild oxidative or acidic cleavage, this treatment generally preserves cellulose crystallinity more effectively than alkaline peroxide systems (Hubbell; Ragauskas, 2010).

For fiber-reinforced composites, the application of acidified-$NaClO_2$ bleaching offers a promising pathway to control lignin content without excessive fiber degradation (Yue et al., 2015). The gradual removal of lignin not only enhances fiber brightness but also increases the accessibility of hydroxyl groups on cellulose and hemicellulose (Abolore; Jaiswal; Jaiswal, 2025). At the same time, residual lignin influences the hydrophobicity of fibers, their dimensional stability, and compatibility with hydrophobic matrices, such as PLA (Kamdem Tamo et al., 2025).

2.5 MANUFACTURING METHODS FOR THERMOPLASTIC COMPOSITES

Manufacturing methods and technologies of polymer composites are intrinsically related to the final thermal and mechanical properties of the produced composites, depending on the set parameters, such as temperature, pressure, the aspect ratio of the reinforcement and its type, relative volume fraction, and in some cases, the stacking sequence, direction of stacking and layer number influence the materials' durability and run to tailor the output properties of the composites (Chohan et al., 2022). As an important preparation step to ensure good final mechanical properties, before the polymer melting manufacturing process, the polymer must undergo a dry process to remove moisture content and prevent excessive hydrolysis that causes

molecular weight drop, especially in the case of PLA, and compromise the physical properties of the polymer and composite (Lim; Auras; Rubino, 2008).

Traditional thermoplastic composites manufacturing comprehend melt-compounding process, solution mixing, injection molding, screw extrusion process, additive manufacturing, calendaring molding, hot pressing molding, and other consolidated and highly repeatable methods that are able to achieve process control and supply high-quality composites (Gupta; Kumar; Sachdeva, 2024; Rajeshkumar et al., 2021; Verma; Goh, 2019; Wu et al., 2023). Also, thermoplastic composite manufacturing processes can be divided into two steps: the first corresponds to the prepreg produced as an intermediate material, and then, the final products are formed from the prepreg material (Jeong et al., 2022).

This section briefly describes the manufacturing methods of melt-compounding as a prepreg operation, injection molding, and hot-press film production as the final production of biocomposites used in the present work.

2.5.1 MELT-COMPOUNDING PROCESS

During the melt-compounding technique, the reinforcement or filler is directly inserted into the matrix. After the polymer's softening point, the characteristic of this process is the operation in batches, which ensures a complete dispersion of the selected amount of reinforcement into the polymer, ensuring homogeneity to the formulation. The heat and shear stresses generated in the melt-compounding result in the mobility of the polymeric matrix chains and diffusion of the reinforcement or filler through the matrix (Cataño et al., 2023).

Melt-compounding is often carried out using an extruder or internal mixer, and specific mixing conditions like barrel/chamber temperature, screws/rotors speed, screws/rotors geometry, and residence time are controlled (Formela, 2023). Different extruder types have been designed to meet the diverse demands of distinct formulations and materials, e.g., single screw, intermeshing or non-intermeshing co- or counter-rotating twin-screw extruders (Albdiry, 2024; Formela, 2023). **Figure 2.8** shows two models of mixer/compounder based on the high-speed thermokinetic principle. The material particles are thoroughly mixed and rapidly heated due to impacts against the chamber wall, mixing blades, and each other. The high-speed leads to the material melting and composite production (DUSATEC, 2012). Despite melt-

compounding also being attributed to the injection molding and extrusion operations, this work is considered a pre-step for composite assemblies.

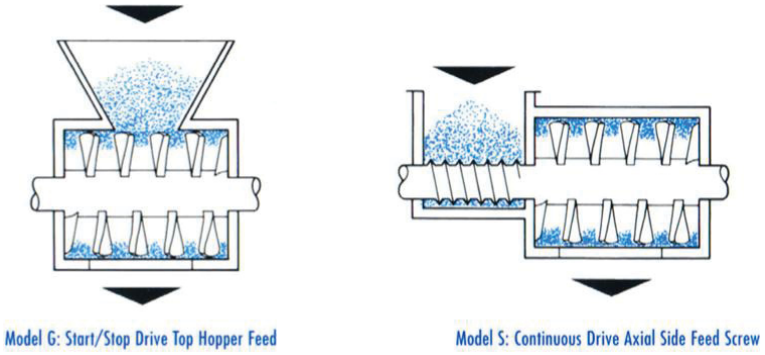

Source: Dusatec, (2012).

Figure 2. 8 Melt-compounding equipment models examples.

Composites manufacturing through melt-compounding is considered a simple, economically favorable method for industrial applications. However, it is usually used as a combined technique, since this process usually generates irregular blocs of composites that need to be milled or pelletized (Albdiry, 2024).

The processing conditions set for the melt-compounding process significantly influence the interface adhesion and compatibility of the materials, which are intrinsically related to the shear stress induced in the polymer melt. In general, the dispersion of inorganic fillers in the polymer matrix is linked to the complex internal shear stresses generated by viscous drag on the fillers along the melt-compounding process. Furthermore, high mechanical shearing during melt processing compromises the natural fibers' structural integrity, and the fibrillated fiber suffers shortening (Albdiry, 2024; Tanahashi, 2010).

2.5.2 INJECTION MOLDING

Injection molding is an essential polymer-processing technique for producing molded parts of polymeric matrices in a cyclic process. Thermoplastic injection molding is driven by important independent process parameters, such as mold and melting temperature, injection and packing pressure, and packing and cooling time. These parameters affect the shrinkage (change in the material size) and deformation of the final product, as well as mechanical performance, dimensional conformity, and appearance (Fernandes et al., 2018; Jeong et al., 2022). The

quality of the final product can be enhanced by optimizing some of these specific parameters and production conditions (Khosravani; Nasiri, 2020).

The manufacturing process of polymeric materials through injection molding holds two basic units, the injection, and the clamping units, as described in **Figure 2.9**. In the injection unit, neat polymers, composites prepreg, or even a mixture of reinforcement particles and polymer pellets are first fed into the hopper (Fernandes et al., 2018). In the filling step, the set injection volume is achieved when the molten and plasticized material in front of the first zone of the screw is pushed back against an adjustable pressure within the hydraulic system, ensuring the required volume to fill the injection unit (Liu, 2012).

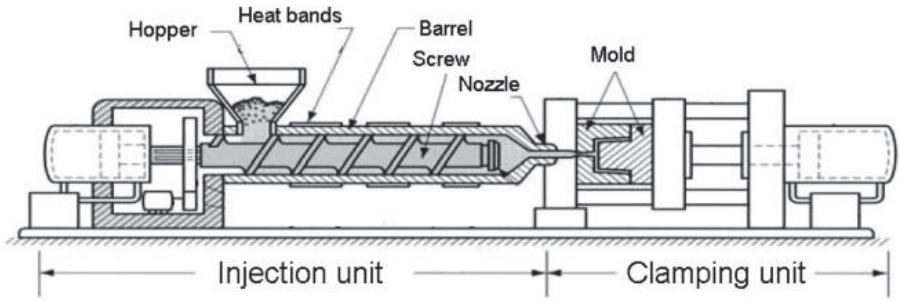

Source: Fernandes et al., (2018).

Figure 2. 9 Injection-molding machine units.

The processing material undergoes through the injection barrel by three functional rotating screws, in which the first zone is responsible for materials feeding, the second for the material transition, and the last corresponds to the metering zone (Greene, 2014). In addition, the screw reciprocates and acts as a battering ram during the filling step, pushing the material along the heated barrel until it reaches the nozzle (Chohan et al., 2022).

In the clamping unit, molten polymer is injected under high pressure into the mold with the cooling system. During the packing phase, the high pressure to fill the mold cavity is essential to prevent shrinkage along with material solidification. The injection cycle usually ranges from 10 to 100 seconds and is controlled by the cooling time of the material to turn rigid enough to be ejected, usually set below the material's glass transition temperature. Simultaneously, in the plasticating stage, the remaining material melts for the next cycle (Fernandes et al., 2018; Liu, 2012).

For neat PLA and natural fiber-reinforced composites, the melt temperature is usually set between 190 and 200 °C, regardless of the type and amount of reinforcement, as described in **Table 2.7**. However, the injection pressure is a determining factor for fiber-reinforced

composites, regardless of the injection mold machine capacity, as well as the injection volume. In general, to ensure good materials processability, during the injection molding, the temperature is increased in the three zones of the screw, the lowest at the feed section, and the highest in the metering zone and the nozzle. The hold pressure improves the stability of the polymer and minimizes warpage (change in the material shape), also enabling the material to keep its dimensional control while the material is cooled (Liu, 2012).

Table 2. 6 Injection parameters applied for different PLA fiber composites.

Injection parameter's	Mofokeng et al., (2012)	Zandi et al., (2020)	Siva et al., (2021)
	PLA/ short sisal fiber	Commercial PLA/wood	PLA/hemp fiber
Injection pressure	600, 700, 740 bar	35–65 bar	92 bar
Screw speed	-	-	300 rpm
Holding pressure	600 bar	35 bar	3 bar
Holding time	20 s	30 s	2 s
Cooling time	30 s	10 s	-
Back pressure	30 bar	-	-
Melt temperature	190 °C	200 °C	190 °C
Mold temperature	20 °C	-	-

Source: The author (2024).

2.5.3 HOT-PRESS FILM PRODUCTION

Hot-pressing is a widely employed method for producing polymeric films and composites, offering a relatively simple, solvent-free, and scalable route to fabricate materials with controlled thickness and morphology (Bajpai; Singh; Madaan, 2014). In this process, polymer powders or preformed sheets are subjected to elevated temperature and pressure between heated plates, which promotes chain mobility, densification, and interfacial adhesion (Wei et al., 2022). Compared to solution casting or extrusion, hot-pressing minimizes the use of solvents, reduces drying times, and enables the production of films with uniform density and good mechanical integrity (Campbell, 2004).

Similar to the clamping unit of an injection molding machine, in which the molten polymer is compressed into a mold, in hot-pressing production of films, the molten polymer is pressed between two flat surfaces, as represented in **Figure 2.10**. In the context of polymeric films, hot-pressing has been applied to materials such as PE, PP, as well as blends and copolymers (Qiao et al., 2023). In addition to conventional thermoplastics, hot-pressing has

been extended to biodegradable and bio-based polymers, such as PLA, polyhydroxyalkanoates (PHAs), and starch-based composite systems (Papadopoulou et al., 2019; Rubio-López et al., 2015; Surendren et al., 2022). The method allows for control over crystalline and molecular orientation by adjusting pressing parameters such as temperature, pressure, and cooling rate (Edebali, 2021). Varying the pressing temperature near or above the polymer's melting point can tailor interfacial bonding and reduce void content. These processing–structure–property relationships are essential in optimizing films for packaging, biomedical, or electronic applications (Li et al., 2024).

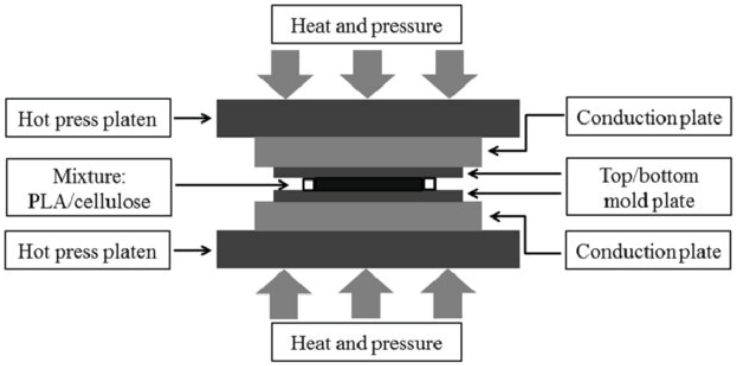

Source: Penjumras et al. (2016).

Figure 2. 10 Schematic representation of the hot-pressing machine.

In composites, the application of pressure during processing enhances the dispersion of fillers and promotes intimate contact between the polymer matrix and reinforcement, which is critical for mechanical performance (Azlin et al., 2020). As research increasingly focuses on sustainable polymeric materials, hot-press film production continues to gain attention as a scalable, eco-friendly, and effective fabrication method (Wei et al., 2022).

2.6 SUMMARY

According to the previous literature review reported in this section, PLA biocomposites reinforced with lignocellulosic fibers demonstrate significant enhancements in mechanical performance, thermal stability, and weight reduction, making them promising materials for high-performance applications in the automotive, aerospace, and packaging sectors. The incorporation of lignocellulosic fibers not only improves the tensile strength and durability of PLA but also preserves the material's environmentally sustainable character.

In addition to fiber reinforcement, the lignin fraction contributes to the overall performance of PLA-based composites. Due to its rigidity, antioxidant capacity, and ultraviolet (UV) shielding properties, lignin can enhance composite stiffness, thermal resistance, and long-term stability. However, the heterogeneous and inherently hydrophobic nature of lignin, as well as the hydrophilicity of lignocellulosic fibers, can hinder interfacial compatibility with the PLA matrix. Consequently, strategies to improve interfacial adhesion are essential for ensuring efficient stress transfer and achieving superior mechanical properties.

Among the compatibilization approaches, silane coupling agents and bleaching treatments are widely recognized in the literature for their effectiveness in modifying natural fibers and isolated lignocellulosic components. Bleaching processes typically employed to reduce lignin content and remove extractives are reported to increase fiber surface cleanliness and reactivity, thereby improving the efficiency of subsequent silanization. Silane coupling agents contain both organic functional groups and alkoxy groups within the same molecule. The alkoxy groups hydrolyze to form silanol groups capable of bonding with hydroxyl-rich substrates such as unmodified natural fibers, bleached fibers, and isolated lignin, while the organic functional groups interact or react with the polymer matrix. This dual functionality promotes improved interfacial adhesion and more efficient stress transfer in PLA-based composites.

Although lignocellulosic fibers have been widely investigated as reinforcements for PLA, most studies have focused on cellulose-rich or chemically purified fibers, often treating lignin as an undesirable component. The potential of lignin as an active interfacial phase remains largely unexplored, particularly in systems where lignin is preserved in its native state. Moreover, the interaction between coupling agents and lignin-rich fiber surfaces has received limited attention, despite the presence of reactive hydroxyl groups that could promote interfacial bonding. In addition, stone groundwood fibers, characterized by high fibrillation and preserved lignin content, remain underutilized in polymer composites.

The present work addresses these gaps by investigating a compatibilization strategy based on the interaction between a coupling agent and the lignin fraction of untreated and partially bleached SGW fibers, as well as examining how structural differences between softwood and hardwood lignin influence coupling-agent interactions. This approach provides insight into a sustainable and efficient route for improving PLA-based composites without extensive fiber modification.

CHAPTER 3 – SILYLATION OF LIGNOCELLULOSIC FIBER: EFFECTS ON THE STRUCTURE AND INTERFACE OF PLA COMPOSITES

Part of this work has been published in the journal Industrial Crops and Products as:
GIULIA HERBST, ROBERTO J. AGUADO, QUIM TARRÉS, MARCOS L. CORAZZA, LUIZ P. RAMOS, PERE MUTJÉ, MARC DELGADO-AGUILAR. Silane-modified high-yield lignocellulosic fibers as reinforcement of polylactic acid: Enhancement of interfacial adhesion for high-performance biocomposites. ***Industrial Crops and Products****, Volume 218, 2024.*
https://doi.org/10.1016/j.indcrop.2024.119027.

Note: All experimental work was developed in the laboratories of the LEPAMAP research group and facilities of the Universitat de Girona, Spain.

3.1 INTRODUCTION

In the last years, the need for developing sustainable and high-performance materials has been highlighted by many actors in society, including policymakers, industrial representatives, and the scientific community (Bhong et al., 2023). These materials are conceived as enablers to promote the transition from a fossil-based to a bio-based economy and, in addition, to leave behind the linear schemes to fully circular value chains (Agarwal et al., 2020; Kılıç et al., 2024; Shanmugam et al., 2021; Uppal et al., 2022). The sustainability of materials can be approached from different perspectives, including their origin, use, and end-of-life management strategies. On the one hand, the use of renewable resources for the development of value-added materials alleviates the pressure over limited resources, such as the case of petroleum (Gurunathan; Mohanty; Nayak, 2015; Yatigala; Bajwa; Bajwa, 2018). However, 90.2 % of the global plastic production in 2021 (390.7 million tons) was fossil-based, while post-consumer recycled plastics accounted for 8.3 %, leaving a residual 1.5 % for bio-based plastics (Plastics Europe, 2022). On the other hand, the end-of-life can be approached by means of recycling strategies or through natural breakdown into simpler compounds (e.g. water, carbon dioxide, and biomass), known as biodegradation or composting, avoiding landfilling and/or incineration (Dammak et al., 2020; Sikorska et al., 2021). According to recent data in the EU27+3, the evolution of post-consumer plastics treatment exhibits a favorable scenario,

having increased recycling by 117 % from 2006 to 2020. Nonetheless, landfilling stills represent around 23 %, and incineration, 42 % (Plastics Europe, 2022). In the use phase, there is an increasing need for lighter materials able to meet the technical requirements of conventional commodity materials that, for instance, can have a positive effect on the associated environmental impact of its use (Delogu et al., 2017).

Composite materials, conceptually, possess the ability to meet these requirements, providing excellent properties (e.g. mechanical, functional, lightweight) with reduced environmental impact (La Mantia; Morreale, 2011). However, the imperative to confront technical challenges has propelled the composite materials industry towards the development of composites reliant on fossil resources. This emphasis often prioritizes properties and production costs yet frequently overlooks the adverse environmental consequences these materials entail throughout their processing, use and disposal (Rodríguez et al., 2018). Thermoplastic materials, such as polypropylene (PP), are often reinforced with short fibers to enhance their properties, achieving unconceivable levels with neat polymers (Mutjé et al., 2006). This is the case of short glass fibers (GFs), which significantly improve the mechanical performance of PP in presence of maleic anhydride functionalized PP (MAPP) as interfacial compatibilizer (Kossentini Kallel et al., 2018). While the environmental superiority of natural fiber (NF)-reinforced compared to GF-reinforced composites has been already demonstrated 20 years ago, the latter still predominates in current market applications (Joshi et al., 2004). The environmental advantages of NF-reinforced composites are evident, encompassing the three stages highlighted above: (i) the production of NF results in lower environmental impact compared to GF, mainly due to their lower energy demands, and the amount of polymer matrix is decreased due to the demand of higher fiber content; (ii) NF are lighter than GF, resulting in lighter composites for the same application; and (iii) even if incinerated, NF-reinforced composites result in energy and carbon credits (Li et al., 2020).

In the recent years, some bio-based and biodegradable alternatives to fossil-based polymers have appeared, such is the case of poly(lactic acid) (PLA), poly(butylene adipate terephthalate) (PBAT) and poly(hydroxy alkanoates) (PHAs) (Ali et al., 2023). Considering that the end-of-life of composite materials still presents some challenges, particularly in terms of sorting and avoiding contamination of current recycling streams, the development of fully bio-based and biodegradable composites (i.e., biocomposites) is attracting the interest of both industry and scientific communities (Chatziparaskeva et al., 2022). As in the case of PP, however, ensuring appropriate interactions between fiber and polymer becomes crucial, and

several efforts have been paid on the generation of well-bonded interfaces by means of incorporating coupling agents or modifying either the fibers or the polymer matrices. While it is true that fiber orientation, distribution, morphology, and dispersion have a significant impact on the resulting biocomposite mechanical properties, successfully generating these interactions ensures appropriate stress transfer between the biocomposite constituents, unlocking the reinforcing potential of the fibers (Birnin-Yauri et al., 2016; Granda et al., 2016).

PLA is one of the most promising and most commonly used bio-based and biodegradable polymers due to its outstanding physic and mechanical properties (Madhavan Nampoothiri; Nair; John, 2010; Pang et al., 2010; Siakeng et al., 2019). Actually, PLA constitutes a competitive alternative to fossil-based polymers, exhibiting a tensile strength that can arouse between 50 and 60 MPa (Madhavan Nampoothiri; Nair; John, 2010). One strategy to further enhance its properties is the development of NF-reinforced PLA composites. However, although successfully described in the literature, uncertainty on the most appropriate surface chemical composition of the fibers still remains. In an attempt to improve interfacial fiber and biopolymer adhesion, studies on fiber surface modification mainly focus on the increase of the surface roughness by lignin removal, creating interdiffusion, and mechanical interlocking of the cellulose fraction using fiber pretreatment processes combined with dispersion agents to induce availability hydroxyl groups, capable of bonding with the polymer matrix creating a strong and stiff component (Balla et al., 2019; Lee; Khalina; Lee, 2021). Some works have reported the suitability of partially bleached fibers to achieve a strong interfacial adhesion with PLA, while others have reported excellent results with fully bleached fibers (Delgado-Aguilar et al., 2018; Granda et al., 2016). However, in some cases, the use of dispersants is required, and the chemical treatments for removing surface lignin inexorably generate a residual stream, questioning the overall process sustainability. Thus, the use of high-yield fibers such as mechanical or thermomechanical fibers is encouraged, as the main lignocellulosic constituents are preserved and the most significant modifications are in terms of morphology (Mujtaba et al., 2023). Concretely, the direct fibrillation of wood fibers generates a significant increase on surface roughness, together with fine elements with high surface area that can improve the fiber reinforcing potential (Graupner et al., 2023). Other strategies encompass the implementation of silane-coupling between fibers and polymers, enhancing fiber hydrophobicity and promoting their dispersion and interactions with PLA (Chen et al., 2021). In previous works, silane coupling agents were efficiently condensed to the fiber surface through reactions involving hydroxyl and alkoxy groups capable of grafting both fiber and

polymer (Chen et al., 2021; Luo et al., 2016; Yang et al., 2023). Also, the presence of lignin increases the availability of hydroxyl groups that can couple with reactive silanol groups. Studies by Zhu et al. (2015), Yeo; Lee; Hwang, (2017), and Wang et al. (2020) demonstrated an increase in tensile strength and improvement in the miscibility of silane-treated lignin composites with unsaturated polyester resins and PLA.

For all the above, the present work aims at elucidating the suitability of incorporating stone groundwood fibers (SGW) from pine into PLA at different fiber contents, together with the influence of (3-glycidyloxypropyl)trimethoxysilane (GPS) as a coupling agent. A comprehensive assessment of the biocomposite properties is provided, as well as a strategy for developing fully bio-based and biodegradable biocomposites using high-yield fibers, constituting a strong alternative to commodity composites (e.g., PP/GF) for several applications.

3.2 MATERIALS AND METHODS

3.2.1 COMPOSITES RAW MATERIALS

PLA with 1.24 g/cm^3 density (Ingeo Biopolymer 4043D) was supplied by Natureworks (Minneapolis, MN, USA) and used as a biodegradable thermoplastic matrix. A commercial grade of stone groundwood pine pulp (SGW) was kindly provided by Zubialde S.A. (Aizarnazabal, Spain). The pulp was supplied in the form of dried blocks, with a moisture content below 10 % by weight. Fibers were modified by the incorporation of modified amounts of (3-glycidyloxypropyl)trimethoxysilane (GPS), also known as silane coupling agent KH560, acquired at Merck (Barcelona, Spain). **Figure 3.1** shows PLA and pine SGW raw materials applied in this research.

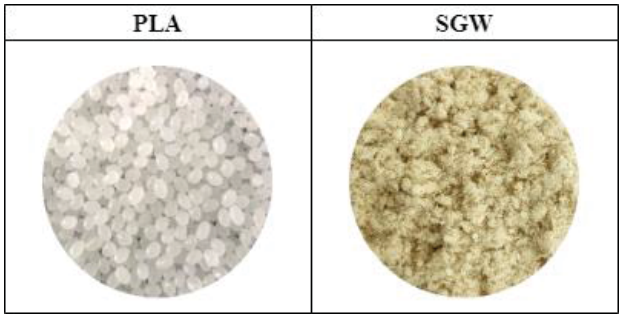

Figure 3. 1 Biocomposites raw materials.

3.2.2 SGW CHEMICAL COMPOSITION DETERMINATION

Neat SGW pulp was chemically characterized according to the Technical Association of the Pulp and Paper Industry (TAPPI) standard methodologies. In order to prepare the samples for characterization, the pulp was air-dried for 24 h at 25 °C as described in T257. The dried SGW was then milled and sieved (40 mesh). Extractives were determined in a Soxhlet apparatus using an ethanol-toluene mixture as solvent (TAPPI T204). The solvent-free sample was then used for lignin determination according to TAPPI standard T222, quantifying acid-insoluble lignin. The cellulose content was determined by high-performance anion exchange chromatography (HPAEC), while the hemicellulose was estimated by subtracting from 100%.

3.2.2.1 Extractives determination

The extractive content determination of SGW pulp was adapted from the TAPPI standard procedure, T2014 (Buchanan, 2012). Approximately 5 g of dry samples for which the experiment was placed in extraction thimbles on the Soxhlet apparatus. The extraction was performed with approximately 150 mL of a mixture of ethanol-benzene 1:2 v/v for 5 h. The experiments were conducted in duplicate, and the extract was dried at 105 °C in an oven until constant weight. The extractives content (%) in ethanol-benzene was determined according to Eq. 3.1, in which $E_{extract}$ refers to the dried weight of extractables and E_{sample} to the dried weight of the original sample.

$$Extractives\ (\%) = \frac{E_{extract}}{E_{sample}}\ x\ 100 \qquad \text{Eq. 3.1}$$

3.2.2.2 Acid-insoluble lignin content

The acid-insoluble lignin content was quantified according to TAPPI standard T222 (Tappi, 2011), with slight modifications. The free-extract samples (approximately 2 dry g) were submitted to acid hydrolysis with 40 mL of 72 % sulfuric acid solution. The experiment was carried out for 2 h under 10 - 20 °C with frequent manual agitation to ensure complete sample dissolution. The solution was then rinsed with approximately 400 mL of distilled water and

diluted to a 3% concentration of sulfuric acid by the addition of distilled water to a total volume of 1540 mL and boiled for 4 h, with additional water frequently added to keep the initial volume. With the end of reaction time and total lignin precipitation, the solution was filtered by filtering crucibles, with the addition of hot water to wash the cake and remove the remaining acid. The acid-insoluble lignin was then dried at 105 °C until constant weight. The acid-insoluble lignin (L_I) content (%) obtained gravimetrically was determined according to Eq. 3.2, in which W_{lignin} refers to the dried weight of lignin and W_{sample} to the dried weight of the original sample.

$$L_I\,(\%) = \frac{W_{lignin}}{W_{sample}}\ x\ 100 \qquad \text{Eq. 3.2}$$

3.2.2.3 Cellulose content

Cellulose content was determined by high-performance anion exchange chromatography (HPAEC), as reported by Tarrés et al., (2017) and previously by Hausser; Marinkovic; Estrine, (2011). For sample preparation, approximately 200 mg (dry weight) of extract-free SGW samples were hydrolyzed in for 60 min in 3 mL of 72% sulfuric acid with constant agitation. After hydrolysis, the samples were diluted by adding 84 mL of deionized water, placed in an autoclave for 60 min at 125 °C, then filtered under vacuum through a 0.22 μm pore-size nylon membrane, and washed twice with deionized water. The prepared samples are subject to high-performance anion exchange chromatography (HPAEC), coupled with a differential refractometer (Waters 410) equipped with a system controller (Waters 600E), and an adsorption column ICSep ICE-ORH-801. Cellulose was quantified using glucose content by comparing the elution band of the sample with the standard solution of glucose.

3.2.3 FIBER SURFACE TREATMENT AND CHARACTERIZATION

3.2.3.1 Fiber silylation

SGW surface treatment was carried out using the silane coupling agent (3-glycidyloxypropyl)trimethoxysilane (GPS). First, SWG pulp was dispersed in water using a baffled pilot-scale pulper at a consistency of 5 wt% at room temperature and 1100 rpm for 30

min, enabling the disintegration of the starting blocks, leading to fiber individualization and pulp dispersion in water. The selected rotor configuration was centered and helicoidal. After fiber dispersion, the pulper was discharged, and the pulp was further diluted with water until reaching a pulp consistency of 3 wt% under mechanical stirring.

The silanization of the SGW fiber was performed by the dropwise addition of GPS at different GPS-to-fiber ratios, ranging from 0 to 10 %, into the SGW pulp dispersed in water (pulp consistency of 3 wt%) under gentle stirring for 30 min. The fibers were then filtered over a 200-mesh nylon cloth and air-dried for 48 h. The samples were named according to the fiber and GPS content (e.g., the sample containing 5 % of GPS was labeled as SGW5).

3.2.3.2 Morphological features of silane-treated and untreated SGW

Fiber morphology, including average fiber diameter and length, fines content (fibers shorter than 75 μm), and size distribution of silane-treated and untreated SGW, was conducted using a MorFi Compact fiber analyzer (TechPap SAS, serial number 1024, France), according to ISO 16065-2:2007, for the determination of fiber length by automated optical analysis using unpolarized light. The equipment consists of a measuring cell with a CCD video camera (connected to a PC), a hydraulic system (mainly composed of a pump, tank, and electro-valves), and a carousel incorporated for analyzing 5 consecutive samples and 1 washing container. For each analysis, 1 g of dry sample was suspended in 1 L of distilled water and fractioned into 4 parts of 250 mL and placed into 4 containers with the addition of distilled water to a total volume of 1 L. Two containers were used for washing the cell between each sample analyzed. The aqueous fibrous suspension flows through the measurement cell, and the optical resolution was set at 10 μm, and the working resolution reached even 4 μm. The mean fiber arithmetic length, mean length-weight fiber length, the percentage of fine content in length, and the fiber distribution in arithmetic length were measured with the StatMorf software (v7.10.19).

3.2.3.3 Fourier transform infrared-attenuated total reflectance spectroscopy (FTIR-ATR)

FTIR-ATR spectroscopy analysis was performed to assess the effect of the coupling agent on the treated and untreated SGW chemical composition using a compact spectrometer

Alpha II (Bruker Corporation, Massachusetts, United States). Spectra were acquired from a platinum ATR accessory at a resolution of 4 cm^{-1} within the 400 to 4000 cm^{-1} wavenumber range.

3.2.4 COMPOUNDING OF PLA/SGW BIOCOMPOSITES

3.2.4.1 Biocomposites melt-compounding

Previously dried SGW samples, both unmodified and GPS-modified, were incorporated at 20 and 30 wt% into the PLA matrix using a high-speed kinetic mixer (Gelimat, Draiswerke Inc, NJ, USA). The SGW fibers were first incorporated into the mixing chamber at a low rotational speed (315 rpm), and then, the PLA fraction was also incorporated. The rotational speed was gradually increased up to 3,000 rpm, reaching a temperature of 195 °C, enabling the melting of the polymeric matrix and fiber wetting and dispersion. Each biocomposite formulation was discharged, separated into small pieces, and milled using a knife mill (SM 100, Retsch GmbH, Haan, Germany) equipped with a 4 mm sieve at the bottom. The samples were stored in an oven at 80 °C to avoid moisture absorption.

3.2.4.2 Injection molding of the biocomposites

The melt-compounding biocomposites pellets, PLA20SGW and PLA30SGW (0, 3, 5, 7, and 10 % of GPS) were used as raw materials in the production of standard specimens for tensile, flexural, and impact tests obtained using an injection molding machine Allrounder (model 320C 500-170, series 205029, Arburg GmbH + Co KG, Lossburg, Germany), with a screw diameter of 25 mm. **Table 3.1** presents the injection molding machine technical properties and the selected parameters for the PLA/SGW biocomposites injection.

Table 3. 1 Technical and selected properties of the injection mold machine.

Properties	Machine capacity	Selected values	Units
Hopper capacity	5	1	kg
Barrel temperature	-	190/200/210/215/220	°C
Injection pressure (max)	2000	1200	bar
Hold pressure	-	800	bar
Motor speed (max)	1800	-	rpm
Screw speed (max)	44	25	m/min
Clamping force (max)	70	-	tons
Mold temperature	-	80	°C
Cooling time	-	15	s

From the feeding zone to the nozzle, the PLA/SGW barrel injection temperature was selected as 190, 200, 210, 215, and 220 °C, as recommended for the PLA fabricants in technical specifications. Approximately 1 kg of biocomposite pellets were filled in the injection molding machine to inject around 25 specimens of tensile, flexural, and impact. The tensile specimen's dimensions with dog-bone shape were 165 mm full length (115 mm distance between grips), 20 mm wide and 3.3 mm thick, according to ASTM D638 (type I, narrow section 57 mm × 13 mm), while the flexural were 127 (51) mm x 12.7 mm x 3.2 mm according with ASTM D790, and impact specimens with 12.7 mm wide x 3.2 mm thick ASTM D4812. **Figure 3.2** shows samples of melt-compound PLA/SGW biocomposites pellets and injected tensile and flexural specimens.

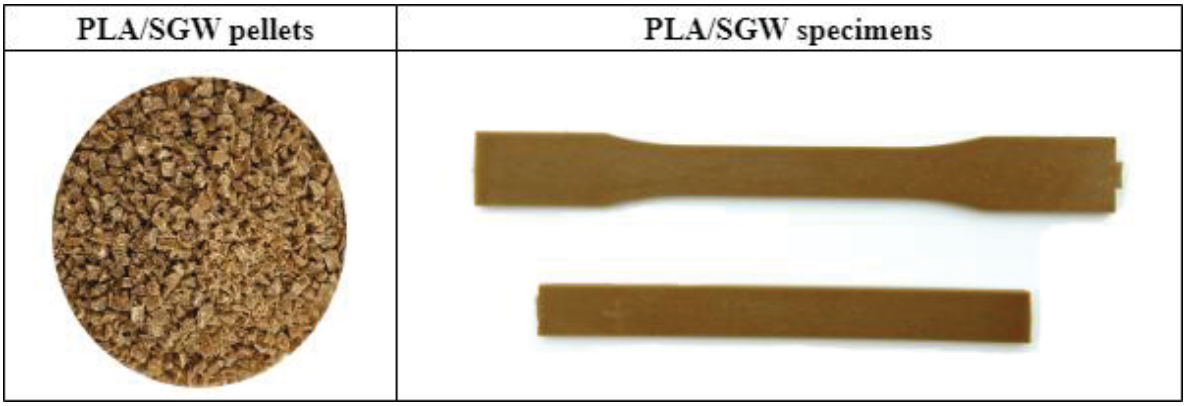

Figure 3. 2 Biocomposite pellets and specimens.

3.2.5 BIOCOMPOSITES CHARACTERIZATION

3.2.5.1 Melt flow index (MFI)

Melt Flow Index (MFI) was determined in a CEAST testing equipment (7082,000, series 17959, Pianezza, Italy), according to ISO 1133 standard. The extrusion rate was determined as the mass extruded over a specified time at 210 °C and a load of 2.16 kg, as suggested by the PLA supplier. Approximately 6 g of each material was placed into the die, and the MFI was expressed in g/10 min, representing the amount of material that flows through the equipment in 10 min.

3.2.5.2 Density

The density of the biocomposites (ρ^C) was determined using the liquid pycnometer method, as specified in the ISO 1183-1 standard. To perform the analysis, approximately 3 g of ground tensile specimens were added to a 50 cm^3 glass pycnometer and filled with distilled water at room temperature (21 °C) as immersion liquid. The composite density was calculated by Eq. 3.3.

$$\rho^C = \frac{W^C}{V - W_{water}\rho_{water}} \quad \text{Eq. 3.3}$$

in which V is the total volume of the pycnometer and ρ_{water} is the density of the water. The weight of the composite and water were represented by w_C and w_{water}, respectively.

3.2.5.3 Melt rheology

The rheology measurements were conducted according to the ASTM D4440-15 standard on a modular rheometer (model MCR 302e, Anton Paar GmbH, Graz, Austria) in oscillatory mode. A parallel plate geometry arrangement with a gap of 1 mm was employed, and the measurements were taken in the PLA melt state at 190 °C. The frequency range used was set between 0.1 and 100 Hz. The linear viscoelastic region was determined using an amplitude sweep deformation of 5 %, with controlled shear deformation. The storage and loss modulus and the complex viscosity of the composites were measured by the TruStrain™ software.

3.2.5.4 Mechanical properties

Neat PLA and PLA/SGW (0, 3, 5, 7, and 10 wt% GPS) biocomposites specimens were conditioned on a climatic chamber (Dycometal, Barcelona, Spain) according to ISO D618 standard for 48 h at 23 °C and 50 % relative humidity. The tensile and flexural strength tests were performed on a universal testing machine (DTC-10, IDM Test S.L, San Sebastian, Spain) equipped with a 5 kN load cell and an extensometer. The tensile strength test was carried out according to ASTM D638 standard at 2 mm/min. For Young's modulus determination, an extensometer was coupled to the specimens, and the test was performed until 0.25% strain on

the stress-strain plot according to the ASTM D638 standard. The flexural strength tests were carried out according to ASTM D790. The impact test was performed on a Resil 5,5 hammer (Ceast, Pianezza, Italy) test machine as described on the ASTM D6110 (Charpy impact), and ASTM D256 (Izod impact) standards, at unnotched specimens. Both mechanical properties were expressed as the average of 5 tested specimens of each sample.

3.2.5.4.1 Statistical analysis of mechanical properties

Statistical analysis of variance (ANOVA) and pairwise multiple comparisons with Tukey's HSD (honestly significant difference) test ($p < 0.05$) were carried out using the Statistica® 10 software (Statsoft Inc., USA) at a 95% level of confidence to identify the effect of fiber load and GPS silane modification degree and its significance in the mechanical properties of PLA/SGW biocomposites.

3.2.5.5 Electron microscopy

The surface of the fractured tensile samples was analyzed by field emission scanning electron microscopy (FE-SEM, Hitachi S-4100, Japan). The samples were previously fixed on a sample holder using conductive carbon tape and coated with a carbon layer using a turbo evaporator device (Emitech K950, Germany) to avoid surface charging during the analysis. Images were taken using the Quartz PCI software at accelerating voltages of 5.0 kV and magnification of 600x, with a secondary electron detector (SED).

3.2.5.6 Thermal analysis

Thermogravimetric analysis (TGA) was performed to assess the effect of incorporating the SGW fibers on the thermal stability of the PLA matrix, using a thermogravimetric analyzer (Mettler-Toledo, LLC, USA). Analyses were performed from 30 to 600 °C at a heating rate of 10 °C min^{-1} under an inert nitrogen atmosphere. The thermal behaviors of neat PLA and PLA/SGW biocomposites were analyzed by differential scanning calorimetry (DSC) to evaluate the physical properties related to the material transition measurement (DSC822e,

Mettler-Toledo, LLC, USA). Samples were analyzed at a heating/cooling rate of 10 °C min^{-1} from 30 to 210 °C under an inert N_2 atmosphere. The degree of crystallinity, *Xc (%)*, was calculated with the first heating scans (given that the thermal history involved curing) as a function of melt and cold-crystallization enthalpy (ΔH_m and ΔH_{CC}, respectively), the PLA theoretical melting enthalpy ($\Delta H°_m$), as shown in Eq.3.4.

$$Xc = \frac{(100\ x\ (\Delta H_m - \Delta H_{CC}))}{(\Delta H°_m x PLA_{fraction})} \quad \text{Eq. 3.4}$$

considering $\Delta H°_m$ as 93.6 J/g for 100 % crystalline PLA (Hakim et al., 2017).

3.2.6 FIBER CHARACTERIZATION AFTER BIOCOMPOSITES COMPOUNDING

3.2.6.1 Morphological features of silane-treated and untreated SGW after injection

To evaluate the extension of fiber morphological degradation and shortening after the injection processes, the fibers were extracted from the composites, and their morphological characteristics were measured, as described in item *3.2.3.2 Morphological features of silane-treated and untreated SGW*. Around 5g of PLA30SGW and PLA30SGW5 samples were solubilized in 50 mL chloroform-DMF (dimethyl formamide) at a 4:1 v/v solution under agitation for 24 h. The extracted fibers were filtered using a vacuum pump, washed with acetone, and with distilled water. The morphological analysis was performed after the samples were oven-dried at 105 °C for 24 h.

3.2.6.2 Fiber density and volume in the biocomposites

The fiber density in the biocomposites (ρ^F) was estimated according to the biocomposites' density using the rule of mixture applied by Equation 3.5 using the data obtained by Equation 3.3.

$$\rho^C = \frac{W^F \rho^C \rho^{PLA}}{W^C \rho^{PLA} - W^{PLA} \rho^C} \quad \text{Eq. 3.5}$$

in which ρ^{PLA} is the density of the matrix, and the weight of the fiber and the PLA matrix were described as w^F and w^{PLA}, respectively.

Further, fiber volume was estimated in function of ρ^F, using Equation 3.5, considering the fiber fraction as x^F.

$$V^F = \left(1 + \frac{\rho^F\,(1-x^F)}{\rho^{PLA}x^F}\right)^{-1} \qquad \text{Eq. 3.6}$$

3.2.7 MICROMECHANICAL MODELLING

The micromechanics of the developed biocomposites was approached by combining the modified rule of mixtures (mRoM), the Hirsch model, and the Tresca and Von Misses criteria for the interfacial shear stress (IFSS) calculation, together with the determination of the critical length (L_c^F). The input data consisted of both stress-strain curves and average data from the matrix and biocomposite tensile tests, as well as the morphological features (average length, diameter, and fines content in length) of the extracted fibers.

The matrix contribution to the biocomposite tensile strength (σ_t^m*) was determined by calculating the tensile strength of the matrix at the elongation at the break of each biocomposite, previously fitting the stress-strain curve of the PLA matrix to a fifth-order polynomial equation (Eq. 3.7). Then, the mRoM was used to determine the value of the fiber tensile strength factor (Eq. 3.8, where V^F stands for the volume fraction of the fiber within the biocomposite), resulting from the product between the coupling factor (fc) and the intrinsic tensile strength of the SGW fibers (σ_t^F) according to Eq. 3.9.

$$\sigma_t^{PLA} = -0.0574\varepsilon_t^5 - 0.6947\varepsilon_t^4 + 5.7427\varepsilon_t^3 - 13.6\varepsilon_t^2 + 29.836\varepsilon_t + 0.8673 \qquad \text{Eq. 3.7}$$

$$\sigma_t^c = FTSF \cdot V^F + (1 - V^F)\sigma_t^{m*} \qquad \text{Eq. 3.8}$$

$$FTSF = f_c \cdot \sigma_t^F \qquad \text{Eq. 3.9}$$

In parallel, the intrinsic tensile modulus of the fiber (E_t^F) was calculated using the Hirsch model (Eq. 3.10).

$$E_t^c = \beta[E_t^F \cdot V^F + E_t^m(1 - V^F)] + (1 - \beta)\frac{E_t^F \cdot E_t^m}{E_t^m \cdot V^F + E_t^F(1 - V^F)} \quad \text{Eq. 3.10}$$

where E_t^c and E_t^m are the elastic modulus of the biocomposite and the matrix, respectively, both obtained during the tensile test, and β is the stress transfer factor (Serra-Parareda et al., 2021). A value of 0.4 was assigned to this factor, as previously reported. The average E_t^F was then calculated and, considering an elastic behavior of the developed biocomposites, the average σ_t^F was obtained.

The IFSS was estimated through the Tresca and Von Misses criteria, τ_T and τ_{VM}, according to Eqs. 3.11 and 3.12, respectively.

$$\tau_T = \frac{\sigma_t^c}{2} \quad \text{Eq. 3.11}$$

$$\tau_{VM} = \frac{\sigma_t^c}{\sqrt{3}} \quad \text{Eq. 3.12}$$

Critical length (L_c^F) was calculated according to Eq. 3.13, considering that most of the biocomposite fibers corresponded to subcritical fibers, the interface factor χ_2 was calculated according to Eq. 3.14, and finally, the fiber orientation factor (χ_1) was determined according to Eq. 3.15,

$$L_c^F = \frac{\sigma_t^F \cdot d^F}{2 \cdot \tau} \quad \text{Eq. 3.13}$$

$$\chi_2 = \frac{\tau \cdot L^F}{\sigma_t^F \cdot d^F} \quad \text{Eq. 3.14}$$

$$f_c = \chi_1 \cdot \chi_2 \quad \text{Eq. 3.15}$$

where d^F and L^F correspond to the fiber diameter and length, both expressed in μm, respectively.

3.3 RESULTS AND DISCUSSION

3.3.1 STONE GROUNDWOOD FIBER CHARACTERIZATION

The chemical composition and the main morphological features of the SGW pulp are shown in **Table 3.2**. This includes the cellulose, hemicellulose, Klason lignin, and extractives contents that comprehend the chemical composition, and the fiber length weighted in length (L^F), average fiber diameter (d^F), and fines content (f) regarding morphology. SGW pulp exhibited a chemical composition similar to that of pine wood, containing 42 to 52 % cellulose, 24 – 28 % hemicelluloses, 22 – 28 % lignin, and 2 – 3 % extractives (Ferraz et al., 2000; Maaoui et al., 2023; Reyes et al., 2013; Sable et al., 2012). These similarities are expected, considering that SGW is a mechanical pulp produced by mechanical fibrillation using cold water as a lubricant, which results in high production yields, slight chemical modifications, and minimized side-stream generation (López et al., 2012). Chemical composition imparts remarkable effects on fiber dispersion and their interaction with the polymer matrix (Yang; Ching; Chuah, 2019). However, the chemical interface between PLA and NF has not been successfully addressed in the literature.

Table 3. 2 Chemical composition and morphological features of SGW.

Chemical composition (%)	
Cellulose	42.3 ± 1.6
Hemicelluloses	27.1 ± 2.1
Klason lignin	29.6 ± 1.8
Extractives	1.9 ± 0.2
Fiber morphology (µm)	
Length	497 ± 31
Diameter	25.9 ± 1.8
Fines	40.5 ± 2.5

The hydrophobic character of PLA should hinder its interactions with hydrophilic natural fibers. Previous studies revealed that the presence of lignin could benefit these interactions, mainly due to its hydrophobic character. Exemplarily, the presence of moderate amounts of lignin in jute fibers enhanced their interfacial adhesion with PLA, boosting tensile strength by 46 % with a 30 wt% addition of partially bleached jute fibers (Delgado-Aguilar et al., 2018). In a previous study, the surface properties of SGW and bleached kraft pine pulp were used to demonstrate that cellulose has a higher affinity for PLA than lignin (Granda et al., 2016). In this sense and aligned with previous works on PLA/lignin composites, the use of GPS should benefit from the improved dispersion provided by lignin, enhancing interface properties by silanization of the fiber surface (Tan et al., 2023; Wang et al., 2020; Zhu et al., 2015).

In addition to chemical composition, fiber morphology also has a pivotal role in the reinforcing potential of fiber-reinforced composites, particularly the length-to-diameter ratio,

known as the aspect or slenderness ratio. As revealed in Table 3.2, SGW exhibited a fiber length and diameter of 497 and 25.9 µm, respectively, leading to an aspect ratio of 19.2. However, during compounding and injection molding, fibers experience shortening due to the shear stress among fibers, with the polymer matrix, and with the cavity of the processing equipment (Wang et al., 2011). This generates a disentanglement of the fiber bundles, exposing more surfaces to be wetted by the matrix and increasing the susceptibility to fiber-matrix interactions (Hasan; Rabbi; Maruf Billah, 2022). **Figure 3.3** compares the fiber length distribution of the unmodified SGW before and after compounding (extracted from the biocomposites at 20, and 30 wt% fiber content) and SGW5.

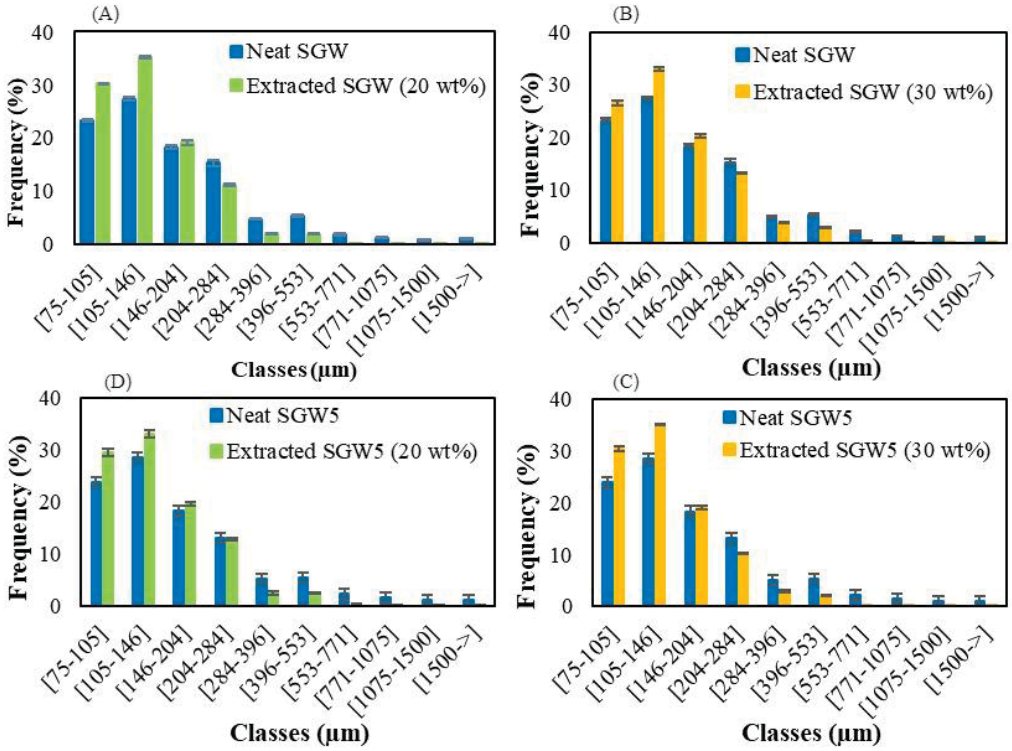

Figure 3. 3 Fiber length distribution before and after injection of untreated 20 wt% SGW (A), untreated 30 wt% SGW (B), 20 wt% SGW5 (C), and 30 wt% SGW5(D).

Figure 3.3 reveals that, as mentioned above, the injection molding generates a significant fiber shortening, shifting the length distribution to the left. In comparative terms, the average fiber length of the untreated SGW decreased from 497 to 205 µm, representing a shortening of 59 %. However, fiber diameter did not experience significant changes. In the case of the SGW5, fiber shortening was of the same magnitude, starting at 493 µm and ending at 192 µm after the injection process, while in the case of the untreated SGW, fiber diameter remained constant.

A significant increase in the fine content was observed in both cases, starting at 43 % approximately for both fibers and ending at around 60 %. This high increase indicates that the compounding and the injection process highly fibrillates the fibers and that some of the fiber particles are not considered in the fiber length distribution from **Figure 3.3**. In addition, fine fibers are expected to exhibit lower diameters. Hence, the MorFi equipment could not detect the effect of these high surface area fibrils on the evolution of biocomposite strength.

The chemical composition and morphology of lignocellulosic fibers play a pivotal role in composite formulation, directly related to the performance of its thermomechanical properties (Granda et al., 2016). However, to enhance the compatibility between the PLA polymer matrix, formed by weakly polar ester bonds, and the hydroxyl groups of the lignocellulose structure, the SGW pulp required partial surface modification. As previously discussed, Granda et al. (2016) explored the use of diethylene glycol dimethyl ether as a dispersant agent for bleached kraft softwood fibers, to avoid fiber agglomeration during compounding. In further studies, Delgado-Aguilar et al., (2018) observed that the mechanical performance of PLA/jute fiber composites increased in the presence of an optimum lignin content after fiber bleaching.

The preservation of the lignocellulosic constituents should be set as a priority, from a resource-efficiency perspective. Lignin concentration is higher at the outer layers of the lignocellulosic fibers and most of the interactions with PLA, in case of using high-lignin fibers as reinforcement, would take place with lignin rather than with cellulose. Studies by Chen et al. (2021), Wang et al. (2020), and Zhu et al. (2015) investigated the application of silane coupling agents for constructing compatible interfaces between PLA/fiber and PLA/lignin and improving its thermo-mechanical properties, since silane reactive groups bind to the carboxyl-terminal groups of PLA and the lignocellulose hydroxyl groups, as represented in **Figure 3.4** (A), resulting in improvements of around 40 and 43 % for bending and tensile strengths, respectively.

Modifications on the SGW chemical structure after 3, 5, 7, and 10 wt% GPS treatment were assessed by FT-IR spectroscopy (**Figure 3.4** B). The main representative bands related to cellulose, hemicelluloses, and lignin were centered at 3313 cm^{-1} for the O−H intra- and intermolecular stretching hydroxyl groups, at 2890 cm^{-1} for the C−H stretching methyl and methylene groups, at 1606 cm^{-1} for aromatic ring vibration attributed to lignin, and at 1018 cm^{-1} for the C–O–C asymmetric stretching in carbohydrates and the C–H in-plane deformation in aromatic groups (Javier-Astete; Jimenez-Davalos; Zolla, 2021; Méndez et al., 2007).

By increasing the GPS concentration from 0 to 10 wt%, a proportional reduction in the O–H stretching vibrations was noticed, demonstrating that part of the available lignocellulose hydroxyl groups were grafted by silanol groups formed after Si−OCH_3 hydrolysis of the coupling agent in aqueous media (Chen et al., 2021). However, there was no clear evidence for fiber silanization, since sharp Si–O–C vibrations at 1000-1200 cm^{-1} and Si−O−Si vibrations (from silanol self-polymerization) at 700-800 cm^{-1} were not present in the spectra (Barczewski; Matykiewicz; Szostak, 2020; Chen et al., 2021; Liu et al., 2019b; Zhang et al., 2022).

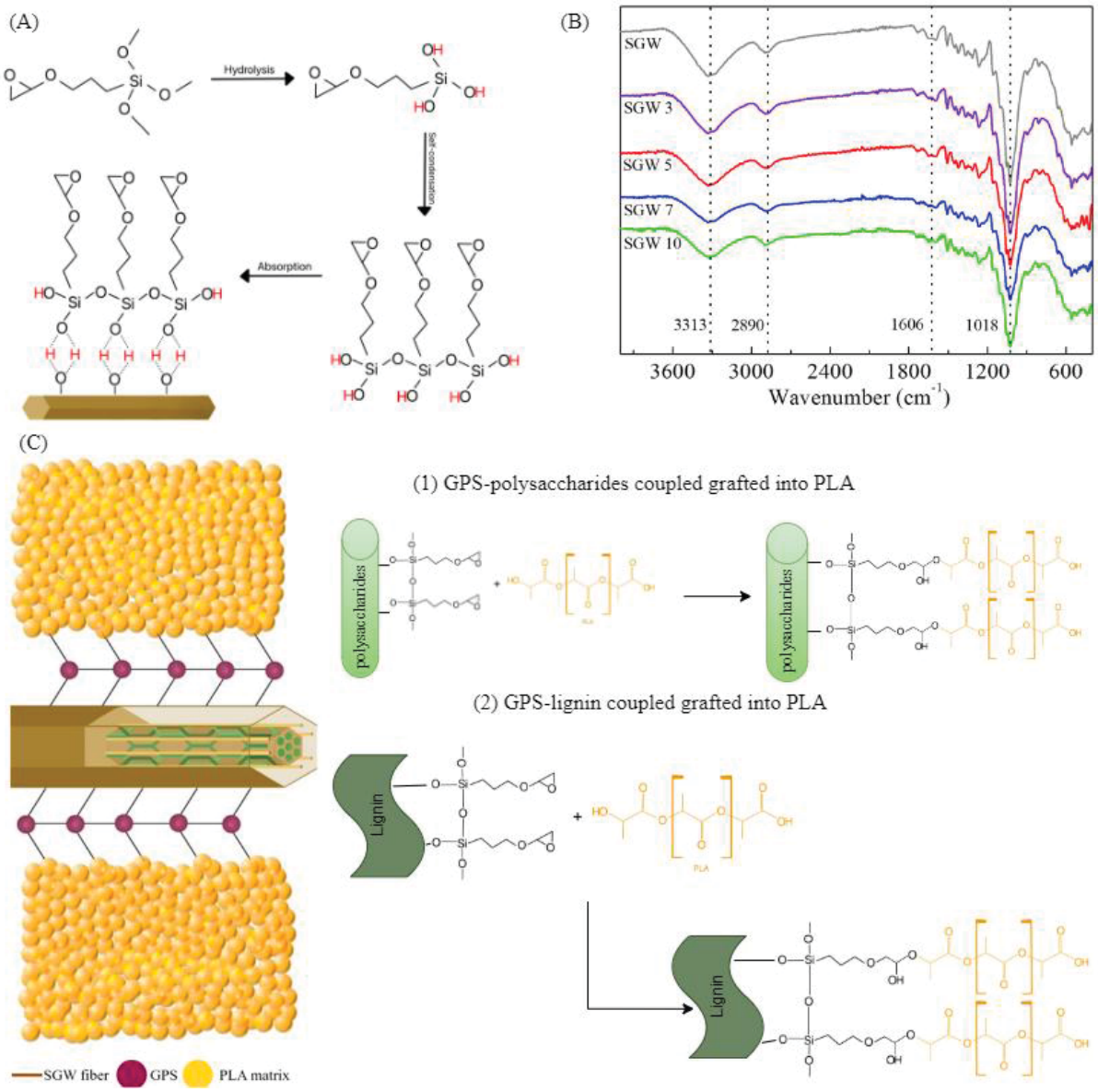

Figure 3. 4 (A) Fiber coupling agent silanization reaction; (B) FT-IR spectra of untreated and GPS-treated SGW at different concentrations; (C) Proposed Fiber-GPS-PLA bonding scheme.

The fiber silanization and grafting mechanism, for both lignin and cellulose into PLA structure, represented in **Figure 3.4** (C) comprise the coupling agent (GPS) hydrolysis, from

silane into silanol groups, possible self-condensation between the silanol hydroxyl groups, due to its high reactivity followed by hydrogen bond formation with the fiber surface, subsequent physical adsorption and grafting, characterized by the formation of covalent bonds from the dehydration of the hydrogen bonds (during the fiber drying process) between the silanols and the hydroxyl groups of the fibers (Arslan; Dogan, 2018; Chen et al., 2021; Del Angel-Monroy et al., 2024; Wang et al., 2020).

3.3.2 PHYSICAL PROPERTIES

Changes in MFI and density provided useful insights of the effects of SGW incorporation into the polymer matrices, both in terms of processability and specific weight of the resulting biocomposites. **Figure 3.5** shows the evolution of both MFI and density at different SGW fiber contents (20 and 30 wt%) and GPS modification degrees.

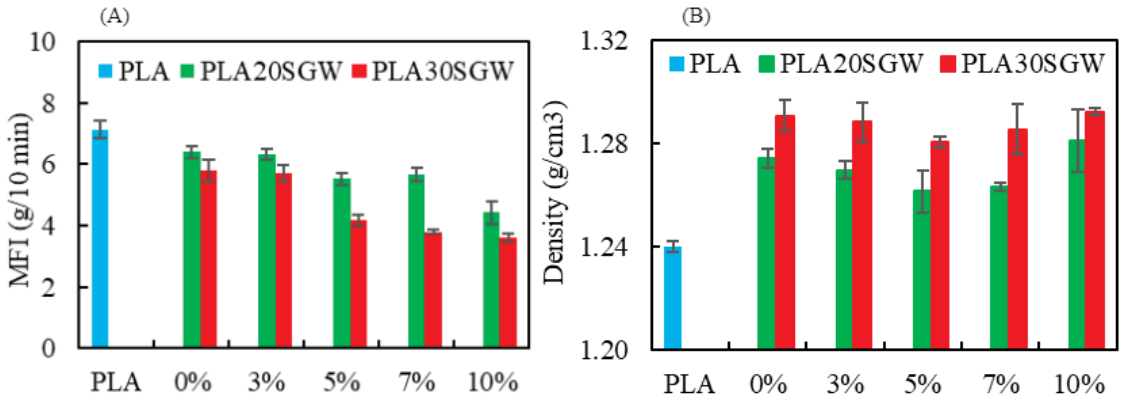

Figure 3. 5 Evolution of Melt Flow Index (A) and density (B) with the incorporation of GPS for the different levels of SGW reinforcement (20 and 30 wt%).

Natural fiber-reinforced composites exhibit shear-thinning behavior that contributes to the decrease of MFI values as fiber content was increased (**Figure 3.5** A) (Awal; Rana; Sain, 2015). The MFI of the PLA matrix decreased from 7 g/10 min to nearly 6 g/10 min at 30 wt% fiber content and found its minimum with 30 wt% of SGW and between 7 and 10 % GPS. Hence, fiber incorporation in the PLA matrix decreases the composite MFI; consequently, the fibers do not melt and contribute to the viscosity of the polymer due to fiber-polymer interactions, leading to higher melt strength than the neat polymer (Awal; Rana; Sain, 2015; Long et al., 2019). Furthermore, as discussed above, SGW is a highly fibrillated pulp, counting on pronounced surface fibrillation due to the processing conditions. This highly fibrillated surface, together with the generation of shorter and finer fibers during compounding,

significantly contributes to the fiber interactions with the polymer and, thus, to its flowability (Bianchi et al., 2019; Hietala et al., 2014; Jalaee; Foster, 2024).

Considering that fiber-polymer interactions also affect chain mobility in the melt state, for certain fiber content, increasing GPS resulted in lower MFI, indicating that the presence of GPS promoted the adhesion of the two biocomposite phases (Luo et al., 2016). Fan et al., (2023) also reported a linear decrease in MFI values as the fiber and the coupling agent contents were increased. Some authors reported that the melt rheology of fiber-reinforced composites provides useful information about fiber-matrix interactions (El Omari et al., 2023; Fourati et al., 2021; Hristov; Vlachopoulos, 2007). **Figure 3.6** shows the storage modulus (G'), loss modulus (G''), complex viscosity (η*), and the loss factor (tan (δ)) of different biocomposites compared to PLA.

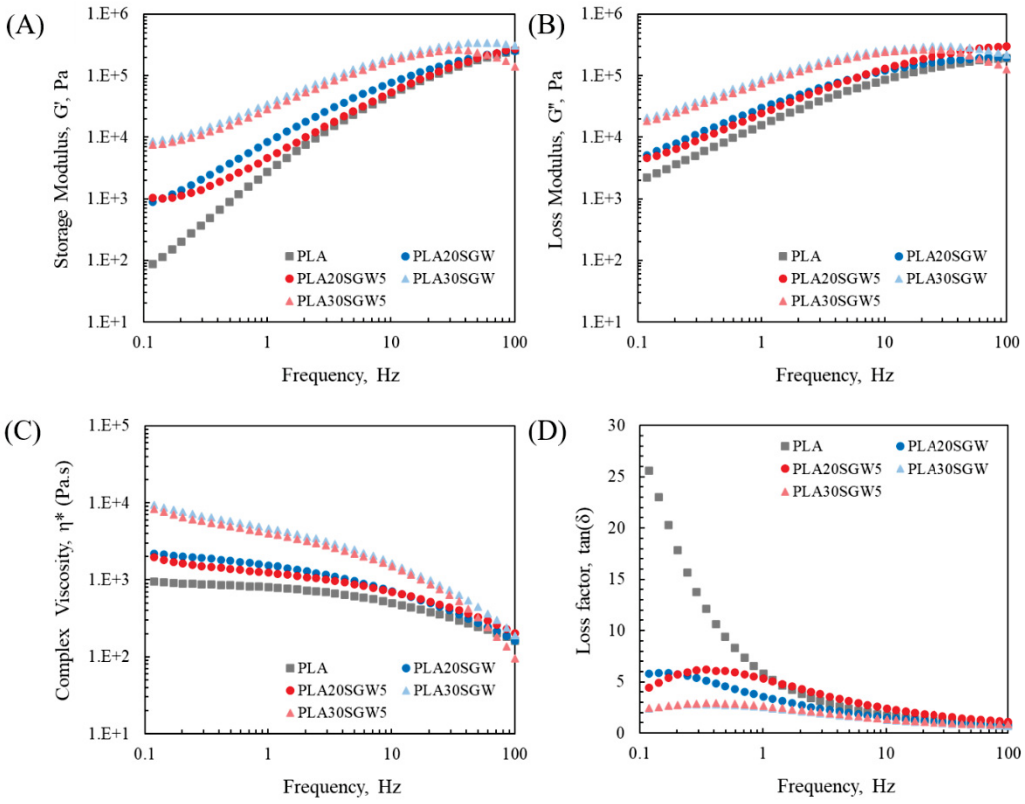

Figure 3. 6 Rheological features of the neat PLA and the PLA composites containing unmodified and 5 wt% GPS-modified SGW (20 and 30 wt%).

Figure 3.6 reveals significant differences at low shear rates with the incorporation of SGW, particularly in terms of G', G'', and η*. At low shear rates, G'' dominated over G', clearly suggesting that materials exhibited predominantly a viscous behavior. However, these differences became lower as the fiber content was increased, as illustrated by **Figure 3.6** D, where the loss factor is provided. At low shear rates, the viscous behavior of PLA was much

more accentuated than in the case of the resulting biocomposites, which exhibited lower loss factor values. This effect, provided by the inclusion of fibers into the PLA matrix, is attributed to the presence of a strong network of fibers within the polymer matrix (Safdari et al., 2018). In addition, at low frequencies, the obtained G' for the biocomposites containing 30 wt% SGW was found to be up to two orders of magnitude higher, confirming these interactions. As the amount of fiber increased in the biocomposites, the loss factor became lower, indicating its predominantly elastic behavior.

In addition, regardless of the fiber content, a crossover point was normally found between 40 and 50 Hz. While the presence of GPS had a direct influence on MFI and as later discussed, on the mechanical properties of the obtained biocomposites, no significant effects were found on its rheological behavior in the melt state, as previously observed for PLA biocomposites reinforced with silane-coupled lignocellulosic fibers (Chen et al., 2021).

3.3.3 MECHANICAL PROPERTIES EVALUATION

3.3.3.1 Tensile properties

Table 3.3 provides the tensile strength characteristics of the obtained biocomposites as a function of fiber and GPS contents. In all cases, regardless of the GPS content, the tensile strength and Young's modulus were increased. The incorporation of neat SGW enhanced the tensile strength of the composite by 14 and 27% for an addition of 20 and 30 wt%, respectively.

For the same fiber content, the incorporation of 5% GPS enhanced tensile properties by 24 and 37%. In addition, the presence of GPS gradually increased the reinforcing capacity of SGW, reaching a plateau between 5 and 7% to be decreased afterward with a 10% addition. This effect was not observed in Young's modulus, where a significant enhancement was obtained regardless of the GPS content.

Tensile strength measurements revealed the potential of PLA biocomposites to replace several commodity PP composites reinforced, for instance, with glass fiber. The incorporation of 20 wt% glass fiber into PP generates materials with tensile strengths of around 60 MPa and densities of 1.35 g/cm^3 (Eftekhari; Fatemi, 2016). These tensile strengths were already achieved with 20 wt% SGW in PLA with densities below 1.28 g/cm^3, representing a competitive advantage for obtaining lighter materials with similar mechanical properties that, in turn, come

from bio-based resources and can be biodegraded at their end of life. Moreover, SGW processing is safe and well-established, while glass fiber handling imparts negative effects on the environment and on human health, particularly for workers directly involved in the process (Gonçalves; Martinho; Oliveira, 2022).

Table 3. 3 Tensile properties of the PLA/SGW biocomposites.

SGW (wt%)	V^f	GPS (wt%)	σ_t^c (MPa)	E_t^c (GPa)	ε_t^c (%)	σ_t^{m*} (MPa)
0	0.0	0	53.27 ± 2.14	3.8 ± 0.1	3.22 ± 0.01	-
20	0.151	0	60.94 ± 1.79	5.2 ± 0.1	3.12 ± 0.09	53.18
		3	62.25 ± 1.38	5.7 ± 0.2	2.80 ± 0.19	51.27
		5	66.15 ± 0.62	5.2 ± 0.1	2.93 ± 0.11	52.39
		7	64.86 ± 0.79	5.3 ± 0.1	2.88 ± 0.09	52.01
		10	64.58 ± 1.19	5.5 ± 0.1	2.87 ± 0.07	51.92
30	0.229	0	67.77 ± 0.65	6.8 ± 0.1	2.62 ± 0.08	49.14
		3	68.36 ± 1.62	7.1 ± 0.3	2.76 ± 0.12	50.85
		5	73.19 ± 2.08	6.8 ± 0.2	2.84 ± 0.28	51.66
		7	74.21 ± 0.79	6.6 ± 0.1	2.78 ± 0.05	51.06
		10	68.89 ± 2.30	6.5 ± 0.1	2.69 ± 0.16	50.04

σ_t^c: tensile strength; E_t^c: Young's modulus; ε_t^c: elongation at break; σ_t^m: contribution of the matrix to tensile strength*

Incorporating a silane coupling agent resulted in reduced fiber debonding from the matrix under stress. In **Figure 3.7**, it is shown that the biocomposites achieved their maximum performance when the SGW content for tensile strength was between 5% and 7% of GPS. Tukey's HSD test of tensile strength results also confirmed that the silane treatment had statistically significantly different effects ($p < 0.05$) for 5% and 7% of GPS compared to untreated SGW. No statistical difference ($p < 0.05$) was evidenced between untreated fiber (0% GPS), 3, and 10% GPS for both SGW content.

The mechanism of silane coupling in lignocellulosic fiber biocomposites has been previously reported, revealing that layers of coupling agents are formed during GPS grafting and adsorption onto the fiber surface as covalent and hydrogen bonds, and the epoxy organo-functional group leads to interdiffusion with the polymeric matrix, contributing to successful reinforcement and efficient stress transfer between the fiber and the matrix (Arslan; Dogan, 2018; Doan; Brodowsky; Mäder, 2012).

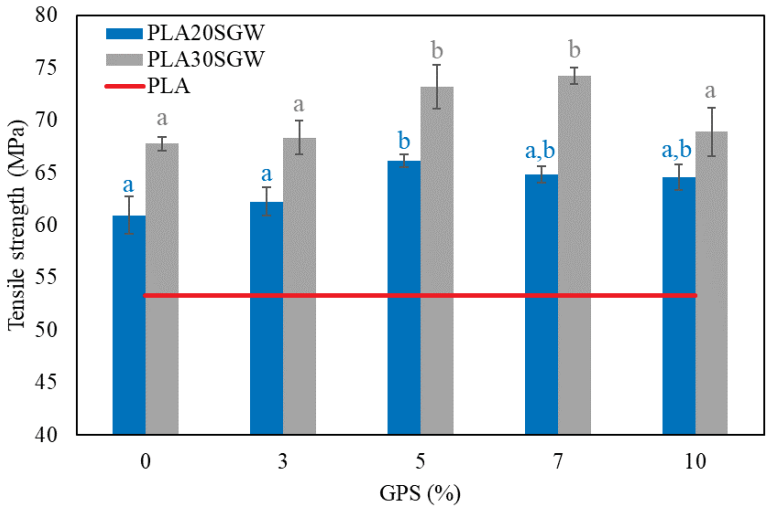

Figure 3. 7 Evolution of tensile strength of the biocomposites at different GPS and SGW contents. Distinct letters represent statistical differences by Tukey's HSD test ($p < 0.05$).

Nandi and Das (2023) reported improvements in the tensile strength of PLA reinforced with 50 wt% Himalayan nettle fibers by 13.33, 18.65, 16.50, and 12.27 % with the presence of 0.5, 1.0, 2.5, and 5.0 % silane coupling agent, respectively. A decrease in tensile strength was observed at high concentrations due to the potential disruption of cellulose crystalline regions. This effect was also observed for biocomposites containing fibers with GPS contents above 7 %. However, the obtained values were still higher than the neat fiber, for both 20 and 30 wt% SGW content. This could also be attributed to the self-condensation structures of silanol groups grafted onto the SGW surface, leading to fiber aggregation. Jandas et al. (2011) enhanced the tensile strength of PLA reinforced with 10, 20, 30, and 40 wt% banana fibers. The best results were obtained with the incorporation of 30 wt% banana fibers. Also, an increase of approximately 15 and 35 % in tensile strength, and 4 and 13 % in tensile modulus upon treatment with two different silane coupling agents, 3-aminopropyltriethoxysilane (APS) and bis-(3-triethoxysilylpropyl) tetrasulfane (Si69), respectively. The Young's modulus of the obtained PLA/SGW biocomposites was significantly enhanced compared to the neat matrix, achieving an average increase of 36 and 79 % for a 20 and 30 wt% SGW addition, respectively, with no clear influence of the GPS content.

As mentioned above, Young's modulus is less influenced by fiber-matrix interactions than other properties such as tensile strength, and more related to aspect ratio, fiber stiffness, and both fiber distribution and dispersion within the polymer matrix (Ku et al., 2011). In addition, other authors observed no significant effect of coupling agents on the elastic modulus (Bartos et al., 2021; Ramachandran et al., 2022). In another work, (Dominguez-Candela et al.,

2022), reported an increase in tensile strength with the incorporation of 15 wt% GPS-treated chia seed flour particles into PLA, with an enhancement of 19.2 %.

Compared to neat PLA, SGW-reinforced composites exhibited a reduction ranging from 10% to 15% in elongation at break when stiffness was increased (Table 3.3). This phenomenon is attributed to the decreased deformability of stiff materials, resulting in diminished fracture resistance and intrinsic ductility. Moreover, the incorporation of SGW limited the macromolecular mobility of the PLA matrix chain, thereby impacting the deformability of the composites (Asaithambi; Ganesan; Ananda Kumar, 2014). Furthermore, the elongation at the break of natural fiber-reinforced composites is influenced by factors, such as fiber entanglement and orientation. In comparison to PLA/jute fiber composites, for instance, PLA/SGW composites demonstrated lower Young's modulus and exhibited less effect on elongation at break (Delgado-Aguilar et al., 2018).

3.3.3.1.1 Composites morphology from tensile specimens

Figure 3.8 shows the tensile fractured surface morphology of the PLA/SGW composites analyzed by a field emission scanning electron microscope, and the effect of the GPS coupling agent treatment on the tensile properties. In general, SGW fibers during the tensile deformation exhibited two main behaviors, fiber debonding or pullout, in which the fiber was detached from the matrix while maintaining its diameter, or fracture and delamination, in which the fiber length was ruptured. However, despite the regular fiber failure, its impregnation in the PLA matrix provides a good homogeneity between PLA/fiber, since the incorporation of 20 and 30 wt% SGW increased the tensile strength, showing a good interfacial adhesion of the composites without undergoing silane treatment.

The silane coupling agent effect was better elucidated in PLA30SGW5 images with a two-thousandfold magnification (15 μm), where a strong interaction between the PLA matrix and SGW fibers was observed without the presence of voids, leading to a 37% increase in tensile strength compared with neat PLA. This confirmed that the silane coupling agent was efficiently bonded to the fiber surface. Since SGW incorporation increases the composite stiffness and decreases the elongation at break, shear yielding of the matrix was not observed in the images.

The presence of silanol self-condensation structures adsorbed onto the SGW surface resulted in fiber aggregation. This was evidenced by a red ellipse in **Figure 3.8** for PLA20SGW10 and PLA30SGW10, which induced points of failure and early rupture of the sample specimens. The reduction in tensile strength with the increase of up to 8 % GPS was also reported by Yang et al. (2023), who observed that with the excessive amount of free coupling agent, the composite's interfacial bonding was affected.

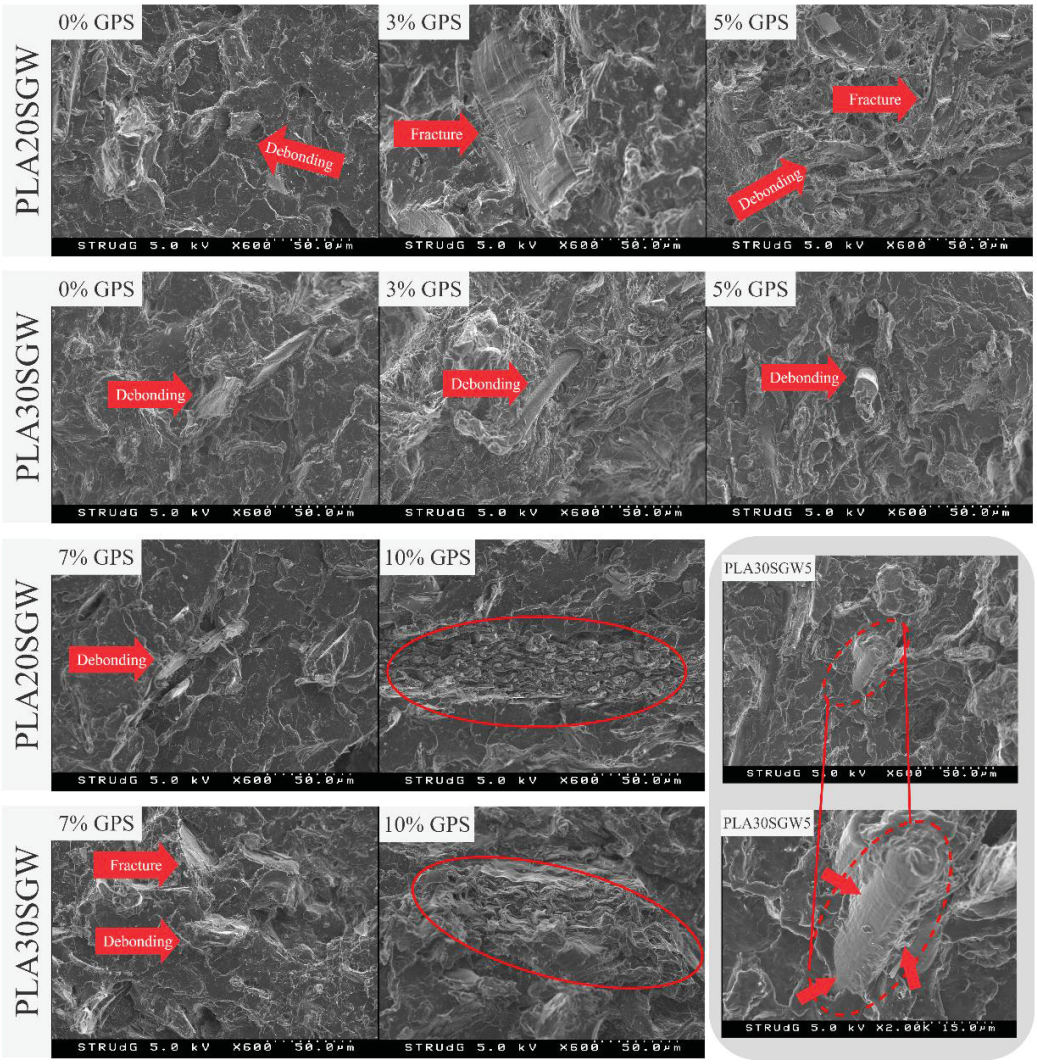

Figure 3. 8 FE-SEM images of PLA/SGW composites at increasing GPS content.

3.3.3.1.2 Micromechanical approach

FTSF has been extensively used for assessing the reinforcing performance of different fibers when incorporated into polymer matrices. It results from the combination of the intrinsic tensile strength of the fiber (σ_t^F) and the coupling factor (f_c). The first parameter is inherently linked to the nature of reinforcement and should remain constant regardless of the fiber-matrix interface, the fiber dispersion, and any other parameter related to composite processing and

properties. The second, on the contrary, is a compounded factor referring to fiber orientation and fiber-matrix interactions, represented by χ_1 and χ_2 factors, respectively. Due to the technical difficulties in determining σ_t^F experimentally, FTSF is commonly used for preliminarily assessing the reinforcing performance of a certain class of fibers when used as reinforcement of a specific polymer matrix. It must be noted that, as the interactions between reinforcement and matrix influence f_c, the FTSF value will vary from one matrix to another despite the same fiber is used. Furthermore, V^F can also influence this value, as fiber dispersion may be influenced by fiber loading. However, the effect of fiber content is residual compared to σ_t^F and f_c, and most of the existing literature provides a mean FTSF value regardless of V^F. **Table 3.4** shows the obtained mean FTSF as a function of the GPS content.

Table 3. 4 Mean FTSF, E_t^F, σ_t^F, and f_c computed by the mRoM and the Hirsch models

GPS (wt%)	E_t^F (GPa)	σ_t^F (MPa)	FTSF (MPa)	f_c
0			117.52	0.15
3			125.66	0.16
5	27.18 ± 4.01	768.91 ± 37.39	144.61	0.19
7			144.64	0.19
10			134.09	0.17

As detailed above, the FTSF is a compounded factor resulting from σ_t^F and f_c. However, due to the inaccuracy of the single-fiber tensile test for determining the intrinsic tensile strength of the fibers, standard deviations of around 25 % are normally reported (Islam; Pickering; Foreman, 2011). Alternatively, the Hirsch model can provide useful insights for its determination, assuming that fibers and the composite experience the same strain at break (Bowyer; Bader, 1972). The Hirsch model allows the theoretical calculation of the intrinsic Young's modulus of the fiber (E_t^F) by assigning a value of 0.4 to orientation and stress concentration (β), as widely reported. Then, σ_t^F can be easily calculated and computed together with the FTSF, leading to an estimated f_c as a function of the GPS content (**Table 3.4**).

The obtained σ_t^F is of the same order of magnitude than in previous works where SGW fibers were used as thermoplastic reinforcement of polypropylene (PP) in presence of maleated polypropylene (MAPP) as the coupling agent (López et al., 2011). Regarding the f_c values of Table 3, the GPS content appeared to directly influence the interactions between the

reinforcement and the polymer matrix, gradually increasing from 0.15 (unmodified SGW) to 0.19 (5 and 7 % GPS) to later decrease to 0.17. Surprisingly, the obtained E_t^F of 27.18 GPa was significantly higher than the previously reported value of 18.2 GPa for the situation in which SGW fibers were used for PP reinforcement. This higher E_t^F can be attributed to the highest rigidity of the PLA matrix, which may have influenced the calculations. Considering the low strain at break of the composites, compared to SGW-reinforced PP composites, this higher value was expected. Considering that the intrinsic tensile strength of the fibers is an inherent property and that, theoretically, it must remain constant regardless the system where fibers are embedded, any change on the FTSF must come from the coupling factor, indicating that interface and orientation exerts a determining role in the fiber reinforcing capacity within the polymer matrix. The obtained f_c value indicates that composites prepared from SGW modified with GPS contents ranging from 5 to 7 % leverage systems with appropriate fiber-matrix interactions. Actually, for randomly oriented fiber-reinforced composites, a coupling factor of 0.20 is an indicator of well-bonded systems.

As previously discussed, f_c results from the combination between fiber orientation and fiber-matrix interfacial features. The interfacial shear stress (IFSS or τ) can be determined by the Bowyer-Bader iterative solution to the Kelly-Tyson model or, in a more simplified scenario, estimated according to the Tresca and/or Von Misses criteria (τ_T and τ_{VM}, respectively). This allows for the determination of the critical length (L_c^F) if σ_t^F and fiber diameter (d^F) are computed together, as described by Eq. 7. Critical length varied from one composite to another, but all values ranged from 242 to 311 μm. In addition, considering the average fiber length weighted in length (**Table 3.2**) of the fibers after the extraction process, this preserves the fiber morphology within the composite, it seems that fibers could be generally considered as subcritical. A more detailed analysis could be performed by considering the fiber length distribution, as previously reported in other studies (Espinach et al., 2024; Tarrés et al., 2018). However, this simplified methodology allows the understanding of the mechanisms taking place during fiber reinforcement of PLA. In this sense, χ_2 can be obtained from Equation 8, and χ_1 can be easily obtained considering the obtained values of f_c.

As depicted from **Table 3.5**, the interface factor χ_2 exhibited an increasing tendency with the GPS content. This is aligned with the previously observed reduction of O-H stretching vibrations by FTIR, potentially generating bonds between lignocellulosic hydroxyl groups and silanol groups that increase the SGW hydrophobicity, which may enhance the fiber-matrix interactions with PLA. The fiber orientation factor χ_1 revealed values between 0.344 and 0.388.

According to the literature, a value of 3/8 (0.375) for the orientation factor can be considered for randomly oriented 2D composites, which is a comparable case to the composites under study due to the thickness of the injected specimens (Garkhail; Heijenrath; Peijs, 2000; Thomason et al., 1996). In any case, the micromechanical analysis reveals that both 5 and 7 % GPS addition provides a good orientation and interface between PLA and SGW, which is aligned with the macromechanical study of the tensile strength.

Table 3. 5 Micromechanical parameters of PLA/SGW composites at increasing SGW and GPS content.

GPS (wt%)	V^F	τ_T (MPa)	τ_{VM} (MPa)	L_c^F (μm)	χ_1*	χ_2*
0	0.151	30.47	35.18	312	0.344	0.432
	0.229	33.89	39.13	276		
3	0.151	31.13	35.94	296	0.386	0.379
	0.229	34.18	39.47	280		
5	0.151	33.08	38.19	283	0.388	0.442
	0.229	36.60	42.26	243		
7	0.151	32.43	37.45	294	0.376	0.523
	0.229	37.11	42.85	249		
10	0.151	32.30	37.29	290	0.353	0.542
	0.229	34.45	39.77	271		

*Calculated using the Von Misses criterion.

3.3.3.2 Flexural and impact properties

Similar to the tensile strength properties, the flexural strength and flexural modulus were improved with the increase in SGW content, as shown in Table 3.6. The flexural properties of GPS-modified PLA/SGW biocomposites in comparison between neat PLA and unmodified fiber, resulted in an increase of approximately 15% and 29% in flexural strength, and 46% and 86% higher flexural modulus, respectively. An opposite effect was observed in flexural elongation at break, which decreases by around 21%, and 39% with fiber content increasing from 20 to 30 wt.%, indicating that the fiber content induces brittleness to the biocomposites, while compared to the matrix.

The incorporation of SGW resulted in a linear increase in the biocomposites' tensile and flexural strength. Flexural strength values of around 93, and 104 MPa for 20 to 30 wt.% SGW were achieved, respectively. This motivates the use of biocomposites for high-performance applications, as these properties allow the evaluation of the anisotropy character of natural fibers (Tarrés et al., 2019).

Table 3. 6 Flexural properties of the PLA/SGW biocomposites.

SGW (wt%)	V^F	GPS (wt%)	σ_F^c (MPa)	E_F^c (GPa)	ε_F^c (%)
0	0.0	0	80.63 ± 1.10	2.30 ± 0.06	6.1 ± 0.1
20	0.151	0	92.94 ± 1.23	3.35 ± 0.10	4.8 ± 0.3
		3	92.83 ± 1.79	3.60 ± 0.07	4.1 ± 0.2
		5	99.85 ± 0.64	3.50 ± 0.10	4.6 ± 0.2
		7	90.35 ± 1.71	3.60 ± 0.20	4.0 ± 0.2
		10	89.08 ± 1.70	3.60 ± 0.17	3.8 ± 0.1
30	0.229	0	104.10 ± 4.01	4.28 ± 0.30	3.7 ± 0.4
		3	102.30 ± 1.52	4.50 ± 0.24	3.5 ± 0.2
		5	103.40 ± 1.84	4.40 ± 0.17	3.8 ± 0.1
		7	104.50 ± 2.74	4.40 ± 0.10	3.8 ± 0.1
		10	87.62 ± 2.82	4.20 ± 0.14	3.1 ± 0.1

σ_F^c: flexural strength; E_F^c: flexural modulus; ε_F^c: elongation at break.

Natural fibers are able to withstand tensile stress more than compressive and flexural stresses due to their thin and elongated shape. As a result, the volume fraction and the position of the cross-section of fibers are crucial in composite materials for determining flexural properties and energy absorption capacity (Li et al., 2019a). Therefore, higher flexural strength was obtained by the 30 wt.% of fiber concentration.

Once compared to polypropylene, PLA not only exhibits higher tensile modulus, and higher storage modulus but also higher flexural properties, since PP's flexural strength is around 40 MPa (Gironès et al., 2011; Yusoff; Takagi; Nakagaito, 2016). Furthermore, López et al., (2013) evaluated the use of SGW as PP reinforcement and obtained flexural strength of 66.10, and 81.60 MPa for 20 and 30 wt.% of SGW, respectively, while Julian et al., (2012) showed flexural strength of PP reinforced with 20 and 30 wt.% glass fiber of 78 and 88.10 MPa, respectively. Thus, the flexural strength results corroborated the application of PLA/SGW composites as an alternative to PP and its derivative composites.

Flexural properties results revealed a significant influence on both properties by the fiber content, even though the polymeric matrix typically plays a crucial role in determining compressive, flexural, and shear properties (Derradji; Wang; Liu, 2018). However, the flexural

modulus was influenced not only by composite composition but is also intrinsically related to fiber orientation and its displacement in the layers within the matrix. While, the material's stiffness is strongly influenced by both the properties of individual components of the composites, and the geometric arrangement of the reinforcement (Greb et al., 2018).

Regarding the fiber silane modification effect on flexural strength, **Figure 3.9** (A), revealed through pairwise multiple comparisons with Tukey's HSD test ($p < 0.05$) that for 20 wt.% of SGW, and 5 wt.% of GPS showed a positive statistically significant effect over flexural strength results compared to untreated fiber and among the remained treatments, once for this condition was obtained the highest flexural strength of 99.85 ± 0.64 MPa. Increasing fiber content to 30 wt.%, no statistically significant effects were observed between untreated SGW and 3, 5, and 7 wt. % of GPS, while a negative statistically significant effect was observed for 10 wt.% of silanization. However, the results were higher and significantly different compared to the PLA matrix.

The effect of fiber content on flexural properties was also observed by Tarrés et al. (2019) in the investigation of the flexural properties of PLA reinforced with bleached kraft softwood fibers in the presence of 2:3 diglyme (diethyleneglycol dimethylether), a linear increase in flexural strength was observed with the increase of fiber content, revealing results from around 80 to 100 MPa, from 15 to 30 wt.% of fiber.

The effect of silane coupling agents' treatment was also observed by Nandi and Das, (2023) in the study of surface-silanized nettle fabric-reinforced PLA composites, at four different mass fractions of silane, ranging from 0.5 to 5 wt.%, at a constant fiber content of 50 wt.%. An increase in flexural strength was observed from around 51 MPA for untreated fiber to 54 MPa for 2.5 wt.% of APTES as a silane agent. Yu et al., (2010) evaluated the effect of 30 wt.% of ramie fiber-reinforced PLA composites treated with alkali and 6% of two different silanes. Flexural strength was increased from around 110 MPa for untreated fiber to 150 MPa for the sample treated with γ-glycidoxypropyltrimethoxy silane, the same agent applied in this research.

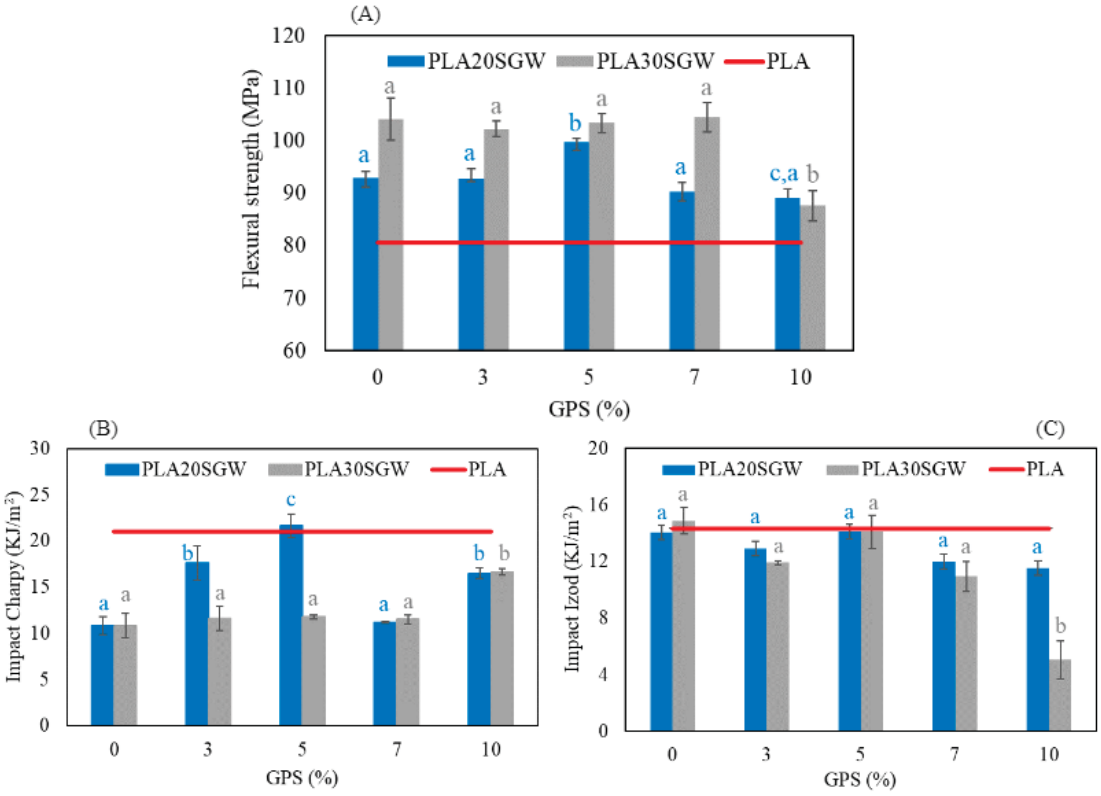

Figure 3. 9 Evolution of (A) flexural strength, (B) Charpy impact strength, and (C) Izod impact strength of PLA biocomposites at different GPS and SGW contents. Distinct letters represent statistical differences by Tukey's HDS test ($p < 0.05$).

The increase in the PLA/SGW biocomposite's flexural modulus increases the material's stiffness, although proportionally decreases the elongation at break, inducing biocomposites' brittleness, influencing other biocomposites' properties as demonstrated by the impact strength results in **Figure 3.9** (B) for Charpy and (C) for Izod.

Charpy impact strength results (specimen located horizontally) were lower for the biocomposites compared to the PLA matrix, however, for 20 wt.% of SGW an increase was observed for the 3 and 5 wt.% of GPS-modified fibers, in which, the sample PLA20SGW5 achieved similar impact strength to the matrix. For 30 wt.% of SGW, no significant statistical effect was evidenced in Tukey's test ($p < 0.05$) for GPS treatment, except for 10 wt.% of GPS with a slight increase of around 35% compared to the untreated fiber. No significant statistical effect was evidenced in Tukey's test ($p < 0.05$) for Izod impact strength (specimen located vertically) between the different fiber loads and GPS modification between PLA matrix, showing that the matrix contribution influence was responsible for Izod's impact results, except for the sample PLA30SGW10 which showed a negative significant statistical difference and the lowest Izod impact result among the biocomposites.

The effect of fiber content on the impact strength of PLA composites was also observed by Oliver-Ortega et al. (2020) by testing the Charpy impact strength of bleached Kraft softwood-reinforced PLA composites. The effect of fiber content was evaluated in six different concentrations ranging from 10 to 35 wt.%. Compared to neat PLA (25.8 ± 2.1 kJ/m^2), a linear decrease in impacted strength was observed by increasing fiber content for un-notched specimens from around 22 to 18 kJ/m^2, for 10 to 35 wt.% of fiber. Nuthong et al. (2013) investigated the effect of notched Izod impact strength of bamboo, coconut, and vetiver grass fiber content in PLA biocomposites treated with 1 wt.% of flexible epoxy resin. For bamboo biocomposites reinforced with 20 and 30 wt.% of fiber, the Izod impact results were similar to those of neat PLA, of around 2 KJ/m^2. For coconut and vetiver grass composites, the impact results decreased with the increase in fiber content.

Bartos et al. (2021) evaluated the effect of fiber content (0 to 30 wt.%) and the influence of functionalized PLA with maleic anhydride coupling agent on the notched Charpy impact of biobased PLA/sugarcane bagasse composites. For short fibers (815 ± 626 μm in length), notched Charpy impact increased from around 1.7 to 3.2 and 3.3 kJ/m^2 for neat PLA, 5 wt.% of fiber, and 5 wt.% of fiber in coupled PLA, respectively. However, with the increase in fiber content from 5 to 30 wt.%, a decrease in impact strength was observed, despite the lowest value achieved for 30 wt.% of fiber being similar to that of neat PLA, and at the same fiber content for coupled PLA, the value was around 2.2 kJ/m^2.

Due to the mechanical anisotropic character of natural fiber as reinforcement in composites, differences in mechanical behavior are expected when tests are performed at different orientations, especially for random fiber orientation, as demonstrated by micromechanics analysis of tensile properties of PLA/SGW biocomposites. The decrease in impact strength could be attributed to the heterogeneous distribution and varying concentration of fiber length, which often introduces defects leading to premature fatigue of the composite material (Qaiss; Bouhfid; Essabir, 2015).

3.3.3.1 Statistical analysis of the mechanical properties

Statistical analysis of PLA/SGW biocomposites with ANOVA, and pairwise multiple comparisons with Tukey's HSD (honestly significant difference) test ($p < 0.05$) revealed that fiber load presented a linear positive influence on both tensile and flexural strength results. For

impact results, both Charpy and Izod showed no effect over the fiber load but were apparently affected by the GPS treatment.

Table 3.7 shows that the variables GPS treatment intensity (from 0 to 10 wt.%) and SGW load (of 20 and 30 wt.%), and the combined effect between the two variables, presented a statistically significant effect on the mechanical properties evaluated in this study, for tensile, flexural, and impact (Charpy and Izod). All the variables showed a p-value of less than 0.05, which indicates a statistically significant effect at the 5% significance level.

Table 3. 7 Two-way **v**ariance analysis results for tensile, flexural, and impact strength.

Property	Effect	SS	Df	F-value	Pr(>F)
Tensile	GPS (wt.%)	203.3	4	27	< 0.0001
	SGW (wt.%)	534.1	1	283.9	< 0.0001
	GPS*SGW	35	4	4.7	0.0035
	Error	75.3	40		
Flexural	GPS (wt.%)	1122.9	4	62.9	< 0.0001
	SGW (wt.%)	754.4	1	169.1	< 0.0001
	GPS*SGW	352.4	4	19.7	< 0.0001
	Error	178.4	40		
Charpy Impact	GPS (wt.%)	125.8	4	30.8	< 0.0001
	SGW (wt.%)	47.7	1	46.6	< 0.0001
	GPS*SGW	85.7	4	21	< 0.0001
	Error	10.2	10		
Izod Impact	GPS (wt.%)	93.2	4	18.1	0.0001
	SGW (wt.%)	13.5	1	10.5	0.0087
	GPS*SGW	32	4	6.2	0.0089
	Error	12.9	10		

SS: sum of squares; Df: degrees of freedom.

Figure 3.10 shows the Pareto chart of standardized effects for tensile and flexural strength at a significant level of $p \geq 0.05$. The SGW fiber load showed the most positive linear relevant effect, of 11.78 percent points (p.p.) for tensile in **Figure 3.10** (A), and 7.47 p.p. for flexural strength in Figure 3.10 (B). As previously reported, the results for tensile (Table 3.3) linearly increased from around 53 for neat PLA to around 61 for 20 wt.% and around 68 MPa for 30 wt.%, and for flexural (**Table 3.6**), the results linearly increased from around 81 for neat PLA to around 93 for 20 wt.% and around 104 MPa for 30 wt.%.

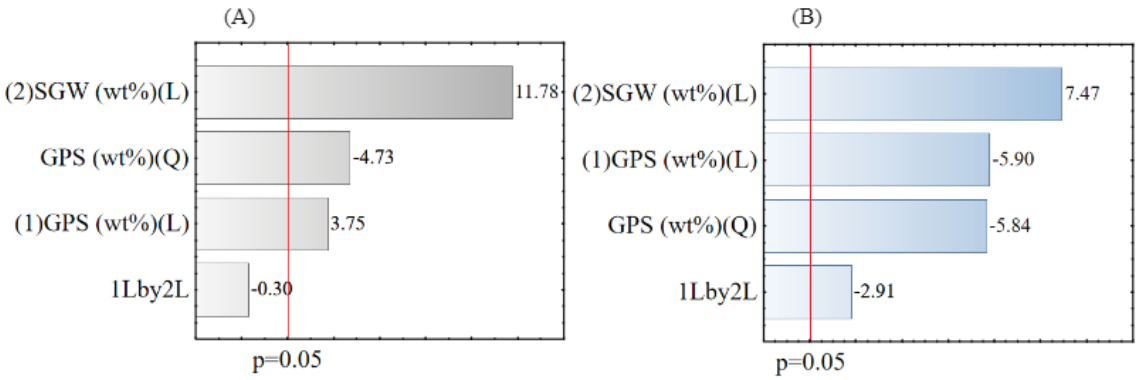

Figure 3. 10 Pareto's chart of standardized effects of (A) tensile, and (B) flexural strength.

The effect of the GPS modification degree showed for tensile results a significant linear (L) positive effect of 3.75 p.p., and a negative effect of -4.73 p.p. in quadratic (Q), since the results in Table 3.3, showed a linear increase in tensile with the linear increase of GPS from 0 to 5 at 20 wt.% of SGW and from 0 to 7 at 30 wt.% of SGW, and at higher coupling agent content, the tensile results started to decrease. For flexural strength, the GPS treatment results showed a significant negative effect for both linear and quadratic of -5.90 and -5.84, respectively, since in **Table 3.6**, the highest value of flexural at 20 wt.% of SGW was obtained at 5 wt.% of GPS (of around 100 MPa), and 30 wt.% of SGW the highest result was achieved for untreated SGW (0 wt.% of GSP, around 104 MPa), demonstrating its ineffectiveness over flexural properties at higher fiber load.

3.3.3.2 Mechanical properties comparison with fossil-based composites

To assess the feasibility of PLA composites reinforced with untreated and GPS-treated SGW fibers from a mechanical performance perspective, **Figure 3.11** compares their tensile and flexural strengths with those of neat PP and PP reinforced with glass fiber (GF). While neat PLA already exhibits higher tensile strength than neat PP, the incorporation of 20 wt.% SGW results in tensile strength values comparable to those of PP reinforced with 20 wt.% GF. Moreover, when 20 wt.% GPS-treated SGW is used, the tensile strength surpasses the ones with PP/GF composite. At 30 wt.% of fiber loads, PP30GF shows higher tensile strength, of around 14 % than PLA30SGW5. In this case, GF provides higher reinforcement efficiency per weight fraction than SGW, due to its higher stiffness and aspect ratio (López et al., 2013).

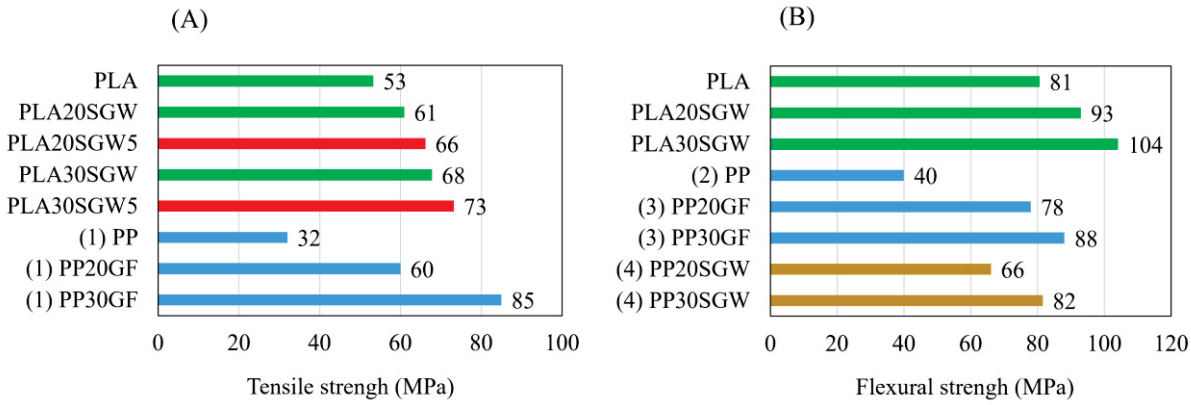

References used to generate the comparison: (1) Eftekhari; Fatemi, (2016); (2) Gironès et al., (2011); (3) Julian et al., (2012); (4) (López et al., (2013).

Figure 3. 11 Comparison between tensile (A) and flexural (B) strength of PLA/SGW and PP composites.

In flexural strength, the incorporation of SGW significantly improved bending resistance, for example, PLA increased from 81 MPa to 93 MPa with 20% SGW and reached 104 MPa at 30% SGW. Even when SGW was added to PP (raising flexural strength from 40 MPa in neat PP to 66 MPa at 20% SGW), the improvement was still lower than in PLA composites at the same fiber loads, confirming a stronger interfacial interaction of SGW with the PLA matrix compared to PP.

Although glass fiber offers reinforcement efficiency in tensile strength, SGW presents a renewable, lighter, and more sustainable alternative. PLA/SGW composites, therefore, represent a viable substitute for PP/GF systems in applications requiring moderate to high mechanical performance, particularly where flexural strength is a key requirement. In addition, the inherent sustainability and biodegradability of PLA/SGW composites expand their potential for use in packaging, automotive interior components, and consumer goods.

3.3.4 THERMAL CHARACTERIZATION

The thermal behavior and stability of the biocomposites reinforced with untreated and silane-treated SGW fibers are shown in **Figure 3.12**, while **Table 3.8** summarizes the composites' thermal parameters. Both TGA and DTG thermograms (**Figure 3.12**, A to D) show that neat PLA and PLA/SGW biocomposites decomposed in a single step. The initial (T_i) and the maximum degradation temperature (T_{max}) of PLA were decreased by the nontreated SGW fiber incorporation.

Table 3. 8 Thermal properties of neat PLA and PLA/SGW biocomposites.

Sample	T_i	T_{max}	T_f	R	T_g	T_{cc}	T_c	T_m	ΔH_{cc}	ΔH_m	X_c
		(°C)		(%)		(°C)			(Jg^{-1})		(%)
PLA	330	363	380	2.5	60.6	-	-	155	-	34.9	37.3
PLA20SGW	290	353	374	4.2	59.9	-	-	145	2.1	22.6	27.4
PLA20SGW3	310	352	372	7.1	65.7	-	-	155	1.9	20.1	25.3
PLA20SGW5	304	342	370	7.3	65.1	123	128	155	1.8	21.3	26.1
PLA20SGW7	294	333	351	7.6	60.1	103	114	151	12.1	18.0	7.9
PLA20SGW10	285	335	360	7.5	60.7	103	116	152	14.0	20.0	8.0
PLA30SGW	303	340	360	9.2	64.5	-	-	155	1.4	17.1	24.0
PLA30SGW3	297	350	385	7.9	62.5	-	-	154	1.5	15.2	20.9
PLA30SGW5	291	347	395	9.4	59.5	100	114	151	1.6	15.8	21.6
PLA30SGW7	307	356	388	10.0	59.6	102	115	152	7.5	15.2	11.8
PLA30SGW10	311	358	383	9.1	59.7	103	114	151	8.3	15.7	11.3

T_i = initial degradation temperature considering 95% residue; T_{max} = maximal degradation temperature; T_f = final degradation temperature; R = residue at 500 °C; T_g = glass transition temperature; T_{cc} = cold crystallization temperature; ΔH_{cc} = cold crystallization enthalpy; T_m = melting temperature; ΔH_m = melting enthalpy; X_c = crystallinity index.

The presence of lignocellulosic fibers affects the thermal stability behavior of polymeric composites, decreasing the onset temperature due to the lower degradation temperature of cellulose, hemicelluloses, and lignin (Eselini et al., 2020; Fang et al., 2022; Jandas et al., 2011; Ozyhar; Baradel; Zoppe, 2020). However, for the silane-treated 20 wt% SGW fibers (**Figure 3.12**, A and B), the addition of 3 and 5 wt% of the coupling agent was able to increase T_i and decrease both $T_{max,}$ and the final degradation temperature (T_f). By contrast, the 3 and 5 wt% silane-treated 30 wt% SGW fibers suffered a decrease in T_i and T_{max}, but a significant increase in T_f. **Figures 3.12** (D) and (E) show an increment in the maximum degradation rate of the silane-treated PLA30SGW, indicating improvements in the composite's thermal stability. Hence, the silane coupling fiber treatment raised the PLA/SGW interfacial adhesion. The presence of greater lignin content in the composites, due to the use of higher fiber contents (*e.g.*, 30 wt% SGW), required more energy for the material degradation, since lignin tends to degrade at higher temperatures, suggesting better adhesion and interaction among the GPS coupling agent, lignin, and the PLA matrix (Fang et al., 2022; Wang et al., 2020).

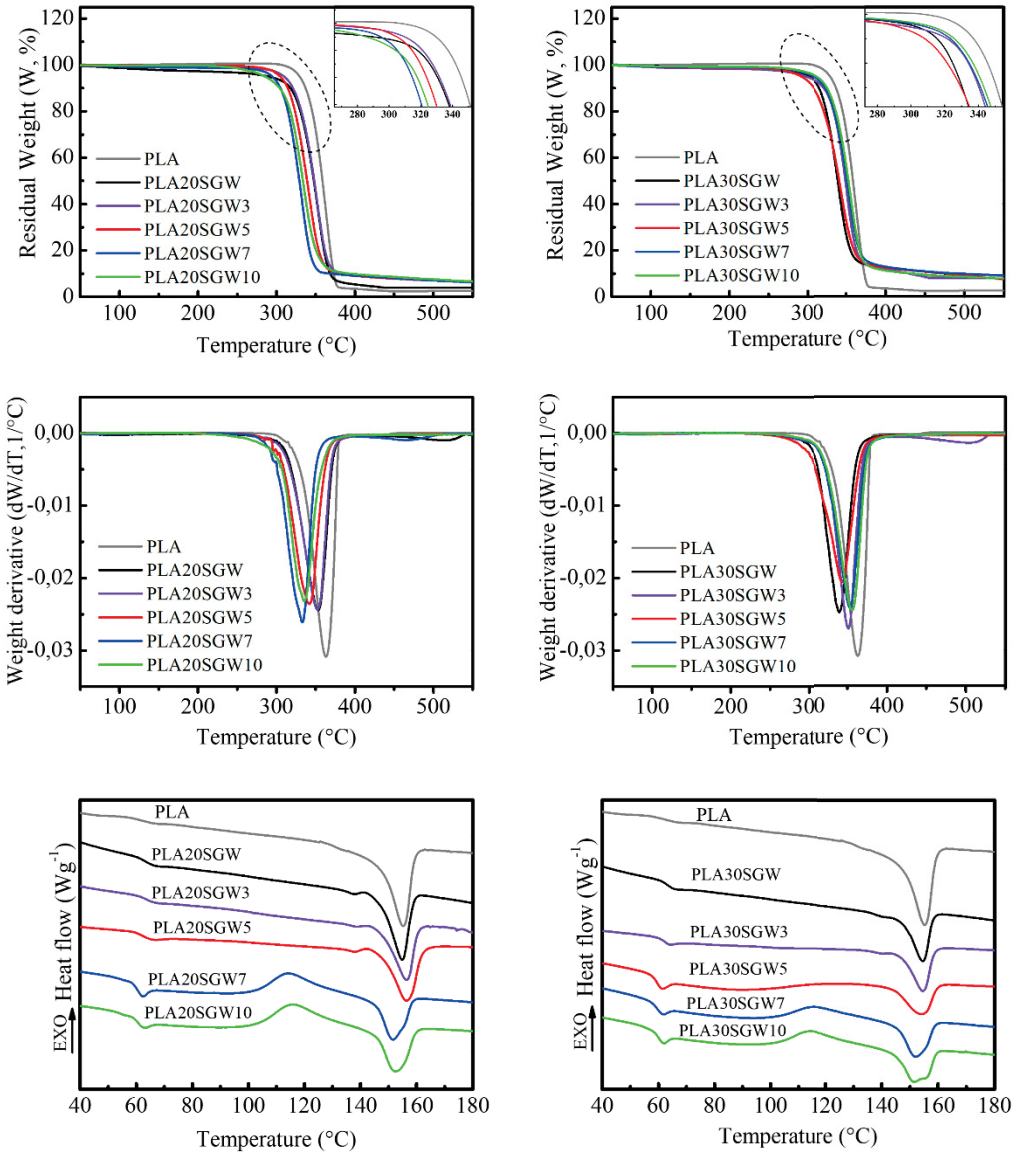

Figure 3. 12 TGA (A, B) and DTG (C, D) measurements of the biocomposites reinforced with 20 and 30 % wt of SGW; DSC thermograms of (E) PLA20SGW and (F) PLA30SGW composites.

The effect of fiber incorporation and coupling agent treatment on the biocomposite's thermal behavior was assessed by DSC. The thermograms of **Figures 3.12** (E) and (F) present a single glass transition temperature (T_g) for all samples, ranging from 59 to 66 °C, as described in Table 3.8. An increment in the T_g was observed for PLA20SGW3, PLA20SGW5, PLA30SGW, and PLA30SGW3, indicating an improvement in the composite's thermal stability by an increase in the fiber-polymer entanglement, while other samples remained like neat PLA.

With the increase in GPS content from 7 to 10 wt%, a cold-crystallization phenomenon was observed for both fiber contents, presenting cold-crystallization temperatures (T_{cc}) between 100 and 123 °C and crystallization (T_c) between 114 and 128 °C. This demonstrates that the silane coupling agent promoted the recrystallization of PLA chains upon heating, promoting molecular entanglement by acting as a nucleating agent due to its epoxy group linkage with the PLA matrix hydroxyl end groups (Chun; Husseinsyah; Osman, 2012). While the PLA melting temperature (T_m) was measured as a single peak at 155 °C, the incorporation of 20 wt% SGW decreased it to 145 °C. However, T_m remained unchanged at 155 °C for 30 wt% SGW. As the presence of 7 to 10 wt% GPS affected both T_{cc} and T_c of PLA, the melting temperature was also changed, displaying a double melting peak and a decrease in the melting enthalpy (ΔH_m).

Regarding the degree of crystallinity (X_c), the neat PLA showed 37.3 % crystalline structure, which was reduced to 27.4 % and 24.0 % with the incorporation of 20 and 30 wt% SGW, respectively, decreasing the nucleation activity of these composites (Table 5). Slight modifications in the crystallinity were observed for the silane-treated composites with 3 and 5 wt% GPS. However, by increasing the GPS content to 7 and 10 wt%, the composite's crystallinity decreased to around 70 % for the 20 wt% SGW and to around 50 % for the 20 wt% SGW. The generation of mobility restrictions in the polymer chains by the higher content of the coupling agent led to changes in polymer rearrangement, decreasing the composite's degree of crystallinity. This was also related to the presence of a cold crystallization peak in these samples, which arises from the reorganization of amorphous domains into crystalline regions on account of the increased macromolecular flexibility upon a temperature increase during the analysis (Jandas et al., 2011).

3.4 CONCLUSION

The present chapter shows the feasibility of incorporating a high-yield mechanical pulp into PLA for the development of high-performance biocomposites through the partial modification of the fibers using a silane-coupling strategy. While a moderate increase in the tensile strength was found with the addition of 20 and 30 wt% SGW, accounting for 14 and 27 %, respectively, this enhancement was further increased when fibers were partially modified with GPS. Concretely, the biocomposites reinforced with 30 wt% SGW and modified with 5 and 7 wt% GPS revealed a tensile strength enhancement of 37.4 and 39.3 %, respectively. This was attributed to an improvement in the PLA-SGW interface, as well as to an appropriate

dispersion of the fibers within the polymer matrix. The micromechanical modeling revealed coupling factors of around 0.2, which have been previously reported for well-bonded systems. Flexural strength increased by around 15% and 29% with the increase of untreated SGW, while GPS coupling treatment most influenced the increase in flexural properties at 20 wt.% of SGW. These biocomposites stand out as a competitive alternative to commodity GF composites, such as the case of GF-reinforced PP, while exhibiting a much lower density. Although the inclusion of SGW influenced the rheological features of PLA, the obtained biocomposites were found to be processable, as revealed by the MFI measurements. There was an increase in complex viscosity and a reduction in the loss factor, suggesting predominantly elastic behavior. In addition, thermal stability was slightly improved, although no significant changes were found in the thermal properties of the biocomposites compared to neat PLA.

CHAPTER 4 – EFFECT OF TWO-STAGE FIBER SURFACE MODIFICATION: BLEACHING PROCESS AND SILYLATION IMPACT ON INTERFACIAL ADHESION OF PLA BIOCOMPOSITES

Note: All experimental work was developed in the laboratories of the LEPAMAP research group and facilities of the Universitat de Girona, Spain, except for the chemical composition of bleached fibers, which were realized at the laboratories of the LACTA research group at Universidade Federal do Paraná, Brazil.

4.1 INTRODUCTION

The performance of PLA-lignocellulosic composites is strongly dependent on the fiber-matrix interface, where the chemical and physical nature of the fiber surface controls adhesion and stress transfer (Oushabi, 2019). Among the fiber constituents, lignin plays a particularly critical role, influencing fiber hydrophobicity, surface energy, and chemical reactivity, thereby affecting the degree of compatibility with the PLA matrix (Mohammadi; Ishak; Sultan, 2024; Oushabi, 2019).

Due to their hydrophilic character and the presence of surface pectins and waxy substances, lignocellulosic fibers exhibit limited reactivity between their hydroxyl groups and polar or hydrophobic organic matrices. As a result, the composite may undergo premature degradation and a reduction in mechanical strength (Mohammed et al., 2022; Oushabi, 2019). One alternative to reduce fiber hydrophobicity and increase adhesion with polymeric matrices is to submit natural fiber to a delignification and/or bleaching process. This process decreases the lignin content of plant fibers, reduces their rigidity, and increases flexibility, since the cellulose fraction provides most of the tensile strength in the fibers (Delgado-Aguilar et al., 2018; Prome et al., 2025).

The bleaching processes commonly used in industry are based on acidic, alkaline, or oxidative methods (Barczewski; Matykiewicz; Szostak, 2020). Among them, acidified sodium chlorite ($NaClO_2$) is a well-established laboratory technique for lignin removal, enabling the evaluation of lignin's influence at the interface of polymeric composites (Yue et al., 2015). Sodium chlorite under acidic conditions generates chlorine dioxide (ClO_2) *in situ*, which acts

as the main oxidizing species. The ClO_2 molecules cleave the aromatic structures and conjugated double bonds within lignin, leading to cleavage of ether linkages (β–O–4) and oxidation of phenolic hydroxyl and carbonyl groups into soluble carboxylic acids and aldehydes (Guo et al., 2023; Kabir et al., 2012; Yue et al., 2015).

The partial removal of lignin and chromophoric compounds from lignocellulosic fibers opens the fiber structure and increases the exposure of surface hydroxyl groups (Khakalo et al., 2019). By disrupting portions of the lignin–hemicellulose, bleaching increases fiber accessibility and surface polarity, which can improve mechanical interlocking in composites but also makes the fiber more hydrophilic and more prone to moisture uptake (Hasan; Rabbi; Maruf Billah, 2022; Pinto et al., 2022). The cellulose-rich surface obtained after this treatment provides more available reactive sites for subsequent surface modification (Fazeli et al., 2024).

Two-step fiber treatment was studied to first activate and then functionalize the fiber surface, aiming to improve the composites' properties (Eng et al., 2014). Following bleaching, silylation can take advantage of the exposed hydroxyl groups to form covalent bonds between silane molecules and the fiber surface. The silane layer can improve adhesion and stress transfer at the fiber–matrix and protect the modified fiber from moisture-induced swelling (Mohammed et al., 2022). The effect of the two-step surface treatment was studied by Barczewski; Matykiewicz; Szostak (2020), on epoxy-based flax/cotton laminates composites. The fibers were bleached with hydrogen peroxide and then silylated, resulting in higher tensile and flexural strength compared to untreated fibers. Indicating that a surface free of impurities and non-cellulosic parts usually allows better polymer saturation, leading to improved physical adhesion at the interface (Mohammed et al., 2023).

In this way, this chapter explores the influence of controlled lignin removal by the acidified sodium chlorite bleaching process and GPS silylation on SGW pine fibers for PLA composites. The lignin content was verified as well as surface functionality, to elucidate how lignin mediates the efficiency of silane coupling and the mechanical and interfacial properties of PLA-lignocellulosic composites.

4.2 MATERIALS AND METHODS

The materials, composite production, and characterization methods employed in this chapter were the same as those presented in Chapter 3, except for the additional fiber bleaching stage, chemical composition of the bleached fiber, and the EDX analysis described below.

4.2.1 SGW BLEACHING AND SILYLATION

SWG fiber was dispersed in water using a baffled pilot-scale pulper at a consistency of 5 wt.% and stirred at 1100 rpm for 30 min at room temperature, promoting the disintegration of the initial fiber blocks and leading to fiber individualization and uniform pulp dispersion. After dispersion, the pulp consistency was verified to ensure it remained at 5 wt.% before being transferred to a 15 L stainless steel rotary reactor.

The bleaching process was carried out using approximately 800 g of dried fiber at a consistency of 5 wt.%. Sodium chlorite ($NaClO_2$, 15 wt.%) was used as the bleaching agent, with acetic acid (CH_3COOH, 10 wt.%) added to maintain the reaction medium at a pH of 3.8 ± 0.5, following a procedure similar to that reported by Yue et al. (2015) research. The reaction was conducted at 70 °C for three different bleaching times: 90 min (sample B1), 180 min (sample B2), and 270 min (sample B3).

After bleaching, the SGW fibers were thoroughly washed until the pH reached approximately 6–7, then air-dried at room temperature for 24 h and subsequently oven-dried at 80 °C for another 24 h. The bleached fraction intended for silylation was further processed by the dropwise addition of 5 wt.% γ-glycidoxypropyltrimethoxysilane (GPS) to the SGW pulp dispersed in water at a consistency of 3 wt.%, under gentle stirring for 30 min. The 5 wt.% GPS concentration was selected based on the optimal coupling agent performance identified in Chapter 3.

4.2.2 DETERMINATION OF LIGNIN AND STRUCTURAL CARBOHYDRATES IN THE BLEACHED FIBERS

The quantification of lignin and structural carbohydrates in bleached SGW pine fiber was carried out following the analytical protocol proposed by Sluiter et al. (2004) (NREL/TP-510-42618). The method enables the determination of acid-insoluble lignin by gravimetry, acid-soluble lignin by ultraviolet spectroscopy, and structural carbohydrates by high-performance liquid chromatography (HPLC), using the same acid hydrolysate.

Approximately 0.3 g of dry sample was hydrolyzed in test tubes with 3 mL of 72% (w/w) sulfuric acid for 1 h at 30 °C, with manual stirring every 5 min using a glass rod. The mixture was subsequently transferred to a glass flask and diluted to 4% sulfuric acid by adding

84 mL of distilled water. The flasks were sealed, homogenized, and autoclaved at 121 °C for 1 h. After cooling, the hydrolysates were filtered through Gooch crucibles at room temperature.

The crucibles were dried at 105 °C for 12 h to constant weight. The mass of the retained residue was used to determine the percentage of acid-insoluble lignin relative to the dry sample, discounting the ash content. The filtrate was quantitatively transferred to a 250 mL volumetric flask and subjected to spectrophotometric analysis at 240 nm to quantify the acid-soluble lignin, using a molar absorptivity of 12 $L \cdot g^{-1} \cdot cm^{-1}$ for pine wood lignin and the optical path length of the cuvette. Total lignin was obtained by the sum of insoluble and soluble lignin.

The hydrolysate was used for the determination of structural carbohydrates by HPLC (Shimadzu LC20AD system) equipped with an autosampler (SIL 10A), mobile phase degasser (DGU 14A), column oven (CTO 10A), and RID10A refractive index detector coupled to an SPD-M10Avp UV detector. Separation was performed on a Rezex RHM column (Phenomenex, 300 × 7.8 mm) at 65 °C, preceded by a Phenomenex pre-column (8.0 × 3.2 mm), using 5 $mmol \cdot L^{-1}$ H_2SO_4 as the mobile phase at a flow rate of 0.6 $mL \cdot min^{-1}$.

Quantification was performed by external standardization using calibration curves for each carbohydrate in the concentration ranges: 0.08–0.8 $g \cdot L^{-1}$ for cellobiose, 0.2–2 $g \cdot L^{-1}$ for glucose, 0.1–1 $g \cdot L^{-1}$ for xylose, 0.08–0.8 $g \cdot L^{-1}$ for arabinose, and 0.1–1 $g \cdot L^{-1}$ for acetic acid. The results were expressed in cellulose content for glucose results, and as hemicellulose for the sum of xylose and arabinose fraction.

4.2.3 SILYLATION EVALUATION BY ENERGY DISPERSIVE X-RAY SPECTROSCOPY (EDX)

Elemental silicon (Si) was identified on the surface of the silylated bleached fibers containing 5 wt.% of GPS, by Energy Dispersive X-ray Spectroscopy (EDX) coupled with Field Emission Scanning Electron Microscopy (FESEM). The analysis was conducted using a TESCAN Clara scanning electron microscope (TESCAN, Brno-Kohoutovice, Czech Republic), operated under high vacuum conditions at an accelerating voltage of 20 kV. This analysis enabled the quantitative determination of the atomic percentages of key elements present in the fiber surface, and possible effects of surface modification on lignin's inorganic content and thermal degradation residues.

4.3 RESULTS AND DISCUSSION

4.3.1 SURFACE TREATMENT INFLUENCE ON FIBER PROPERTIES

In order to assess the effect of structural fiber modification, **Table 4.1** provides a comparative analysis of the chemical composition and fiber morphology of the three bleaching stages of SGW fiber. The bleaching treatment progressively modified the fiber structure by removing partial lignin and hemicellulose fractions. The cellulose content increased from 42.3% in the untreated SGW (B0) to 49.5% in B3, reflecting the increase of cellulose as lignin and hemicellulose fractions were removed. The lignin content decreased by approximately 9%, 16%, and 29% for stages B1, B2, and B3, respectively, indicating a gradual delignification. In parallel, hemicelluloses decreased by approximately 35% after the first bleaching stage and remained nearly constant in subsequent stages, suggesting that most hemicellulose removal occurred during the B1 stage.

Table 4. 1 Chemical composition and morphological features of SGW bleaching stages.

Chemical composition (%)	B0	B1	B2	B3
Cellulose	42.3 ± 1.6	47.91 ± 1.1	48.40 ± 0.8	49.5 ± 1.0
Hemicelluloses	27.1 ± 2.1	17.5 ± 0.3	17.4 ± 0.4	17.5 ± 0.5
Klason lignin	29.6 ± 1.8	26.9 ± 1.1	24.7 ± 0.7	21.0 ± 1.5
Extractives	1.9 ± 0.2	-	-	-
Fiber morphology				
Length (μm)	497 ± 31	438 ± 42	428 ± 34	373 ± 27
Diameter (μm)	25.9 ± 1.8	24.3 ± 2.1	23.9 ± 1.6	23.2 ± 1.4
Fines (%)	40.5 ± 2.5	41.6 ± 1.3	42.1 ± 0.7	45.5 ± 1.1

Source: The author (2025).

In terms of morphology, bleaching resulted in progressive fiber shortening and a slight reduction in fiber length, with average lengths decreasing from 497 μm (B0) to 373 μm (B3) and diameters from 25.9 μm to 23.2 μm. The increase in fines content (from 40.5% to 45.5%) indicates partial fiber fragmentation induced by chemical treatment, caused by the removal of lignin that acts as a binding matrix, reducing fiber stiffness and promoting fibrillation (Yadav et al., 2022; Zhang et al., 2013). The presence of fines increases the specific surface area and exposes cellulose hydroxyl groups, promoting fibrillation that could enhance interfacial interactions with the polymer matrix, as a result of lignin removal, thereby improving the affinity for surface compatibilizers. However, the increase in fines content also contributes to the reduction of fiber stiffness, and the shortening of fibers may limit stress transfer efficiency and hinder the formation of an effective fiber network (Cosse et al., 2023; Sandquist; Thumm;

Dickson, 2019). Yemele et al. (2010) studied the influence of fines content in bark fibers/HDPE composites, and the results show lower modulus of elasticity and tensile strength, as well as less linear and more ductile stress-strain curves. These observations were attributed to poor dispersion of fine fibers in the plastic matrix, leading to stress concentration and low adhesion between the fibers and the matrix, as the fine content in the fiber fraction was increased.

In this way, fibrillation of the SGW fibers can be observed in **Figure 4.1** (A) by microscopy images of the unbleached fibers (B0) and the fibers bleached sequentially at 90 min intervals (B1, B2, and B3). However, no significant morphological changes were detected among the different bleaching stages. In **Figure 4.1** (B), the EDX micrographs highlight in green the presence of silicon (Si), the inorganic component of the GPS coupling agent, on the surface of the silylated fibers, confirming that the coupling reaction successfully occurred.

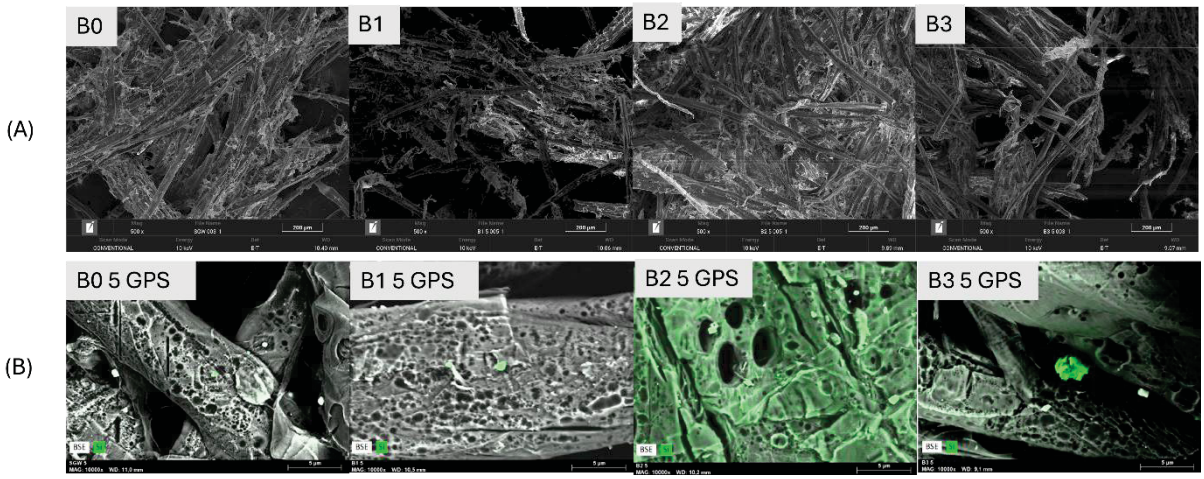

Figure 4. 1 Characterization of SGW fibers before and after surface modification: (A) microscopy image of bleached fibers; (B) EDX spectrum confirming elemental changes following silylation with 5% GPS.

4.3.3 BIOCOMPOSITES THERMO-RHEOLOGICAL PROPERTIES

Figure 4.2 (A) shows the thermal decomposition thermograms of bleached (B1, B2, and B3) and silylated biocomposites (5 wt.% % GPS) at SGE fiber concentration of 30 wt.% in comparison with unbleached fibers (B0). The composites display a single, dominant mass-loss event in the temperature range expected for PLA degradation, with the major weight-loss occurring roughly between 300–400 °C and a single, sharp peak in the derivative

thermogravimetry (**Figure 4.2** B). The overall maximum degradation temperature is around 380 °C and is similar across bleaching stages (from B0 to B3) and non-silylated and silylated samples, indicating that the principal thermal decomposition mechanism is driven by the PLA matrix. Minor differences were evident in the composites containing unbleached fiber (B0), showing a slightly higher residual mass at 600 °C than composites with bleached fibers (B1–B3). This trend is consistent with the higher lignin content of B0 (**Table 4.1**), since lignin is more thermally stable and tends to increase char yield. The presence of GPS does not markedly change the onset or peak decomposition temperatures, although small shifts in Tmax were observed.

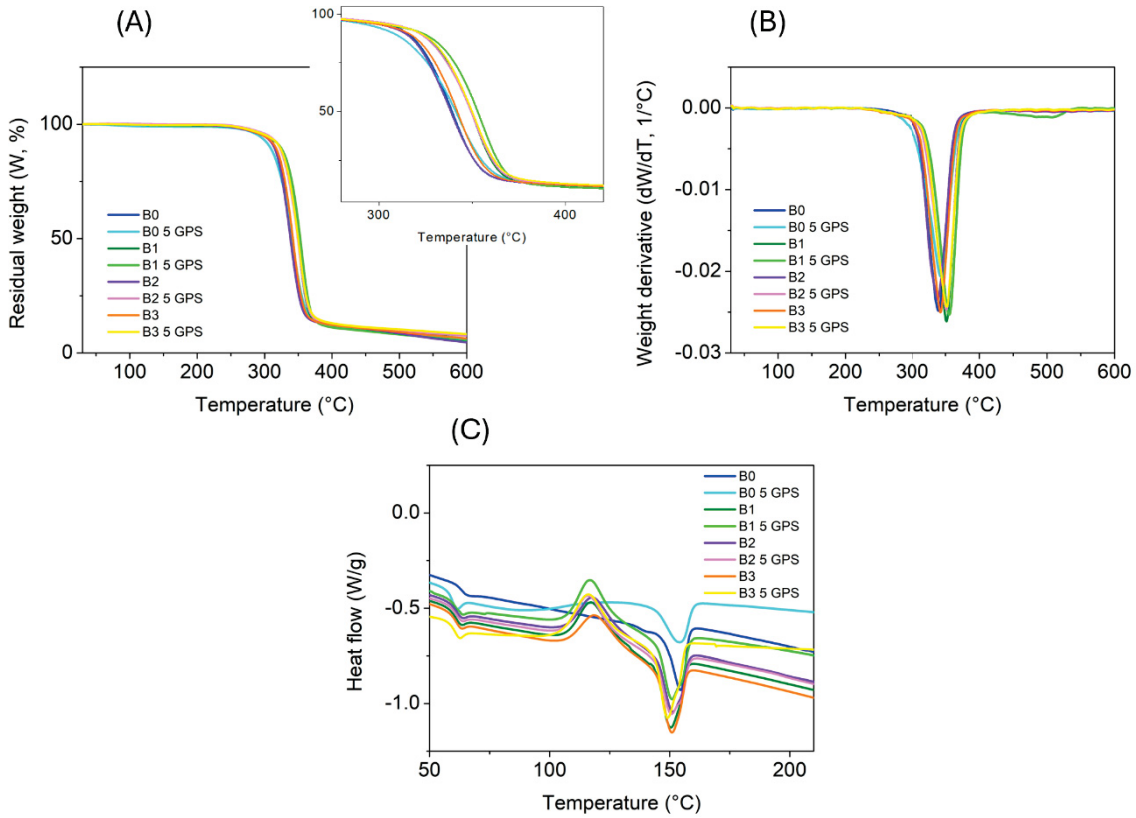

Figure 4. 2 TGA (A) and DTG (B) thermal decomposition thermograms and DSC (C) thermal events of the PLA and bleached SGW fiber composites.

The DSC thermal events in **Figure 4.2** (C) show the typical thermal transitions of semi-crystalline PLA, comprising a glass transition followed by cold crystallization and melting. All composites exhibit a Tg between 57 and 61 °C, which decreases progressively with increasing bleaching intensity, affected by the partial amorphous lignin removal (Fernandes et al., 2017; Rayung et al., 2014). However, the bleached fibers (B1-B3), which are richer in

cellulose and contain more fines, tend to modify the profile of the cold/melt crystallization peaks relative to B0, consistent with a change in nucleation efficiency and restriction of the mobility of the PLA chains near the fiber surface. Tcc and Tm values of the composites slightly increased from 115 to 118 °C, and from 149 to 151 °C, respectively, with the silylated samples exhibiting approximately 0.6 °C higher than the non-silylated ones.

Although the silylated samples show only modest changes in the thermal stability compared to non-silylated composites. These changes are consistent with improved fiber-matrix coupling that slightly alters the local chain mobility and the energetics of cold crystallization (Mlhem; Abu-Jdayil; Iqbal, 2023).

The rheological behavior of the PLA composites containing 30 wt.% SGW fibers with different bleaching stages is shown in **Figure 4.3**. The composites exhibited overall higher storage modulus (G′), loss modulus (G″), and complex viscosity (η*) than neat PLA across the entire frequency range, indicating an overall increase in melted elasticity and resistance to flow due to the presence of the fibrous phase (Qiao et al., 2021). This behavior evidences the formation of a solid-like structure in the melt, attributed to the restricted mobility of PLA chains caused by fiber–fiber and fiber–matrix interactions (Spiridon; Darie; Kangas, 2016).

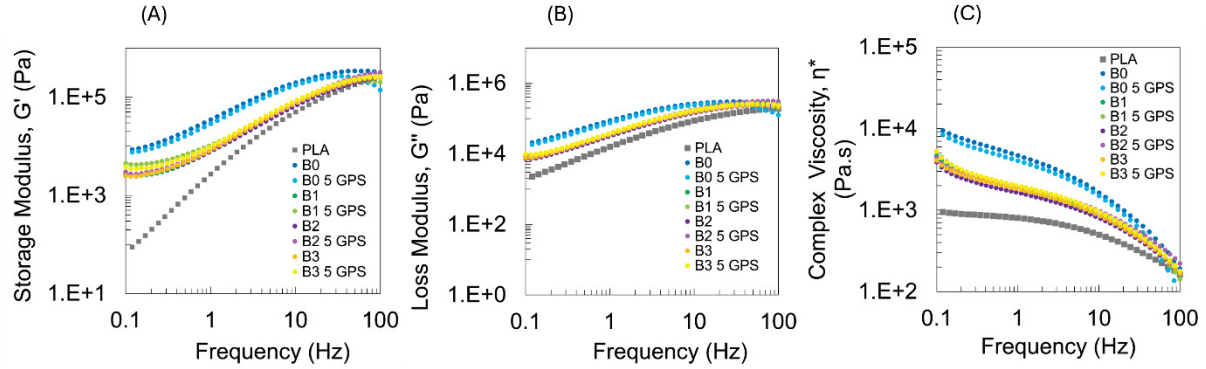

Figure 4. 3 Rheological properties of treated PLA and SGW composites.

Among the composites, the formulation containing unbleached fibers (B0) showed the highest values of G′ and η*, especially at low frequencies. This suggests a higher network structure resulting from the longer fibers, higher lignin content, and greater inter-fiber adhesion of the untreated material. Longer fibers create a more extended and interconnected network throughout the melt, and the presence of lignin promotes stronger inter-fiber adhesion (OA, 2017; Zhang et al., 2011). This structural arrangement restricts fiber mobility and hinders polymer chain flow, resulting in a composite that is less sensitive to shear rate. In contrast, bleaching and consequent fiber shortening reduce the aspect ratio and weaken fiber–fiber

interactions (Ilyas et al., 2022). Under these conditions, the fibers can more easily orient in the flow direction at elevated shear rates, facilitating melting flow and leading to a lower η* value and enhanced shear-thinning behavior (Zhang et al., 2011).

Such structural features enhance the elastic character of the melt and promote stronger fiber–fiber contact, thereby increasing the overall melt stiffness. In contrast, progressive bleaching (B1–B3) led to a gradual reduction in G', G'', and viscosity. The removal of lignin and hemicellulose, coupled with fiber shortening and the generation of fines (**Table 4.1**), weakened the percolated structure within the PLA matrix. Consequently, the bleached fibers displayed reduced ability to form network-like arrangements, resulting in lower melting elasticity (Cui et al., 2021).

The silylation with 5 wt.% of GPS coupling agent moderated an increase in both G′ and η* for all bleaching levels, suggesting improved interfacial adhesion between the modified fibers and PLA. In Chapter 3, in the study of unbleached SGW composites, the incorporation of the coupling agent led to a slight decrease in complex viscosity. This effect can be attributed to the plasticization promoted by silylation at the fiber-matrix interface, reducing inter-fiber interactions, and enhancing chain mobility within the PLA melt. As a result, the overall melt flowability increases despite the inherently higher aspect ratio of the unbleached fibers (Yang et al., 2020b). However, after bleaching, the silylated fibers promote a slight increase in the composite's complex viscosity. This behavior is attributed to the greater exposure of cellulose microfibrils following lignin removal, which enhances the availability of hydroxyl groups for silane bonding (Chen et al., 2021).

4.3.4 MECHANICAL PROPERTIES

The tensile strength of the PLA composites containing 30 wt% SGW fibers at different bleaching stages is shown in **Figure 4.4**. The incorporation of fibers significantly modified the mechanical behavior of PLA. Composites reinforced with unbleached fibers (B0) exhibited the highest tensile strength among all formulations, reaching values around 70 MPa for the non-silylated and above 75 MPa for the silylated fibers. These values represent a considerable improvement compared to neat PLA (around 53 MPa), indicating efficient stress transfer between the PLA matrix and the unbleached fibers. The higher tensile results for B0 composites can be attributed to their higher lignin content and longer fiber length (**Table 4.1**), which promotes stronger inter-fiber cohesion and a more continuous reinforcing network. The high

melt stiffness observed in rheological tests for these formulations (**Figure 4.3**) also supports the presence of a well-developed fiber network contributing to load-bearing capacity in the solid composite.

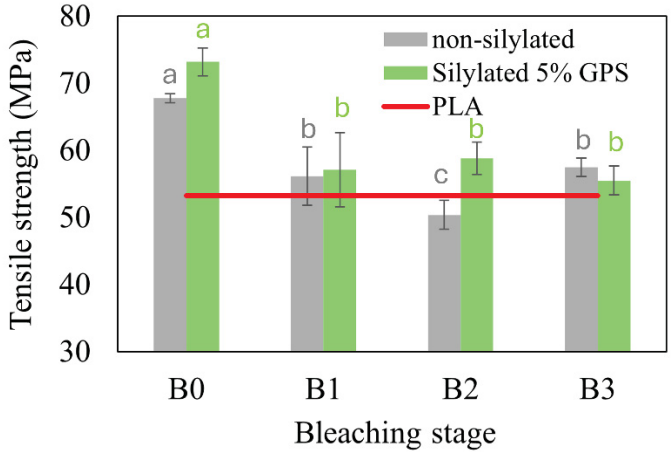

Figure 4. 4 Tensile results of the mechanical properties of PLA composites and modified fibers. Distinct letters represent statistical differences by Tukey's HSD test ($p < 0.05$).

On the other hand, progressively bleached fibers (B1, B2, B3) resulted in lower tensile strengths, with values decreasing to around 50-55 MPa, comparable to or slightly below neat PLA. The loss of reinforcing efficiency can be associated with the weakening of the fiber structure, reducing fiber length, and limiting the mechanical interlocking with the matrix. Additionally, the higher fines content and smoother fiber surfaces after bleaching may hinder stress transfer, leading to premature debonding under tension (Pickering; Efendy; Le, 2016). This reflects the decrease in overall tensile properties, such as Young's modulus and elongation at break, as shown in **Table 4.2**.

Table 4. 2 Tensile properties of bleached SGW-PLA composites

Sample	σ_t^c (MPa)	E_t^c (GPa)	ε_t^c (%)
PLA	53.27 ± 2.14 a (a)	3.8 ± 0.1	3.22 ± 0.01
B0	67.77 ± 0.65 b	6.8 ± 0.1	2.62 ± 0.08
B0 5 GPS	73.19 ± 2.08 (b)	6.8 ± 0.2	2.84 ± 0.28
B1	56.16 ± 4.32 a	2.1 ± 0.6	2.76 ± 0.39
B1 5 GPS	57.14 ± 5.53 (c)	2.0 ± 0.3	3.21 ± 0.35
B2	50.39 ± 2.15 a	2.7 ± 0.1	2.19 ± 0.19
B2 5 GPS	58.83 ± 2.42 (c)	2.4 ± 0.2	2.91 ± 0.13
B3	57.49 ± 1.39 a	2.0 ± 0.4	2.84 ± 0.28
B3 5GPS	55.49 ± 2.15 (c)	2.4 ± 0.3	3.75 ± 0.20

σ_t^c: tensile strength; E_t^c: Young's modulus; ε_t^c: elongation at break.
Distinct letters represent statistical differences by Tukey's HSD test ($p < 0.05$) for σt^c results: a, b, and c for comparison between lignin concentrations and (a), (b), and (c) for comparison between GPS concentrations.

Although the increase in fines content enhances the specific surface, which could promote greater interaction with silane coupling agents such as GPS, this effect does not compensate for the structural losses associated with fiber fragmentation, also leading to fiber aggregation (Xie et al., 2010). The reduced fiber length and stiffness limit effective stress transfer and hinder the formation of a mechanically efficient fiber network (Mallick, 2018). As a result, the reinforcing potential of the fibers is diminished, and the system behaves more like a particulate-filled composite rather than a fiber-reinforced material (Chaudhary; Rajput; Bajpai, 2017). Therefore, despite the improved interfacial chemistry, excessive fibrillation leads to an overall reduction in mechanical performance.

Silylation significantly ($p < 0.05$) increased the tensile strength only for the unbleached (B0) and moderately bleached (B2) fibers. However, the treatment was more aggressive for B2, resulting in a reduction in tensile strength value. Overall, the two-stage fiber treatment, bleaching followed by silylation, led to lower mechanical performance of the composites compared with those produced using untreated fibers. Although GPS promotes better interfacial adhesion and is effective even in partially delignified fibers, the two-stage treatment created a limit on reinforcement efficiency due to the loss of fiber integrity, and the aspect ratio cannot be fully compensated by improved interface bonding (Pickering; Efendy; Le, 2016).

Asim et al. (2016) investigated the effects of alkali and silane treatments on the mechanical performance and interfacial adhesion of kenaf and pineapple leaf fibers, reporting that silane treatment alone produced the highest tensile strength. The maximum tensile modulus was also achieved in fibers treated exclusively with the silane solution. However, when delignification was combined with silylation, the tensile strength decreased, indicating that the removal of lignin and the associated reduction in structural integrity outweighed the benefits of improved interfacial bonding. Residual lignin plays an important role as an interfacial mediator between cellulose fibers and coupling agents such as silanes. Due to its aromatic structure and the presence of phenolic and aliphatic hydroxyl groups, lignin can act as a natural primer, improving silane anchoring and interfacial compatibility. However, lignin also contributes significantly to the mechanical integrity of the fiber cell wall, particularly in the S2 layer, where it provides stiffness and structural cohesion (Dong et al., 2020; Li et al., 2025).

In composites, Barczewski; Matykiewicz; Szostak, (2020) studied the effect of two-step surface treatment by hydrogen peroxide and silylation of flax/cotton fabrics on epoxy-based laminates, obtaining lower tensile strength results for the composites containing bleached fibers, while further silylation slightly increased. However, the results were lower than those

using untreated fibers. This may be caused by the excessive lignin removal during bleaching, although beneficial for surface activation and fibrillation, which leads to fiber weakening, increased fragmentation, and reduced load-bearing efficiency (Klunklin et al., 2023; Najahi et al., 2023).

4.4 CONCLUSION

The progressive bleaching of SGW fibers induced simultaneous changes in their chemical composition and morphology, which directly influenced the structure–property relationships of the PLA composites. The removal of lignin and hemicellulose (up to approximately 29% and 35%, respectively) increased cellulose purity but also shortened the fibers and generated a higher fines content. These structural modifications weakened the fiber network formed within the PLA matrix, as evidenced by the reduction in storage modulus (G′) and complex viscosity (η*) in the rheological analyses.

Consequently, the unbleached fibers (B0), which presented higher lignin content and aspect ratio, promoted more pronounced melt structuring and produced composites with the highest tensile strength. On the other hand, extensive bleaching (B3) reduced fiber–fiber connectivity and the efficiency of mechanical reinforcement, despite facilitating melt flow and processability. The addition of 5 wt% of the GPS coupling agent consistently improved interfacial adhesion, increasing tensile strength and slightly enhancing melt elasticity, particularly for less-bleached fibers, in which the residual lignin provided abundant reactive sites for silane bonding.

These results demonstrate a clear relationship between fiber chemical structure, morphology, and interfacial compatibility. However, bleaching combined with silane treatment limited reinforcement efficiency due to the loss of fiber integrity. This couldn’t achieve a balanced compromise between processability, interfacial adhesion, and mechanical performance in PLA/SGW composites, where lignin plays an important role in SGW fiber composites.

CHAPTER 5 – LIGNIN SILYLATION INFLUENCE ON PLA BIOCOMPOSITES: A COMPARISON BETWEEN SOFT AND HARDWOOD LIGNIN

This work has been published in the journal ACS Biomacromolecules as:
GIULIA HERBST, GABRIELA ADRIANA BASTIDA, QUIM TARRÉS, MARCOS LÚCIO CORAZZA, LUIZ PEREIRA RAMOS, MARC DELGADO-AGUILAR. Silylated Softwood and Hardwood Lignin: Impact on Thermomechanical and Interfacial Properties of PLA Biocomposites. ***ACS Biomacromolecules****, Volume 26, 2025.*
https://doi.org/10.1021/acs.biomac.5c01179

Note: All experimental work was developed in the laboratories of the LEPAMAP research group and facilities of the Universitat de Girona, Spain.

5.1 INTRODUCTION

Effective compatibilization remains one of the main challenges in developing functional poly (lactic acid) (PLA) biocomposites (Tham et al., 2022). Surface compatibilization is critical in determining the performance of polymer biocomposites reinforced with particulate or fibrous fillers (Mohammed et al., 2022b). Effective stress transfer, uniform dispersion, and interfacial stability are dependent on the chemical and physical compatibility between the polymer matrix and the filler surface (Fredi; Dorigato, 2024). In many cases, inherent differences in polarity, surface energy, or functional group availability led to poor interfacial adhesion, resulting in phase separation, agglomeration, and compromised mechanical or barrier properties (Zhou; Fan; Chen, 2016).

PLA offers a renewable platform for a sustainable, competitive alternative to fossil-based polymers, especially for packaging and film applications. Its intrinsic brittleness and low barrier performance limit broader utility (Tripathi; Misra; Mohanty, 2021). Lignin, with its aromatic content, antioxidant properties, and UV-blocking properties, has been proposed as a multifunctional additive in the field of food packaging, biomedicine, agriculture, and biomass conversion (Shu et al., 2021). However, as with many fillers, its incorporation often results in poor dispersion and phase separation due to limited compatibility with PLA (Mariana et al., 2021). Lignin's chemical heterogeneity, driven by both its botanical origin and extraction

process, strongly influences its behavior in polymer matrices, even though its hydroxyl groups are capable of forming numerous hydrogen bonds (Alam et al., 2024; Andriani; Lawoko, 2024; Zhang et al., 2024a). In particular, softwood lignins are typically rich in guaiacyl, exhibiting a more recalcitrant structure due to higher quantities of β-5′ and 5-5’ linkages. In contrast, hardwood lignins have a higher syringyl-to-guaiacyl ratio, demonstrating a less recalcitrant and more accessible structure, which affects their polarity, branching, and reactivity (Mei et al., 2019; Suota et al., 2021; Trentin et al., 2025). Due to lignin's distinct structural characteristics, selecting an appropriate lignin type is crucial for optimizing polymer-lignin interactions and determining a suitable surface modification strategy.

Lignin acetylation (Johansson et al., 2023), esterification (Luo; Cao; McDonald, 2017), synthetic chain grafting (Bhadane et al., 2025; Kim; Chung, 2024), and silylation (Sekar et al., 2023) are techniques that confer lignin polarity or introduce reactive groups that improve interfacial bonding. Silylation has been widely applied due to its ability to introduce organofunctional silane groups that can act as molecular bridges between the lignin surface and the polymer matrix, improving dispersion and adhesion by bonding with available hydroxyl groups present in the lignocellulosic fraction of natural fibers (Buono et al., 2016; Sayadi; Brouillette, 2024; Trejo-Cáceres; Martín-Alfonso; Franco, 2025). In previous research, silane coupling agents were successfully grafted onto lignocellulosic fiber surfaces via condensation reactions, especially improving the mechanical properties of PLA biocomposites (Herbst et al., 2024).

Although several studies have investigated individual modification methods, without systematic comparisons between different lignin sources, particularly in the context of surface-modified PLA biocomposites, remain limited. For instance, Zhu et al., (2015) studied the effect of three different silane coupling agents at 2 wt.% concentration on the silylation of lignin and obtained the maximum tensile strength and Young’s modulus improvement at 5 wt.% of lignin, with an increase of around 10% compared to neat PLA. Similarly, Wang et al., (2020) investigated a technical lignin silylated at multiple concentrations (1, 3, and 5 wt.%) in PLA and found minimal improvements in tensile strength, accompanied by persistent agglomeration and low dispersion in both the unmodified and silylated forms.

This study investigates the impact of two chemically distinct technical lignins, softwood (LS) and hardwood lignin (LH), on the structural and functional properties of PLA-based composite films before and after surface modification by silylation. Lignin’s inherent molecular structure, polarity, and functional group variability were approached, and its

influence on dispersion, compatibility, and interfacial bonding within the PLA matrix was assessed by film production. This comparative study provides insights into lignin-biopolymer systems through source-specific compatibilization strategies.

5.2 MATERIALS AND METHODS

5.2.1 MATERIALS

Poly (lactic acid) pellets (PLA, Ingeo™ Biopolymer 4043D) purchased from NatureWorks LLC (Plymouth, Minnesota, USA), with a specific gravity of 1.24 g/cm^3, melt flow index (210 °C/ 2.16 kg) of 6 g/10 min, and an average molecular weight of 111 kDa were used as the matrix to produce biocomposites. Kraft softwood and hardwood lignin (LignoForce™) were provided by FPInnovations (Pointe-Claire, QC, Canada). The softwood lignin (LS) was produced from the black liquor of a wood mixture of pine (*Pinus contorta*), spruce, and fir trees at a ratio of 74:25:2, with a molecular weight of 9813 mol/g, and a total OH groups of 6.4 ± 0.4 mmol/g. The hardwood lignin (LH) was produced from the black liquor of aspen wood, with a molecular weight of 4224 mol/g and a total OH groups of 5.8 ± 0.4 mmol/g. Lignin full characterizations were provided by Suota et al (2021)(Suota et al., 2021b). (3-glycidyloxypropyl) trimethoxysilane (GPS), acquired at Merck (Barcelona, Spain), was selected as a coupling agent, aiming at enhancing the interfacial strength of the produced biocomposites.

5.2.2 SOFTWOOD AND HARDWOOD LIGNIN SILYLATION REACTION

Lignin was dispersed in water at a concentration of 10 wt.% under mechanical agitation at 700 rpm at room temperature. Silane coupling agent (GPS) was added dropwise at 1, 3, and 5 wt.% concentrations (concerning the dry weight of lignin) and kept under stirring for 30 min. The lignin-dispersed solution was oven-dried at 60 °C until a moisture content of around 4 wt.% was achieved. To complete the silylation reaction, the samples were placed in an oven at 80 °C for 24 hours before the biocomposites' melt-compounding.

5.2.3 SILYLATED LIGNIN CHARACTERIZATIONS

FTIR-ATR spectroscopy analysis was performed to assess differences in lignin structure and the effect of the coupling agent on unmodified and silylated (1, 3, and 5 wt.% of GPS) LS and LH lignin's chemical composition using a compact spectrometer Alpha II (Bruker Corporation, Massachusetts, United States). Spectra were acquired from a platinum ATR MIR single-reflection accessory at a resolution of 4 cm^{-1}, scanned at a wavenumber within the range from 400 to 4000 cm^{-1}. Analysis of spectra was performed using OPUS_7.5.18 software.

Thermal analysis was conducted to identify evidence of silylation after GPS addition. Thermogravimetric analysis (TGA) was conducted in a temperature range from 30 to 600 °C at a heating rate of 10 °C min^{-1} under an inert nitrogen atmosphere. Glass transition temperatures (T_g) of the unmodified and modified lignin were obtained from differential scanning calorimetry (DSC, DSC822e, Mettler-Toledo, LLC, USA) and analyzed at a heating/cooling rate of 10 °C min^{-1} from 30 to 210 °C under an inert N_2 atmosphere. TGA and DSC analyses were performed over both LS and LH lignins, unmodified and modified with a 5 wt.% addition of GPS.

The ash content of both unmodified and silylated (containing 1, 3, and 5 wt.% of GPS) LS and LH lignin was determined according to TAPPI T211 Ash in wood, pulp, paper, and paperboard (TAPPI, 2007). The samples were ignited in a muffle furnace at 525 ± 25 °C, starting at 250 ºC for one hour, then 350 ºC for another hour, and finally the temperature increased to 525 ºC until constant weight was achieved.

The elemental composition of the ash residues from both unmodified and silylated lignin (containing 1, 3, and 5 wt.% of GPS) was analyzed using Energy Dispersive X-ray Spectroscopy (EDX) coupled with Field Emission Scanning Electron Microscopy (FESEM). The analysis was conducted using a TESCAN Clara scanning electron microscope (TESCAN, Brno-Kohoutovice, Czech Republic), operated under high vacuum conditions at an accelerating voltage of 20 kV. This analysis enabled the quantitative determination of the atomic percentages of key elements present in the ash, and possible effects of surface modification on lignin's inorganic content and thermal degradation residues.

5.2.4 COMPOSITE MELTING-MIXING AND HOT-PRESSING FILM PRODUCTION

PLA and lignin were compounded using an internal mixer plastograph (Brabender® GmbH & Co. KG, Duisburg, Germany). The equipment consists of a measuring mixer chamber equipped with two counterrotating screws with a processing volume of approximately 55 cm^3.

The raw material was loaded through the top opening into the heated mixer bowl, homogenized by two mixing blades with a roller shape and a rotor speed of 80 rpm, at 195 °C, until a constant torque of the melt compound. Both LS and LH lignins (unmodified and modified) were added at 5, 10, and 15 wt.%, respectively. The biocomposites were discharged, cooled down, and milled using a knife mill (SM 100, Retsch GmbH, Haan, Germany) equipped with a 4 mm sieve at the bottom.

Neat PLA and its biocomposites containing unmodified and silylated LS and LH lignin films were produced by hot press molding, in an IDM TEST equipment (Madrid, Spain). Approximately 3 g of each sample, previously oven-dried at 80 °C for 24 h, were placed between high-strength polyester films to facilitate removal from the hot-press metal plates and then molded at 200 °C. The samples were preheated for 60 s, pressed at 45 bar for more than 60 s, and then cooled to room temperature. The resulting film thicknesses were approximately 0.18 ± 0.01 mm for the PLA biocomposites, 0.17 ± 0.02 mm for PLA-LS, and 0.18 ± 0.01 mm for PLA-LH.

5.2.5 THERMAL AND RHEOLOGICAL BEHAVIOR OF THE BIOCOMPOSITES

TGA and DSC analyses of the obtained biocomposites were conducted as described in the item “5.2.3 Silylated lignin characterizations”. Melt flow index (MFI) measurements were conducted in CEAST testing equipment (7082,000, series 17959, Pianezza TO, Italy), according to ISO1133. The extrusion rate was determined as the mass extruded over a specified time under prescribed conditions of 210 °C and a load of 2.16 kg, as described in the datasheet of the PLA applied in this work. The rheological properties, including storage modulus, loss modulus, and complex viscosity of the biocomposites, were measured following the ASTM D4440–15 standards using a modular rheometer (model MCR 302e, Anton Paar GmbH, Graz, Austria). The measurements were taken in oscillatory mode, at the PLA melt state at 190 °C, between a parallel plate geometry arrangement with a gap of 1 mm. The frequency range used was set between 0.1 and 100 Hz. The linear viscoelastic region was determined by an amplitude sweep deformation of 5 %, with controlled shear deformation.

5.2.6 TENSILE PROPERTIES OF PLA/LIGNIN FILMS

Tensile properties were evaluated using an INSTRON 3340 testing machine equipped with a 100 N load cell, in accordance with ASTM D882 for thin plastic films under 1mm thick. Measurements were performed on strips with dimensions of 15 mm width and 80 mm length at a crosshead speed of 5 mm/min.

5.2.7 BARRIER AND SURFACE PROPERTIES OF PLA/LIGNIN FILMS

The obtained PLA/lignin films' UV-shielding properties were accessed by a Shimadzu UV-1280 spectrophotometer (Duisburg, European branch office) in the wavelength range 200–800 nm, which was used to measure the transmittance (%) spectra of the specimens. This wavelength range covered both UV and visible light. All samples were cut into a rectangular shape (4 cm × 0.8 cm), placed in a cuvette, measured in triplicate, and used air as a reference.

The water vapor transmission rate (WVTR) of the films was estimated by the dry cup method according to the ASTM E-96 standard. The films were cut into circles with a diameter of 6.0 cm and placed in impermeable O-ring cups containing silica gel. The cups were sealed and conditioned at 23 °C with a relative humidity of 50%. After 24 h, the overall weight of the cup, silica gel, and film was measured. The difference was assigned to the moisture uptake of the silica gel, and the WVTR value corresponding to each sample was determined.

The surface hydrophobicity of PLA/lignin films was evaluated by measuring the static water contact angle using a DSSA25 droplet shape analyzer (Krüss GmbH, Germany) equipped with Krüss Advance software. Measurements were performed at room temperature, with data acquisition at a rate of two measurements per second.

5.2.8 STATISTICAL ANALYSIS

Analysis of variance (ANOVA) and pairwise multiple comparisons with Tukey’s HSD (honestly significant difference) test ($p < 0.05$) were performed using Excel to identify significant differences between LS and LH lignins composition, as well as the impact of the

GPS coupling agent on mechanical and barrier properties, including water vapor transmission rate (WVTR) and water contact angle (WCA).

5.3 RESULTS AND DISCUSSION

5.3.1 EFFECT OF GPS INCORPORATION ON LIGNIN SAMPLES

The structural differences between the LS and LH lignins were investigated by FTIR-ATR analysis, as shown in **Figure 5.1**. Typical vibrations of both lignins were shown around 3300 cm^{-1} corresponding to phenolic OH and aliphatic OH groups, followed by vibrations at around 2900 and 2800 cm^{-1} corresponding to methoxyl and methyl. Also, C=O stretch in ketones, aldehydes, and carboxylic acid groups bands in 1700 and 1650 cm^{-1}, aromatic skeletal vibrations between 1595 and 1510 cm^{-1}, at around 1460 cm^{-1} C-H deformation in $–CH_3$ and $–CH_2$ groups, and C-C, C-O, C=O stretching at 1225-1274 cm^{-1}. Primary alcohol and aliphatic ester C-O stretching were observed in 1085-1030 cm^{-1} (Zhou et al., 2016).

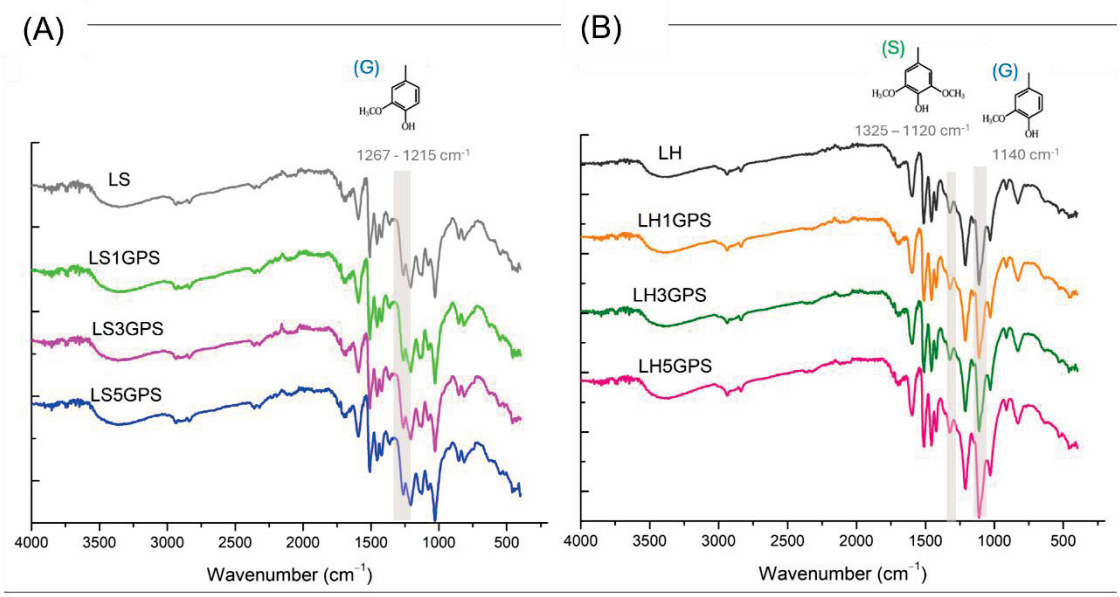

Figure 5. 1 FT-IR spectra of unmodified and silylated soft (A) and hardwood (B) lignin.

Figure 5.1A shows LS specific strong vibrations on 1267 cm^{-1} for the guaiacyl ring (G), 1215 cm^{-1} for C–O stretching in G, and at 835 $cm^{-1,}$ C-H aromatic bending deformation (Rashid; Kait; Murugesan, 2016). While for LH, **Figure 5.1B**, 1325 cm^{-1} vibrations of syringyl ring (S), 1120 cm^{-1} C-H plane deformation of S units, and at 1140 cm^{-1} for G units (Zhou et al., 2016). Although silylation did not produce observable changes in either LS or LH for the

applied GPS concentration, this may be attributed to the limited sensitivity of the characterization method employed.

The lignin silylation was evaluated by assessing the differences in thermal properties of both LS and LH lignins at a 5 wt.% GPS addition and compared to the unmodified ones. **Figure 5.2A** shows the degradation profile of both unmodified and silylated lignins in a single step between 30 and 600 °C. Three thermal events were observed, as depicted from the derivative thermogravimetric curve (DTG, **Figure 5.2B**), corresponding to moisture release (around 100 °C), followed by the breaking of more labile chemical bonds (between 360 and 380 °C), and the breakage of more stable C–C bonds at temperatures higher than 450 °C. Evaluating the data presented in **Table 5.1**, the silylation showed no effect on softwood lignin (LS5%GPS), maintaining its thermal stability as neat LS. Suota et al. (2021) characterized both LS and LH technical lignins used in this work and attributed the higher thermal stability of LS lignin to the predominance of guaiacyl units, which tend to undergo condensation at the free C5 position. These reactions lead to the formation of thermally stable carbon-carbon bonds, including 5-5' and β-β' bonds. On the other hand, the silylation of hardwood (LH5%GPS) was able to shift both degradation initial temperatures (T_{onset}) at 5% and 50% mass loss, promoting an increase of around 30 °C and 90 °C, respectively, indicating effective crosslinking between LH and the coupling agent GPS.

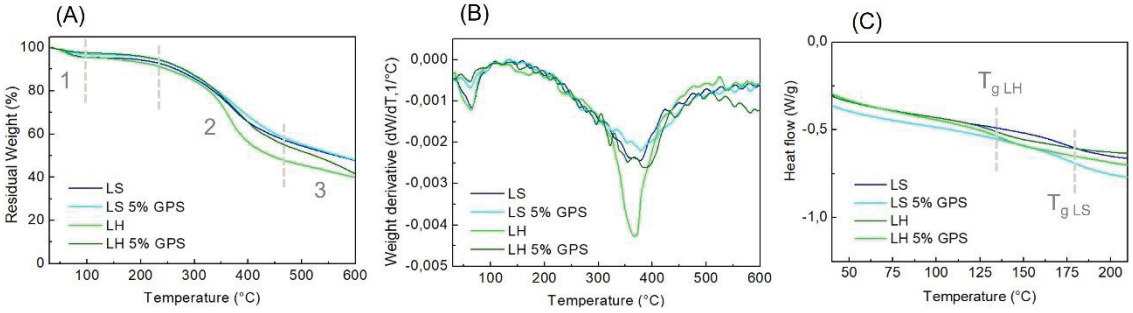

Figure 5. 2 TGA (A), DTG (B), and DSC (C) thermograms of unmodified and silylated soft and hardwood, and lignins.

The GPS also induced shifts in the lignin T_g, increasing by around 3 and 7 °C for LS5%GPS and LH5%GPS, respectively, compared to their unmodified counterparts. Buono et al. (2016) (Buono et al., 2016) found that silylation using tert-butyldimethylsilyl chloride (TBDMSCl) led to an increase in T_g. This was attributed to the introduction of bulky silyl groups that restrict the mobility of the lignin chains, thereby raising the T_g.

Table 5. 1 Thermal properties of unmodified and silylated LS and LH lignins.

Lignin sample	T_{onset} (°C)[a]	T_{50} (°C)[b]	Residual (%)	DTG $_{max.}$	T_g (°C)[c]
LS	232.3	564.3	48.1	377.0	177.3
LS 5% GPS	233.3	564.3	48.1	378.2	180.5
LH	213.8	433.3	41.7	366.7	132.7
LH 5 % GPS	240.8	523.6	40.2	386.6	139.3

[a] T_{onset} = first temperature of degradation registered at 5% mass loss.
[b] T_{50} = 50 % mass loss temperature.
[c] T_g = glass transition temperature determined by DSC.

In order to verify lignin silylation reaction, a simple technique as the ash determination, was applied to evaluate the degree of GPS coupling. **Figure 5.3** shows the variation in the color of ash at varying GPS content. Ash color is essentially related to the inorganic composition of materials (Rodela; Chowdhury; Hohner, 2022). Unmodified LS showed white coloring due to the higher amounts of calcium in its composition (around 4% of total ash content), while LH presented a light orange coloring due to higher amounts of potassium (around 4 % of total ash content)(Suota et al., 2021b). High concentrations of calcium and magnesium promote the formation of light-colored oxides such as CaO and MgO, typically resulting in white or light gray ash residues. Conversely, high potassium levels often contribute to yellow-orange hues due to the formation of potassium-based salts (Werkelin; Skrifvars; Hupa, 2005). However, the final ash coloration is a complex outcome determined by the combined effects of all the present inorganic elements in the original biomass, including but not limited to iron, which can also impart reddish-brown tones, and manganese, potentially leading to greenish or blackish coloration (Bodí et al., 2014; Magdziarz et al., 2018). The interaction and potential formation of complex compounds among these elements further contribute to the diversity of observed ash colors.

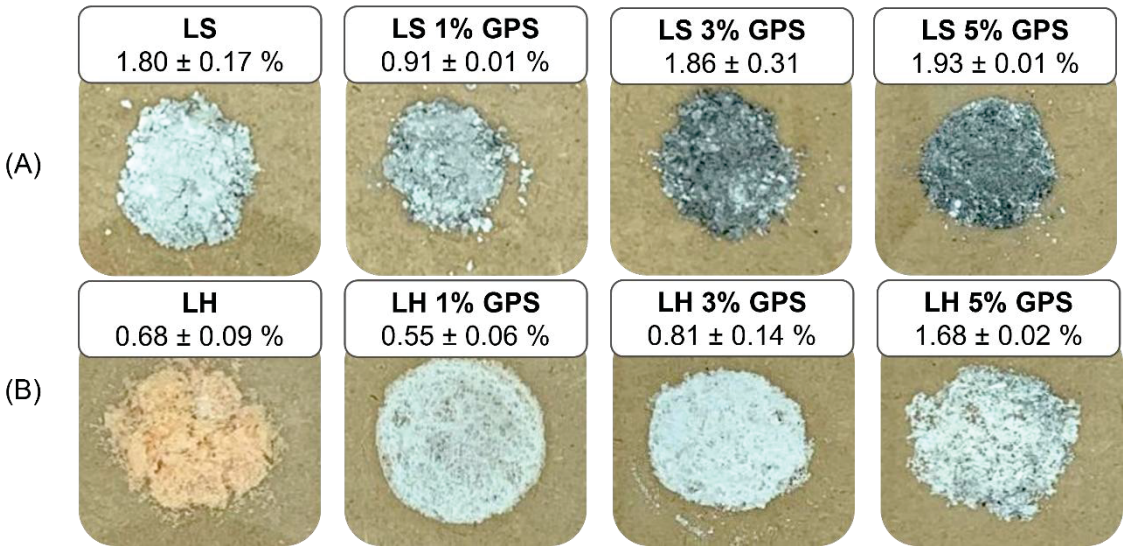

Figure 5. 3 Visual appearance of LS (A) and LH (B) samples after combustion for ash determination at different GPS content.

The silylation degree reflected changes in the material's thermal decomposition behavior and inorganic composition. As the concentration of the GPS coupling agent increases, the silylation promoted LS coloring turns from light to dark gray. The incorporation of organosilicons alters the combustion process, often resulting in lighter-toned ash due to higher silica content and reduced carbonaceous residues (Rodela; Chowdhury; Hohner, 2022). **Figure 5.4** shows the ash elemental average composition of the unmodified and silylated lignins.

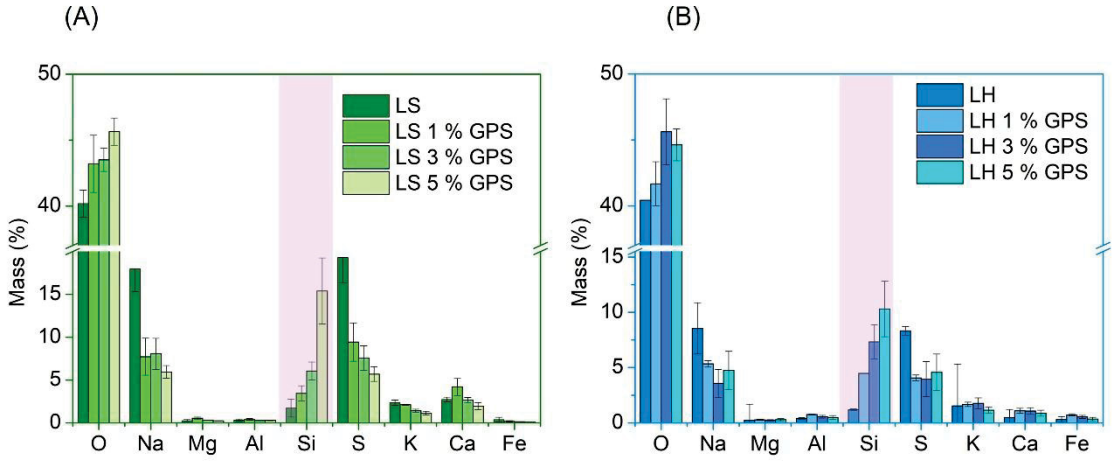

Figure 5. 4 Ash average elemental composition of unmodified and silylated LS (A) and LH (B) with 1, 3, and 5 wt.% of coupling agent.

Sodium (Na) and sulfur (S) were the predominant elements found in both lignin ash samples, excluding oxygen (O), and the not showed carbon content of around 40% presented in all the samples as a consequence of the sample preparation. Silicon (Si) was also detected in

small amounts, due to its natural absorption by plants (Oo et al., 2021). However, after the silylation reaction with concentrations of 1, 3, and 5% of GPS, the silicon content in the lignin ash increased proportionally, indicating successful grafting and retention of silane moieties.

5.3.2 THERMAL PROPERTIES OF PLA/LIGNIN BIOCOMPOSITES

The rheological properties of unmodified LS and LH PLA-filled biocomposites compared to the neat matrix at 190 °C and as a function of frequency are shown in **Figure 5.5**. Both storage modulus (elastic, G') and loss modulus (viscous, G'') slightly decreased in the presence of both LS (**Figure 5.5A**) and LH (**Figure 5.5B**) lignins, indicating that the composite materials are softer and more compliant, especially at lignin loadings of 5 and 15 wt.%.

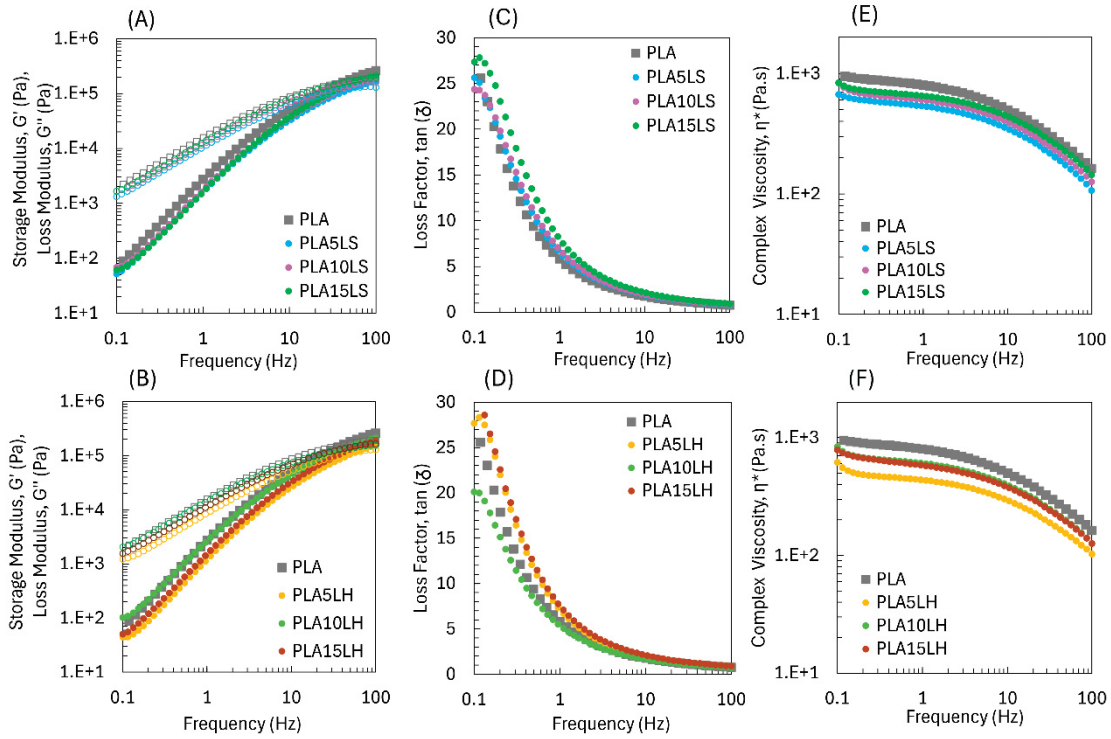

Figure 5. 5 Rheological curves of unmodified softwood and hardwood lignin on PLA.

In addition, both the composite materials and neat PLA exhibited predominantly viscous behavior, as indicated by higher G″ values compared to G'. This observation is further supported by the loss factor (tan δ) results shown in **Figure 5.5C** for softwood lignin, where the biocomposites displayed crossover points (tan δ = G'/G'' = 1) at higher frequencies, ranging from 50 to 75 Hz, in contrast to neat PLA, which showed a crossover around 40 Hz. This shift toward higher frequencies suggests that the biocomposites maintain a viscous-dominated response over a broader frequency range, possibly due to restricted chain mobility or increased

interfacial interactions introduced by lignin (Guo et al., 2019). While for LH, **Figure 5.5 D**, at 10 wt.%, the crossover point (37 Hz) was slightly lower than that of neat PLA, showing a more elastic behavior, suggesting stronger interactions between the hardwood lignin and the PLA matrix.

Moreover, G' and G" showed a linear behavior at low frequencies; consequently, a strong relationship between viscosity and shear rate, evidencing a strong power-law dependence (Gupta et al., 2017). The data presented in **Table 5.2** illustrate this phenomenon during the evaluation of the rheological percolation threshold for a uniform dispersion at low frequencies (ranging from 1 to 10 rad/s).

Table 5. 2 Low frequency slopes of G' and G" for unmodified and silylated lignin biocomposites.

Samples	**G'**	**G"**	**Samples**	**G'**	**G"**
PLA	1.60	0.91	-	-	-
Unmodified softwood			Unmodified hardwood		
PLA5LS	1.58	0.92	PLA5LS	1.62	0.89
PLA10LS	1.45	0.76	PLA10LS	1.53	0.84
PLA15LS	1.59	0.90	PLA15LS	1.59	0.88
Silylated softwood			Silylated hardwood		
PLA10LS1GPS	1.54	0.84	PLA10LH1GPS	1.49	0.82
PLA10LS3GPS	1.58	0.86	PLA10LH3GPS	1.55	0.85
PLA10LS5GPS	1.59	0.88	PLA10LH5GPS	1.57	0.86

The observed reduction in the slope values of G' and G" at a concentration of 10 wt.% for both softwood (slope G' and G" of 1.45 and 0.76, respectively) and hardwood (slope G' and G" of 1.53 and 0.84, respectively) indicates improved lignin dispersion through the matrix and the possible formation of a network.

Regarding the materials' processability evaluated by complex viscosity (η*), PLA-lignin biocomposites present typical thermoplastics shear-thinning behavior, meaning that with the increase in shear rate, the viscosity decreases (Alshammari; Ameli, 2024). As observed, the addition of a lignin loading of 5 wt.% decreased the viscosity of the biocomposites regardless of the type of lignin that was incorporated, as shown in **Figure 5.5 (E, F)**, and slightly increased at loads of 10 and 15 wt.%, however, behaving as neat PLA. In this case, lignin acted as a plasticizer agent, requiring less resistance to deformation, showing lower degrees of

intercalation, while increasing the free volume of the PLA matrix with the higher loads of lignin (Anuar et al., 2023; Terzopoulou et al., 2025). Studies by Ding et al. (2023) also found that the addition of 2.5 and 10 wt.% of kraft lignin significantly decreases the composite viscosity at a low shear rate, which was attributed to the lower molecular weight of lignin compared to PLA.

Thus, both LS and LH were modified through silylation reaction to enhance the interfacial adhesion between lignin and PLA, expressed by the low value obtained for storage modulus (G') and complex viscosity arising from polarity and structure differences. The influence of GPS, as a coupling agent, on the rheological properties of PLA-lignin biocomposites was measured at a constant lignin fraction of 10 wt.% at 190 °C as a function of frequency (**Figure 5.6**).

The rheological parameters, represented by G', G", and η*, gradually increased with increasing GPS content in the selected lignins, revealing higher values than neat PLA and the unmodified 10 wt.% PLA/lignin biocomposites (Figures 6A and 6B). Silylation of lignin allowed the formation of localized bonding interactions along the PLA matrix, restricting chain mobility and increasing biocomposite complex viscosity, as well as a significant change in its flow behavior (Alshammari; Ameli, 2024; Gupta; Kumar; Sachdeva, 2024).

In previous research, highly fibrillated lignocellulosic fibers, originally from a stone groundwood pulp, were silylated at 3, 5, 7, and 10 wt.% GPS contents and incorporated into the PLA (Herbst et al., 2024). The lowest degree of silylation (3 wt.% of GPS addition) showed the highest enhancement of both G' and G" of the biocomposites due to the covalent bond formation between the available hydroxyl groups and the hydrolyzed forms of GPS silanol groups, while its epoxy terminal groups were able to undergo to open-ring rection with PLA ends during melt processing (Arslan; Dogan, 2018; Chen et al., 2021b; Herbst et al., 2024; Sekar et al., 2023). On the one hand, this bond formation creates a strong network between filler and matrix, and possibly a percolation threshold. On the other hand, the excess coupling agent leads to system plasticization or over-compatibilization due to possible GPS self-condensation and steric interference at the filler-matrix interface (Sekar et al., 2023).

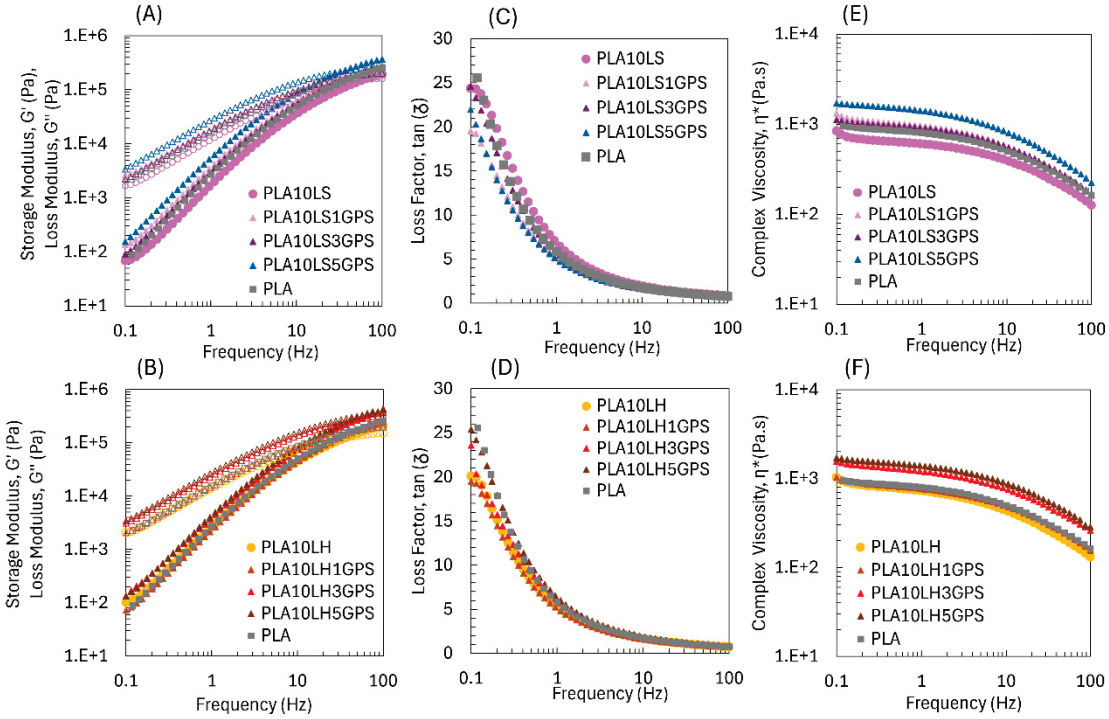

Figure 5. 6 Rheological curves of silylated softwood and hardwood lignin on PLA.

In **Table 5.2**, the slopes of G' and G" for silylated lignin biocomposites presented lower values at 1 wt.% of GPS content, suggesting optimization of lignin percolation by the coupling agent and better dispersion of both LS and LH up to around 3 wt.% of GPS content. This leads to an improved interface and consequently enhances further mechanical properties. However, up to 3 wt.%, the slope increased, suggesting weakening of the network, and consequently leading to lower mechanical properties.

The silylation of lignin directly affected the complex viscosity of the biocomposites, as shown in **Figure 5.6 (E, F)**. In addition, as the concentration of GPS increased, η* was intensified, reflecting on the biocomposite flowability, as depicted from the MFI values (**Figure 5.7**). PLA/LH biocomposites presented higher MFI than PLA/LS (**Figure 5.7A**), which is attributed to the higher linearity and condensed structure of LH, contributing to the plasticizing effect and inducing free volume between PLA chains. Something similar was observed with the PLA/LS biocomposites, although the higher complexity of the LS structure and tendency to form aggregates resulted in a decrease in MFI values (Park et al., 2019; Suota et al., 2021). The incorporation of the GPS coupling agent led to a significant reduction in the MFI values of both LS and LH biocomposites. In particular, 10 wt.% of LH silylated with 5 wt.% GPS exhibited an MFI comparable to that of neat PLA. This suggests that lignin modification

enhanced interfacial interactions within the molten composite, promoting greater cohesion with the PLA matrix(Zhang et al., 2024b).

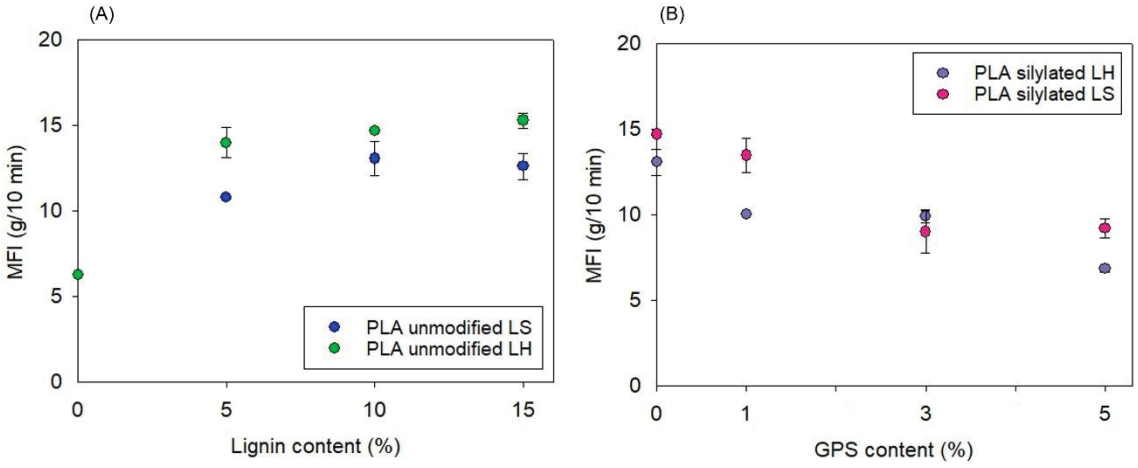

Figure 5. 7 MFI of unmodified and silylated lignin PLA biocomposites.

In summary, the melt rheology indicated that PLA/LS and PLA/LH exhibited lower complex viscosity and higher MFI than neat PLA. Furthermore, lignin silylation introduced interfacial binding sites into the PLA matrix, facilitated by the two distinct reactive groups present in the coupling agent. This modification contributed to the increase in viscosity and may have enhanced the formation of nucleation sites, thus promoting crystallization in the biocomposite (Ma et al., 2023; Shorey; Gupta; Mekonnen, 2021). **Figure 5.8** shows the thermal events of unmodified and silylated PLA biocomposites during the second heating scan. Neat PLA presents an amorphous structure after melt-processing, indicating limited recrystallization during the cooling phase. However, the lignin incorporation was able to induce cold crystallization followed by melting, for all the LS compositions, as shown in **Figure 5.8A**. The presence of rigid lignin molecules possibly restricts the mobility of PLA chains, limiting their ability to organize and crystallize during cooling. As a result, a higher cold crystallization enthalpy is observed during heating, suggesting a reduced nucleation efficiency in the composite (Yang et al., 2021). Although for LH, **Figure 5.8B**, as the amount of LH increases, the cold crystallization and melting events were minimized, due to the amorphous and less condensed nature of this lignin type (Spiridon et al., 2015).

After silylation, both cold crystallization and melting events were observed for LS lignin, as shown in **Figure 5.8C**. These events were maximized for LH as the GPS concentration increased, compared to the untreated 10 wt.% of LH, which is displayed in **Figure 5.8D**. The presence of cold crystallization and melting events could lead to an increase in the crystallinity degree of modified lignin PLA biocomposites (Frasca et al., 2024), supported

by the significant increase in its G' observed in the rheological properties of **Figure 5.6 (A** and **B)**.

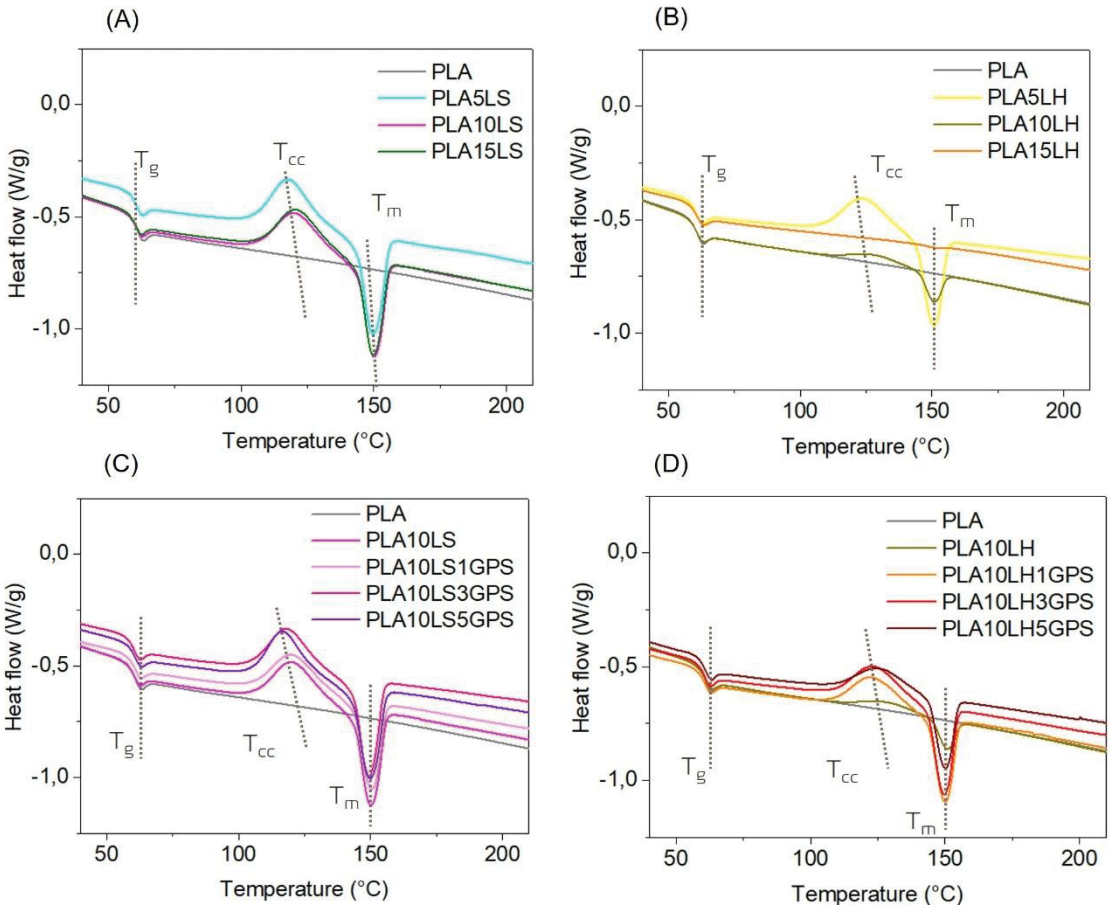

Figure 5. 8 DSC thermograms of unmodified and silylated lignin PLA biocomposites.

The effect of unmodified and silylated lignins on the T_g and crystallization of PLA is provided in **Table 5.3**. All the biocomposites showed a T_g of around 61 °C, characteristic of neat PLA. The presence of a single T_g in the DSC thermogram suggests that lignin and PLA are at least partially miscible at the molecular level (Johansson et al., 2023). As discussed, the selected PLA presents an amorphous structure after melting, showing no crystallinity index (X_c). Once LS is incorporated at 5, 10, and 15 wt.%, the X_c of the biocomposites increases to around 3%, due to its more condensed structure, which promotes a weak but more effective nucleation of PLA crystals. Despite lignin-induced crystallinity, overall levels remained low since lignin does not act as a strong nucleating agent, in some cases, slowing down or inhibiting the formation of crystalline domains (Righetti; Faedi; Famulari, 2024), as in the case of LH, in which X_c values range from 0.1 to 1.1%. However, the LS and LH silylation had no clear effect on the PLA crystallization. LS provided the highest X_c for 3 wt% of GPS, while in the case of LH, it was found at 1 wt% of GPS addition.

Table 5. 3 Effect of lignin silylation on the thermal properties of softwood and hardwood PLA biocomposites.

Lignin	GPS	T_g[a]	T_{cc}[b1]	T_m[c1]	ΔH_{cc}[b2]	ΔH_m[c2]	X_c[d]
(%)		(°C)			(Jg^{-1})		(%)
PLA	0	61.1	-	-	-	-	0
Softwood							
5	0	61.0	118	149	21.6	24.5	3.2
10	0	60.8	120	150	20.4	22.9	3.0
10	1	61.1	120	150	21.8	24.5	3.2
10	3	60.7	118	149	17.7	21.5	4.5
10	5	61.3	117	150	20.5	21.9	1.6
15	0	60.5	121	150	20.6	22.9	3.0
Hardwood							
5	0	61.0	124	150	17.7	17.8	0.1
10	0	61.3	128	151	4.7	5.6	1.1
10	1	61.0	123	150	18.2	19.5	1.5
10	3	60.8	123	149	18.5	19.4	1.1
10	5	61.1	125	150	14.2	14.4	0.3
15	0	61.3	-	150	0.0	0.2	0.3

[a] T_g = glass transition temperature.

[b1] T_{cc} = cold crystallization temperature / [b2]ΔH_{cc} = cold crystallization enthalpy.

[c1] T_m = melting temperature / [c2]ΔH_m = melting enthalpy.

[d]X_c = crystallinity index.

5.3.3 MECHANICAL PROPERTIES OF PLA-LIGNIN FILMS

The mechanical properties of neat PLA and its biocomposites with lignin derived from unmodified and silylated LS and LH are shown in **Table 5.4**. The effect of lignin on PLA is strongly dependent on its composition and structure, which are, in turn, strongly influenced by its botanical origin and extraction process (Li et al., 2025; Rencoret et al., 2023). Lignin derived from softwood species is typically richer in guaiacyl units than hardwood-derived lignin. On the contrary, hardwood lignin, characterized by a higher syringyl content, interacts differently with the PLA matrix and, thus, results in biocomposites with distinct mechanical performance

(Terzopoulou et al., 2025). **Figure 5.9** shows the evolution of tensile strength at increasing unmodified LS and LH contents, as well as the influence of silylation reaction through the increase of GPS content at lignin weight fraction set at 10 wt.%.

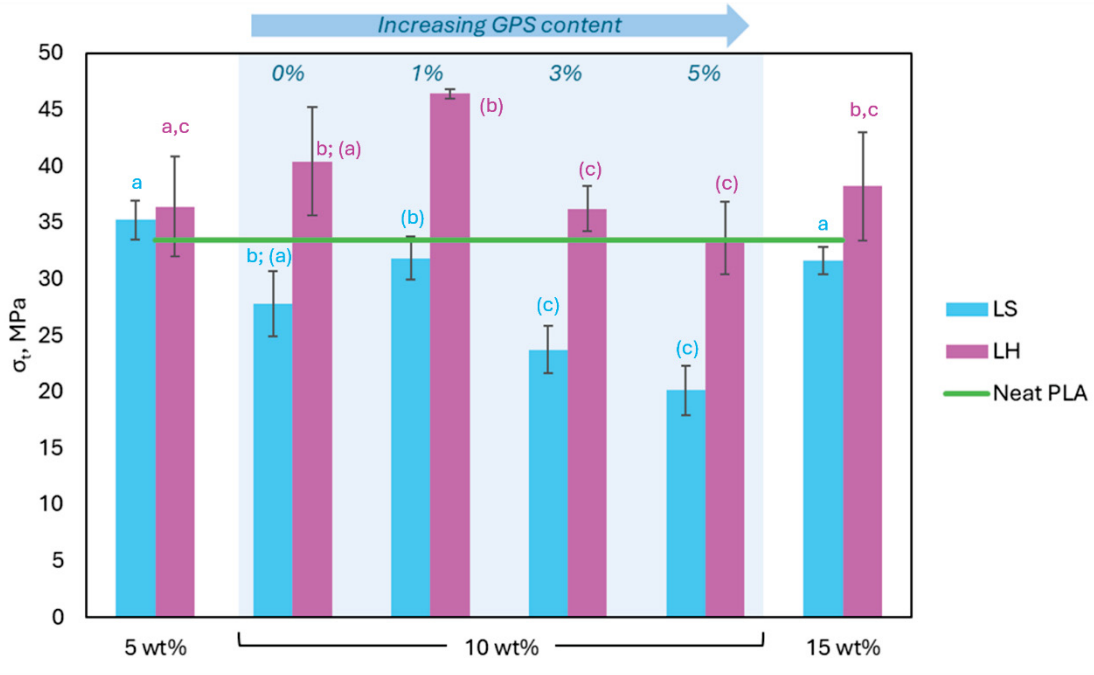

Figure 5. 9 Influence of unmodified and silylated lignin type over tensile strength of different lignin loads, and GPS content of 10 wt.% filled biocomposites. Letters indicate statistical differences according to Tukey's HSD test ($p < 0.05$): a, b, and c for comparison between lignin concentrations and (a), (b), and (c) for comparison between GPS concentrations.

The incorporation of 5 wt.% of both lignins into PLA resulted in improvements in tensile strength of approximately 5% and 8% for LS and LH, respectively, as the lignin content increased to 10 wt.%, LH continued to enhance the tensile strength of the composite, achieving an overall improvement of approximately 13%. On the contrary, LS at 10 wt.% did not contribute to the tensile strength of the obtained biocomposites, resulting in a reduction of this property when compared to the neat PLA. In this case, reinforcement appears to be driven by mechanical interlocking, and at higher loads, tensile strength decreased due to low compatibility or agglomeration (Wasti et al., 2021; Wu et al., 2025). On the other hand, LH tends to form stronger interfacial bonds, promoting better stress transfer and dispersion within the matrix. Furthermore, the lower glass transition temperature (T_g) of hardwood lignin, approximately 130 °C, compared to softwood (around 177 °C), suggests better thermal compatibility with PLA during melting processing, leading to a more homogeneous mixing and improved interfacial adhesion (Mariana et al., 2021).

Table 5. 4 Tensile properties of composite films according to lignin and coupling agent load.

Lignin	GPS	Tensile strength (σ_t)	Young modulus (E_t)	Elongation (ε)
wt.%	wt.%	MPa	GPa	%
0	0	33.4 ± 2.2 [a]	2.7 ± 0.1[a]	3.40 ± 0.31 [c]
LS				
5	0	35.2 ± 1.7 [a]	2.9 ± 0.1 [a]	2.04 ± 0.30 [a]
10	0	27.8 ± 2.9 [b,(a)]	3.2 ± 0.2 [a; (a)]	1.45 ± 0.19 [b; (a)]
10	1	31.8 ± 1.9 [a; (b)]	3.2 ± 0.2 [(a)]	1.77 ± 0.20 [(b)]
10	3	23.7 ± 2.1[(c)]	2.7 ± 0.3 [(b)]	1.92 ± 0.42 [(b)]
10	5	20.1 ± 2.2 [(c)]	2.6 ± 0.2 [(b)]	1.62 ± 0.39 [(a,b)]
15	0	31.6 ± 1.2 [a]	3.0 ± 0.4 [a]	1.59 ± 0.27 [b]
LH				
5	0	36.4 ± 4.4 [a,c; (a,b)]	2.7 ± 0.1[a; (a)]	2.77 ± 0.18 [a; (a)]
5	1	38.4 ± 3.2 [(a)]	2.7 ± 0.3 [(a)]	2.78 ± 0.42 [(a)]
5	3	38.6 ± 1.9 [(a)]	2.9 ± 0.3 [(a)]	2.56 ± 0.25 [(a)]
5	5	34.2 ± 2.7 [(b)]	2.9 ± 0.3 [(a)]	2.71 ± 0.21 [(a)]
10	0	40.4 ± 4.8 [b; (a)]	2.6 ± 0.1[a; (a)]	2.53 ± 0.35 [a; (a)]
10	1	46.4 ± 0.4 [(b)]	3.0 ± 0.1 [(b)]	3.10 ± 0.12 [c; (b)]
10	3	36.2 ± 2.0 [(c)]	3.1 ± 0.2 [(b)]	2.28 ± 0.17 [(a)]
10	5	33.6 ± 3.2 [(c)]	3.2 ± 0.2 [(b)]	2.37 ± 0.30 [(a)]
15	0	38.2 ± 4.8 [b,c; (a)]	3.2 ± 0.2 [b; (a)]	2.09 ± 0.19 [a; (a)]
15	1	32.1 ± 3.9 [(a,c)]	2.9 ± 0.2 [(a)]	2.01 ± 0.17 [(a)]
15	3	31.8 ± 2.3 [(c)]	3.1 ± 0.2 [(a)]	1.80 ± 0.23 [(a)]
15	5	35.9 ± 2.2 [(a,b)]	3.1 ± 0.1 [(a)]	2.04 ± 0.14 [(a)]

Superscript letters indicate statistical differences according to Tukey's HSD test ($p < 0.05$): a, b, and c for comparison between lignin concentrations and (a), (b), and (c) for comparison between GPS concentrations.

The difference in mechanical behavior can be attributed to the different interactions between each type of lignin and the PLA matrix. LH exhibited a lower content of aliphatic and phenolic hydroxyl (OH) groups, along with a higher methoxy content, reflected in a syringyl/guaiacyl (S/G) ratio of 1.97 (Suota et al., 2021b). A lower hydroxy group concentration typically results in reduced polarity, which can improve compatibility with the PLA matrix, leading to better dispersion and interfacial adhesion. Furthermore, a higher methoxy content

and a higher S/G ratio are associated with a more linear and less condensed lignin structure, which increases chain flexibility and reduces the tendency to aggregation (Österberg et al., 2023; Rosado et al., 2025). These characteristics promote uniform dispersion and enable more effective stress transfer within the composite, contributing to improved tensile strength. In contrast, the higher hydroxy group content and the presence of mainly guaiacyl units can lead to stronger lignin-lignin interactions than lignin-PLA, leading to phase separation and poor mechanical performance at higher loads (Terzopoulou et al., 2025).

Once silylated, the 10 wt.% LH biocomposites at 1 wt.% GPS showed an improvement of around 13% compared to their unmodified per and around 28% to neat PLA. The attached organosilane groups at the lignin surface increase the dispersion in PLA and improve interfacial adhesion (Huo et al., 2025; Zhu et al., 2015). As a result, the biocomposites based on silylated lignin often exhibit enhanced mechanical performance, especially for LH biocomposites. However, as the GPS content increases to 3 and 5 wt.%, the tensile strength of the samples decreases independently of the type of lignin.

As observed in the rheological properties, this phenomenon could be related to the excess coupling agent and system plasticization due to possible over-compatibilization, induced by the GPS self-condensation (Sekar et al., 2023). In the case of silylated lignin, excessive GPS loading may result in the formation of a rigid interphase surrounding the lignin particles, limiting molecular mobility and leading to stress concentration sites, as happens in natural fiber polymeric composites with excessive coupling agent in natural fiber composites, which leads to a decline in mechanical properties rather than continued enhancement (El-Sabbagh, 2014). This effect can counterbalance the benefits of improved interfacial bonding, resulting in increased brittleness rather than enhanced mechanical performance.

Silylated lignins generated an increase in complex viscosity of PLA, as discussed above, indicating enhanced interfacial interactions and possibly restricted chain mobility due to better lignin dispersion or partial crosslinking effects, caused by covalent bonds formed between GPS and lignin during the drying process, anchoring the coupling agent, that upon melt mixing with PLA, GPS can also react with PLA's carboxyl end groups, strengthening interfacial adhesion and enhancing the composite's mechanical properties leading to significant improvement in the tensile strength of the LH composite, overcoming neat PLA (Arslan; Dogan, 2018; Herbst et al., 2024). As supported by the Young's modulus results in **Table 5.4**, LH biocomposites showed higher values in comparison to neat PLA. At the same time, at 10 wt.% of unmodified LH, it was slightly lower, meaning that stiffness was reduced, indicating

that at this lignin concentration, the composite was more flexible, and more recommended for film application (Fazeli et al., 2024). However, after the silylation, the lignin induces a low degree of crystallization (observed by the DSC analysis in **Table 5.3**), leading to an increase in Young's modulus. In contrast, the LS composite showed a decline in tensile strength with the lignin incorporation and after silylation, despite increased viscosity, suggesting that compatibility improvements were insufficient to overcome the inherently lower miscibility or more rigid structure of guaiacyl-rich softwood lignin, leading to an increase in Young's modulus, suggesting that the biocomposites became more brittle, as its elongation at break results also decrease (Ridho et al., 2022).

5.3.4 BARRIER PROPERTIES

Figure 5.10 shows the visual of the films, and the barrier properties of PLA biocomposites containing unmodified and silylated LS and LH were assessed through ultraviolet light (UV) shielding, water vapor transmission rate (WVTR), and water contact angle (WCA). These properties determine how effectively a film can be applied as a packaging material, protecting contents from external factors such as moisture, extending shelf life, and preserving product quality (Cheng et al., 2024). In polymeric films, barrier performance is influenced by the material's molecular structure, crystallinity, and the presence of additives or fillers (Wu; Misra; Mohanty, 2021), as in the case of LS and LH.

Differences in transparency and color intensity with increasing LS and LH content were shown in **Figures 5.10 A** and **5.10 B**, corroborating the UV-shielding performance of the biocomposites, as presented in **Figures 5.10 C** and **5.10 D**, corresponding to the LS and LH biocomposites, respectively, based on transmittance (%) measurements in the 200–800 nm wavelength range. Neat PLA exhibited high transmittance, ranging from 60% to 85% in the UVA and UVB regions, and approximately 90% transparency at 660 nm, indicating limited UV-blocking capability. Conversely, PLA biocomposites containing 5 wt.% LS lignin shows a significant reduction in transmittance, reaching values between 0% and 10% in the UV region and approximately 10% at 660 nm, demonstrating improved UV-shielding capability. As the lignin content increased, the UV-blocking efficiency was enhanced for both LS and LH, attributed to the effective suppression of UV light (transmittance equal to zero). However, this improvement in UV protection suppresses visible light transparency.

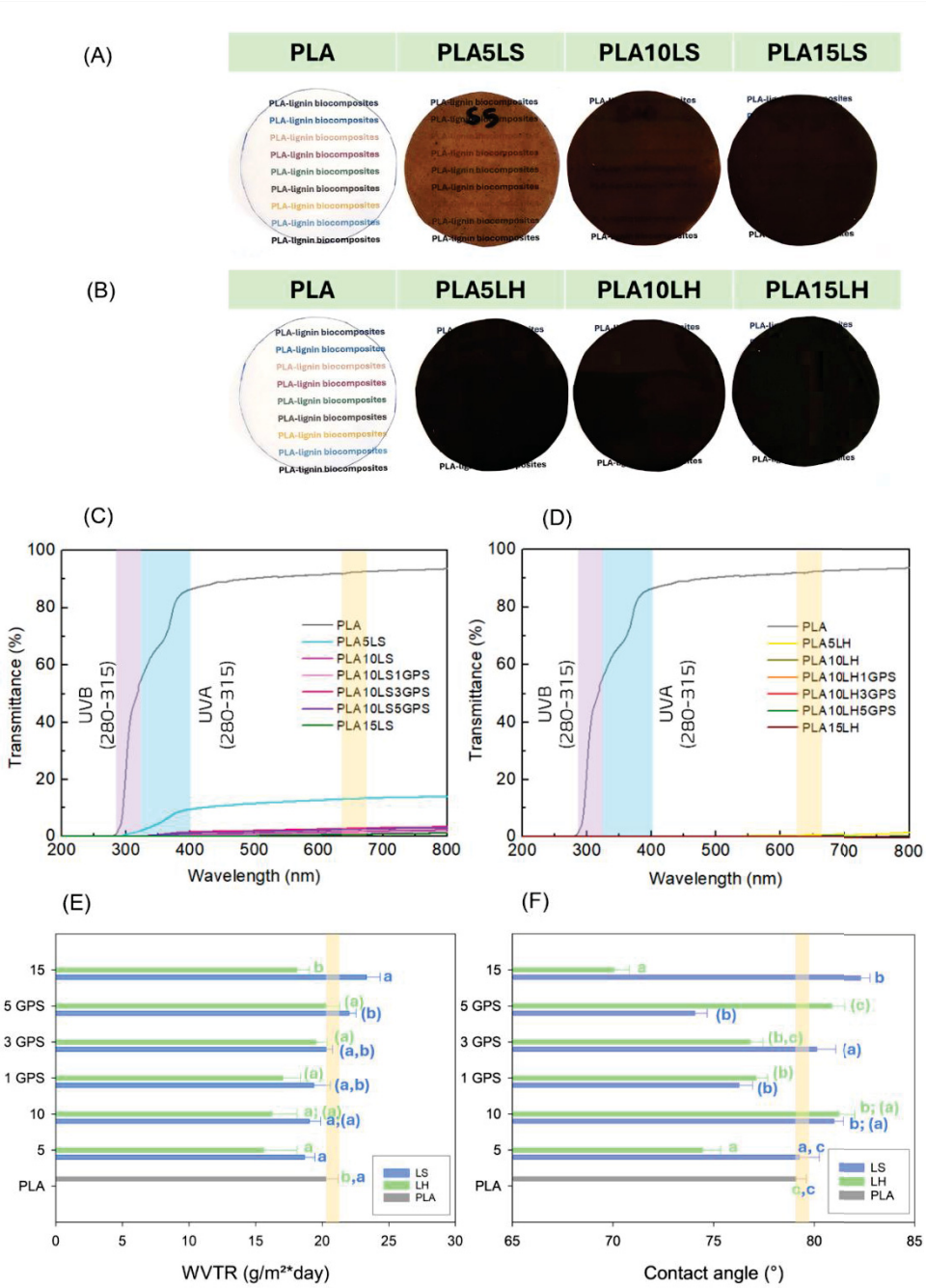

Figure 5. 10 Unmodified and silylated soft and hardwood lignin PLA films' barrier properties: Photograph of (A) LS and (B) LH films; Transmittance of (C) LS and (B) LH films; (E) Water vapor transmission rate and (F) water contact angle of LS and LH films, in which the letters indicate statistical differences according to Tukey's HSD test ($p < 0.05$): a, b, and c for comparison between lignin concentrations and (a), (b), and (c) for comparison between GPS concentrations.

The difference in the refractive indices of PLA in particles promotes light scattering, leading to a reduction in optical transparency (Ye et al., 2023). This effect becomes more pronounced at higher lignin loadings, which explains the progressively darker and more opaque

appearance observed for films containing increased amounts of LS or LH, due to chromophore groups within lignin's complex aromatic structure (He et al., 2025; Wu et al., 2024).

Chromophores, such as conjugated aromatic rings, facilitate π-π* electronic transitions, which are primarily responsible for UV absorption. This effect is further enhanced by the functional groups like phenolic hydroxyls, methoxy (-OCH_3), and carbonyl (-CO), that can interact with the aromatic system, inducing a redshift in the π-π*, intensifying UV absorption across a wider spectral range (Duan et al., 2022; Wu et al., 2024; Zhang et al., 2025). However, the same chromophore groups are responsible for the characteristic dark brown color of lignin (Li et al., 2019b), which leads to no transparency of PLA-lignin biocomposites. Although this characteristic does not necessarily limit the applicability of the developed biocomposites. In several applications, transparency is not a critical requirement. For instance, in drug delivery systems, the functional performance of the carrier, such as UV protection and barrier properties, can contribute to the protection of photosensitive active compounds (Wang et al., 2021; Witzler et al., 2018).

In addition to UV-shielding properties, the water vapor transmission rate (WVTR) plays a significant role in polymeric films, especially for food packaging applications, and the results are shown in **Figure 5.10 E**. Compared to neat PLA, the WVTR of the biocomposites generally slightly decreased as the load of both lignin types increased, due to lignin's inherently amphiphilic characteristics, presenting both hydrophobic and hydrophilic groups in its structure (Agustin et al., 2023), allowing partial compatibility with the PLA matrix. LS displayed values ranging from 18 to 22 g/m²·day, while LH showed lower values from 15 to 20 g/m²·day. In composite films, micro- and nanofillers act as impermeable obstacles within the PLA matrix, creating a tortuous diffusion pathway that forces water vapor molecules to get cross-dispersed. Reducing the WVTR, thereby improving the barrier performance of the material (De Lima et al., 2025; Yang et al., 2020a). Gas barrier properties are often influenced by the crystalline content of the polymer matrix, as crystalline regions are less permeable than amorphous ones (Safandowska et al., 2022).

The DSC results presented in this work (**Table 5.3**) indicate that the PLA matrix remained predominantly amorphous. However, the addition of lignin slightly promoted crystallization by introducing a limited number of crystalline domains. These formed crystalline regions may have contributed to a modest reduction in WVTR, although the effect was minor compared to pure PLA. Boarino et al (2022) (Boarino et al., 2022) studied the effect of PLA blends containing lignin, lignin nanoparticles, and PLA-grafted lignin nanoparticles with 1, 5,

and 10 wt.% lignin content in PLA films, and observed a slight reduction in the WVTR as the lignin load was increased, regardless of the lignin form, but especially for the PLA-grafted nanoparticles.

Changes in surface wettability, driven by lignin functional groups, distribution, and structural factors, can also affect the water contact angle of the PLA-lignin biocomposites, as reported in **Figure 5.10F**. LS lignin biocomposites showed WCA values ranging from 74 to 82°, with the highest value obtained for 15 wt.% of lignin, exceeding the values obtained by LH due to the higher hydrophobic character of LS lignin. Regardless of LS silylation, the sample with 3 wt% GPS exhibited the highest WCA, suggesting that higher GPS loadings may increase moisture uptake, due to unreacted GPS or ungrafted free radicals in lignin or PLA. However, for LH containing biocomposites, corresponding to the one that showed improved mechanical properties, indicating better interactions with the PLA matrix, yielded WCA values ranging from 70 to 82°, with the silylated sample at 1 wt.% of GPS showing the highest value. While at 15 wt.% of lignin, the value decreased to 70°. Despite the differences between LS and LH, the WCA values only decrease or increase by around 10 % of the neat PLA WCA.

5.4 CONCLUSION

This study demonstrated that both lignin type and silylation significantly affect the thermal, mechanical, and rheological properties of PLA-lignin composite films. FTIR analysis identified structural differences between LS and LH lignins (guaiacyl and syringyl groups), though GPS functional groups were not detected. Silylation increased the Tg of LS and LH by 3 °C and 7 °C, respectively, confirming reaction effectiveness. The degree of silylation was visually supported by lignin ash color change: LS from white to dark gray, and LH from light orange to white with increasing GPS content. Rheological analysis showed that LH at 10 wt.% and GPS at up to 3 wt.% were well dispersed. Both lignin types decreased the complex viscosity (η*) of the biocomposites; however, once silylated, η* increased, suggesting enhanced interactions and network formation within the PLA matrix. MFI values increased from around 6 to 16 g/10min for both LS and LH, and with the increase of GPS concentration, the values decreased from 6 to 16 g/10min to 10 wt.%. Despite significant changes in the rheology properties, crystallinity increased slightly with GPS (4.5% for LS, 1.5% for LH), with minimal Tg variation (60.5 – 61.3 °C). Mechanically, LH-based composites outperformed LS due to their structure and lower molecular weight. LS at 5 wt.% reached 35.2 ± 1.7 MPa (statistically

similar to neat PLA), while LH at 10 wt.% improved tensile strength by around 20% (40.04 ± 4.8 MPa). With 1 wt.% GPS, LH composites showed around 40 % tensile strength increase (46.4 ± 4 MPa) over neat PLA, confirming enhanced interfacial adhesion. However, silylation had minimal impact on barrier properties (UV blocking, WVTR, and WCA). Overall, the findings highlight the important role of lignin type and surface modification in improving PLA biocomposites for sustainable uses. Future research could explore the effect of shorter-chain silanes and compare the performance of grass lignin with LS and LH to enhance interfacial interactions. Evaluating the long-term stability, biodegradation behavior, and scalability of processing for silylated PLA-lignin systems would also provide valuable insights for future application development.

6. FINAL CONSIDERATIONS

This study demonstrates that the performance of PLA-based biocomposites is ruled by the relationship between the chemical structure of lignocellulosic reinforcements, their surface reactivity, and their resulting interfacial interactions with the polymer matrix. By systematically comparing untreated SGW fibers, bleached SGW fibers, and isolated softwood and hardwood lignins, the work clarifies how differences in morphology and chemistry influence the effectiveness of silane-based interfacial engineering.

Untreated high-yield SGW fibers exhibited the highest intrinsic reinforcing efficiency, achieving tensile strength improvements of up to 27% at 20 and 30 wt% fiber loadings without chemical modification. This behavior is primarily attributed to their high aspect ratio and preserved lignin-rich surface, which promotes effective stress transfer through mechanical interlocking and network formation within the PLA matrix. In these systems, lignin acts not only as a structural component but also as a compatibilizer, whose reactivity becomes particularly relevant after silylation, enhancing fiber–matrix adhesion without compromising the morphology-driven reinforcement mechanism.

In contrast, progressive bleaching substantially altered both the chemical composition and morphology of SGW fibers. While increased cellulose purity improved surface reactivity toward silane coupling, fiber shortening and fines formation reduced aspect ratio and disrupted the physical fiber network. Consequently, bleached fibers displayed reduced geometry-driven reinforcement. However, these systems benefited more strongly from silylation, as evidenced by increased complex viscosity and improved interfacial structuring at intermediate GPS contents. This shift highlights a transition from morphology-dominated reinforcement in untreated SGW to chemistry-dominated interfacial control in bleached SGW, demonstrating that optimal composite performance results from a balanced preservation of lignin and fiber geometry combined with targeted surface modification.

The comparison between fiber-based composites and PLA–lignin systems further emphasized the critical role of interface design. In lignin-filled PLA, in which reinforcement depends entirely on interfacial interactions rather than particle geometry, silylation proved particularly effective. Both softwood and hardwood lignins exhibited improved dispersion and matrix compatibility after modification, with the strongest effects observed at low lignin contents (1 wt%). Notably, LH showed a more pronounced response to silylation, leading to enhanced rheological structuring, increased glass transition temperature, and improved mechanical performance in selected formulations. These differences can be linked to inherent

structural variations between LS and LH, which influence silane grafting efficiency and interfacial bonding with PLA.

Across all material systems, the results consistently indicate that interfacial phenomena emerge from the combined effects of chemical functionality, surface accessibility, and morphological integrity. Excessive chemical treatment, whether through extensive bleaching or high silane loadings, tended to disrupt this balance. However, moderate modification levels provided the most favorable compromise between reinforcement efficiency, rheological behavior, and processability. Overall, this work highlights that controlled interfacial engineering, rather than maximal chemical modification, is the key to developing high-performance, sustainable PLA biocomposites, positioning SGW fibers and lignin as viable, multifunctional alternatives to conventional fossil-based fillers, comparable to PP reinforced composites.

7. FUTURE PERSPECTIVES

Examine how different lignin types, including grass-derived lignins, can provide deeper insights into their structure–property relationships and their influence on polymer–filler interactions. Additionally, fractionating lignin based on molecular weight could enable the selective use of fractions with tailored properties, facilitating targeted functionalization and improved compatibility with polymer matrices, including PLA and other biopolymers. Furthermore, lignin could be explored as a precursor for compatibilizer development, acting not only as a reinforcing filler but also as a natural interface modifier in biopolymer systems. These approaches may expand the potential of lignin to enhance both mechanical performance and processability in sustainable biocomposites.

REFERENCES

ABDELMOULEH, M. *et al.* Modification of cellulosic fibres with functionalised silanes: Development of surface properties. International Journal of Adhesion and Adhesives, v. 24, n. 1, p. 43–54, 2004.

ABOLORE, Rasaq S.; JAISWAL, Swarna; JAISWAL, Amit K. A comprehensive review on sustainable lignin extraction techniques, modifications, and emerging applications. Industrial Crops and Products, v. 235, p. 121696, 1 nov. 2025.

AFSHAR, Sevil V. *et al.* Degradation of biodegradable plastics in waste management systems and the open environment: A critical review. Journal of Cleaner Production, v. 434, p. 140000, 1 jan. 2024.

AGARWAL, Jyoti *et al.* Progress of novel techniques for lightweight automobile applications through innovative eco-friendly composite materials: A review. Journal of Thermoplastic Composite Materials, v. 33, n. 7, p. 978–1013, 12 jul. 2020.

AGUADO, Roberto J. *et al.* Comparative Study on the Stiffness of Poly(lactic acid) Reinforced with Untreated and Bleached Hemp Fibers. Polymers, v. 15, n. 13, p. 2960, 6 jul. 2023.

AGUSTIN, Melissa B. *et al.* Lignin nanoparticles as co-stabilizers and modifiers of nanocellulose-based Pickering emulsions and foams. Cellulose, v. 30, n. 14, p. 8955–8971, 29 set. 2023.

AHMAD, R.; HAMID, R.; OSMAN, S. A. Physical and Chemical Modifications of Plant Fibres for Reinforcement in Cementitious Composites. Advances in Civil Engineering, v. 2019, p. 1–18, 12 mar. 2019.

ALAM, Mohammad Mahbubul *et al.* Efficient and environmentally friendly techniques for extracting lignin from lignocellulose biomass and subsequent uses: A review. Cleaner Materials, v. 13, p. 100253, 1 set. 2024.

ALBDIRY, Mushtaq. Effect of melt blending processing on mechanical properties of polymer nanocomposites: a review. Polymer Bulletin, v. 81, n. 7, p. 5793–5821, 2024.

ALI, Sameh Samir *et al.* Bioplastic production in terms of life cycle assessment: A state-of-the-art review. Environmental Science and Ecotechnology, v. 15, p. 100254, jul. 2023.

ALSHAMMARI, Shallal; AMELI, Amir. Improved Performance of Polylactic Acid Biocomposites at High Lignin Loadings through Glycidyl Methacrylate Grafting of Melt-Flowable Organosolv Lignin. ACS Omega, v. 9, n. 33, p. 35937–35949, 20 ago. 2024.

ANDERSON, Eric M. *et al.* Differences in S/G ratio in natural poplar variants do not predict catalytic depolymerization monomer yields. Nature Communications, v. 10, n. 1, p. 2033, 2 maio 2019.

ANDREW, J. Jefferson; DHAKAL, H. N. Sustainable biobased composites for advanced applications: recent trends and future opportunities – A critical review. Composites Part C: Open Access, v. 7, p. 100220, mar. 2022.

ANDRIANI, Fika; LAWOKO, Martin. Oxidative Carboxylation of Lignin: Exploring Reactivity of Different Lignin Types. Biomacromolecules, v. 25, n. 7, p. 4246–4254, 8 jul. 2024.

ANUAR, Hazleen *et al.* Novel soda lignin/PLA/EPO biocomposite: A promising and sustainable material for 3D printing filament. Materials Today Communications, v. 35, p. 106093, 1 jun. 2023.

ARSLAN, Cagrialp; DOGAN, Mehmet. The effects of silane coupling agents on the mechanical properties of basalt fiber reinforced poly(butylene terephthalate) composites. Composites Part B: Engineering, v. 146, n. January, p. 145–154, 2018.

ASAITHAMBI, B.; GANESAN, G.; ANANDA KUMAR, S. Bio-composites: Development and mechanical characterization of banana/sisal fibre reinforced poly lactic acid (PLA) hybrid composites. Fibers and Polymers, v. 15, n. 4, p. 847–854, 2014.

ASIM, Mohammad *et al.* Effect of Alkali and Silane Treatments on Mechanical and Fibre-matrix Bond Strength of Kenaf and Pineapple Leaf Fibres. Journal of Bionic Engineering, v. 13, n. 3, p. 426–435, 1 jul. 2016.

AVCI, Ali *et al.* Water absorption characterization of boron compounds-reinforced PLA/flax fiber sustainable composite. International Journal of Biological Macromolecules, v. 233, p. 123546, abr. 2023.

AVEROUS, L.; BOQUILLON, N. Biocomposites based on plasticized starch: thermal and mechanical behaviours. Carbohydrate Polymers, v. 56, n. 2, p. 111–122, jun. 2004.

AWAL, A.; RANA, M.; SAIN, M. Thermorheological and mechanical properties of cellulose reinforced PLA bio-composites. Mechanics of Materials, v. 80, n. Part A, p. 87–95, 2015.

AZLIN, M. N. M. *et al.* Natural Polylactic Acid-Based Fiber Composites: A Review. Advanced Processing, Properties, and Applications of Starch and Other Bio-based Polymers, p. 21–34, 1 jan. 2020.

BAJPAI, Pramendra Kumar; SINGH, Inderdeep; MADAAN, Jitendra. Development and characterization of PLA-based green composites. Journal of Thermoplastic Composite Materials, v. 27, n. 1, p. 52–81, 22 jan. 2014.

BAJPAI, Pratima. Pulping Fundamentals. *In*: Biermann's Handbook of Pulp and Paper. *[S.l.]*: Elsevier, 2018. p. 295–351.

BALLA, Vamsi Krishna *et al.* Additive manufacturing of natural fiber reinforced polymer composites: Processing and prospects. Composites Part B: Engineering, v. 174, p. 106956, out. 2019.

BARCZEWSKI, Mateusz; MATYKIEWICZ, Danuta; SZOSTAK, Marek. The effect of two-step surface treatment by hydrogen peroxide and silanization of flax/cotton fabrics on epoxy-based laminates thermomechanical properties and structure. Journal of Materials Research and Technology, v. 9, n. 6, p. 13813–13824, 2020.

BARTOS, András *et al.* Biobased PLA/sugarcane bagasse fiber composites: Effect of fiber characteristics and interfacial adhesion on properties. Composites Part A: Applied Science and Manufacturing, v. 143, 2021.

BASBASAN, Angel J. *et al.* Emerging challenges on viability and commercialization of lignin in biobased polymers for food packaging: A review. Food Packaging and Shelf Life, v. 34, p. 100969, 1 dez. 2022.

BELGACEM, Mohamed Naceur; GANDINI, Alessandro. The surface modification of cellulose fibres for use as reinforcing elements in composite materials. Composite Interfaces, v. 12, n. 1–2, p. 41–75, 2005.

BERGSTRÖM, Jörgen S.; HAYMAN, Danika. An Overview of Mechanical Properties and Material Modeling of Polylactide (PLA) for Medical Applications. Annals of Biomedical Engineering, v. 44, n. 2, p. 330–340, 2016.

BHADANE, Rupali *et al.* Lignin-Grafted Poly(*n* -Butyl Acrylate) Copolymers as Soft Materials for Adhesive Applications: A Comparison of Hardwood, Softwood, and Straw Lignin. Biomacromolecules, 12 jun. 2025.

BHAT, Asrar Rafiq; KUMAR, Rajiv; MURAL, Prasanna Kumar S. Natural fiber reinforced polymer composites: A comprehensive review of Tribo-Mechanical properties. Tribology International, v. 189, n. September, p. 108978, 2023.

BHONG, Mahesh *et al.* Review of composite materials and applications. Materials Today: Proceedings, out. 2023.

BIANCHI, Sauro *et al.* Medium density boards made of groundwood fibres: an analysis of their mechanical and physical properties. European Journal of Wood and Wood Products, v. 77, n. 1, p. 71–77, 30 jan. 2019.

BIKIARIS, Nikolaos D. *et al.* Recent Advances in the Investigation of Poly(lactic acid) (PLA) Nanocomposites: Incorporation of Various Nanofillers and their Properties and Applications. Polymers, v. 15, n. 5, p. 1196, 27 fev. 2023.

BIRNIN-YAURI, Abubakar Umar *et al.* Influence of kenaf core fiber incorporation on the mechanical performance and dimensional stability of oil palm fiber reinforced poly(lactic acid) hybrid biocomposites. BioResources, v. 11, n. 2, p. 3332–3355, 2016.

BOARINO, Alice *et al.* Uniformly Dispersed Poly(lactic acid)-Grafted Lignin Nanoparticles Enhance Antioxidant Activity and UV-Barrier Properties of Poly(lactic acid) Packaging Films. ACS Applied Polymer Materials, v. 4, n. 7, p. 4808–4817, 8 jul. 2022.

BODÍ, Merche B. *et al.* Wildland fire ash: Production, composition and eco-hydro-geomorphic effects. Earth-Science Reviews, v. 130, p. 103–127, 1 mar. 2014.

BOEY, Jet Yin; LEE, Chee Keong; TAY, Guan Seng. Factors Affecting Mechanical Properties of Reinforced Bioplastics: A Review. Polymers, v. 14, n. 18, p. 3737, 7 set. 2022.

BOWYER, W. H.; BADER, M. G. On the re-inforcement of thermoplastics by imperfectly aligned discontinuous fibres. Journal of Materials Science, v. 7, n. 11, p. 1315–1321, 1972.

BUCHANAN, Michael. Solvent extractives of wood and pulp. Nanofibers - Production, Properties and Functional Applications, 2012.

BUHAUG, Halvard *et al.* Climate-driven risks to peace over the 21st century. Climate Risk Management, v. 39, p. 100471, 1 jan. 2023.

BUONO, Pietro *et al.* New Insights on the Chemical Modification of Lignin: Acetylation versus Silylation. ACS Sustainable Chemistry & Engineering, v. 4, n. 10, p. 5212–5222, 3 out. 2016.

CABRERA, Isis Castro *et al.* Chemical functionalization of nano fibrillated cellulose by glycidyl silane coupling agents: A grafted silane network characterization study. International Journal of Biological Macromolecules, v. 165, p. 1773–1782, 2020.

CAMPBELL, F. C. Commercial Composite Processes: These Commercial Processes Produce Far More Parts than the High-performance Processes. Manufacturing Processes for Advanced Composites, p. 399–438, 2004.

CATAÑO, Francisco A. *et al.* Green composites based on thermoplastic starch reinforced with micro- and nano-cellulose by melt blending - A review. International Journal of Biological Macromolecules, v. 248, p. 125939, set. 2023.

CHAND, Navin; FAHIM, Mohammed (ORGS.). Wood reinforced polymer composites. *In*: Tribology of Natural Fiber Polymer Composites. *[S.l.]*: Elsevier, 2008. p. 180–196.

CHANG, Boon Peng; MOHANTY, Amar K.; MISRA, Manjusri. Studies on durability of sustainable biobased composites: a review. RSC Advances, v. 10, n. 31, p. 17955–17999, 2020.

CHATZIPARASKEVA, Georgia *et al.* End-of-Life of Composite Materials in the Framework of the Circular Economy. Microplastics, v. 1, n. 3, p. 377–392, 20 jul. 2022.

CHAUDHARY, Vijay; RAJPUT, Akash Kumar; BAJPAI, Pramendra Kumar. Effect of Particulate Filler on Mechanical Properties of Polyester based Composites. Materials Today: Proceedings, v. 4, n. 9, p. 9893–9897, 1 jan. 2017.

CHEN, Hongzhang. Biotechnology of lignocellulose: Theory and practice. *[S.l.: S.n.]*.

CHEN, Kang *et al.* Effect of silane coupling agent on compatibility interface and properties of wheat straw/polylactic acid composites. International Journal of Biological Macromolecules, v. 182, n. May, p. 2108–2116, 2021.

CHENG, Heli *et al.* Hemicellulose Extraction and Applications as Hydrogels: A Review. Journal of Applied Polymer Science, v. 142, n. 29, 5 ago. 2025.

CHENG, Juan *et al.* Applications of biodegradable materials in food packaging: A review. Alexandria Engineering Journal, v. 91, p. 70–83, 1 mar. 2024.

CHIHAOUI, Belgacem *et al.* Lignin-containing cellulose fibrils as reinforcement of plasticized PLA biocomposites produced by melt processing using PEG as a carrier. Industrial Crops and Products, v. 175, n. June 2021, 2022.

CHOHAN, Jasgurpreet Singh *et al.* Manufacturing techniques and applications of polymer matrix composites: a brief review. Advances in Materials and Processing Technologies, v. 8, n. 1, p. 884–894, 2022.

CHRISTIAN, Sarah J. Natural fibre-reinforced noncementitious composites (biocomposites). *In*: Nonconventional and Vernacular Construction Materials. *[S.l.]*: Elsevier, 2020. p. 169–187.

CHUN, Koay Seong; HUSSEINSYAH, Salmah; OSMAN, Hakimah. Mechanical and thermal properties of coconut shell powder filled polylactic acid biocomposites: Effects of the filler content and silane coupling agent. Journal of Polymer Research, v. 19, n. 5, 2012.

CORREA, Juan P.; MONTALVO-NAVARRETE, Juan M.; HIDALGO-SALAZAR, Miguel A. Carbon footprint considerations for biocomposite materials for sustainable products: A review. Journal of Cleaner Production, v. 208, p. 785–794, jan. 2019.

COSATE DE ANDRADE, Marina F. *et al.* Life Cycle Assessment of Poly(Lactic Acid) (PLA): Comparison Between Chemical Recycling, Mechanical Recycling and Composting. Journal of Polymers and the Environment, v. 24, n. 4, p. 372–384, 20 dez. 2016.

COSSE, Renato Lemos *et al.* The effect of size and delignification on the mechanical properties of polylactic acid (PLA) biocomposites reinforced with wood fibres via extrusion. RSC Sustainability, v. 1, n. 4, p. 876–885, 2023.

CRUZ-GONZÁLEZ, O. L. *et al.* Effective behavior of long and short fiber-reinforced viscoelastic composites. Applications in Engineering Science, v. 6, p. 100037, jun. 2021.

CUI, Lu *et al.* Rheology of PLA/regenerated cellulose nanocomposites prepared by the pickering emulsion process: Network formation and modeling. Materials & Design, v. 206, p. 109774, 1 ago. 2021.

DAMMAK, Mohamed *et al.* Blends of PBAT with plasticized starch for packaging applications: Mechanical properties, rheological behaviour and biodegradability. Industrial Crops and Products, v. 144, p. 112061, fev. 2020.

DE BUYL, François; KRETSCHMER, Axel. Understanding hydrolysis and condensation kinetics of γ-glycidoxypropyltrimethoxysilane. Journal of Adhesion, v. 84, n. 2, p. 125–142, 2008.

DE JONG, Ed; JUNGMEIER, Gerfried. Biorefinery Concepts in Comparison to Petrochemical Refineries. Industrial Biorefineries and White Biotechnology, p. 3–33, 1 jan. 2015.

DE LIMA, Gabriel Goetten *et al.* Enhancing Barrier and Antioxidant Properties of Nanocellulose Films for Coatings and Active Packaging: A Review. ACS Applied Nano Materials, v. 8, n. 9, p. 4397–4421, 7 mar. 2025.

DEBNATH, Mrittika *et al.* Soft mechanical treatments of recycled fibers using a high-shear homogenizer for tissue and hygiene products. Cellulose, v. 28, n. 12, p. 7981–7994, 25 ago. 2021.

DEL ANGEL-MONROY, M. *et al.* Effect of coconut fibers chemically modified with alkoxysilanes on the crystallization, thermal, and dynamic mechanical properties of poly(lactic acid) composites. Polymer Bulletin, v. 81, n. 1, p. 843–870, 6 jan. 2024.

DELGADO-AGUILAR, M. *et al.* Bio composite from bleached pine fibers reinforced polylactic acid as a replacement of glass fiber reinforced polypropylene, macro and micro-mechanics of the Young's modulus. Composites Part B: Engineering, v. 125, p. 203–210, set. 2017.

DELGADO-AGUILAR, Marc *et al.* The role of lignin on the mechanical performance of polylactic acid and jute composites. International Journal of Biological Macromolecules, v. 116, p. 299–304, 2018.

DELOGU, M. *et al.* Innovative composites and hybrid materials for electric vehicles lightweight design in a sustainability perspective. Materials Today Communications, v. 13, p. 192–209, dez. 2017.

DENG, Qian; LI, Shi; CHEN, Youping. Mechanical properties and failure mechanism of wood cell wall layers. Computational Materials Science, v. 62, p. 221–226, 2012.

DERRADJI, Mehdi; WANG, Jun; LIU, Wenbin. Fiber-Reinforced Phthalonitrile Composites. *In*: Phthalonitrile Resins and Composites. *[S.l.]*: Elsevier, 2018. p. 241–294.

DING, Ruonan *et al.* Enhancement of 3D printability and mechanical properties of polylactic acid/lignin biocomposites via interface engineering. Industrial Crops and Products, v. 194, p. 116286, 1 abr. 2023.

DOAN, Thi Thu Loan; BRODOWSKY, Hanna; MÄDER, Edith. Jute fibre/epoxy composites: Surface properties and interfacial adhesion. Composites Science and Technology, v. 72, n. 10, p. 1160–1166, 2012.

DOKL, Monika *et al.* Global projections of plastic use, end-of-life fate and potential changes in consumption, reduction, recycling and replacement with bioplastics to 2050. Sustainable Production and Consumption, v. 51, p. 498–518, 1 nov. 2024.

DOMINGUEZ-CANDELA, Ivan *et al.* Novel compatibilizers and plasticizers developed from epoxidized and maleinized chia oil in composites based on PLA and chia seed flour. European Polymer Journal, v. 173, n. April, p. 111289, 2022.

DONATE, Ricardo; MONZÓN, Mario; ALEMÁN-DOMÍNGUEZ, Mariá Elena. Additive manufacturing of PLA-based scaffolds intended for bone regeneration and strategies to improve their biological properties. E-Polymers, v. 20, n. 1, p. 571–599, 2020.

DONG, Zhen *et al.* Enhancement of Interface between Lignocellulosic Fibers and Polypropylene Matrix via the Structure Alteration of Lignin at Elevated Temperatures. Materials, v. 13, n. 23, p. 5428, 28 nov. 2020.

DUAN, Xuejun *et al.* A citric acid/cysteine based bioadditive for plasticization and enhancing <scp>UV</scp> shielding of poly(vinyl chloride). Polymer International, v. 71, n. 2, p. 227–231, 19 fev. 2022.

DUSATEC. Gelimat ™ Technology Gelimat ™ Technology. Disponível em: <https://www.dusatec.com/images/Gelimat_brochure_final.pdf>.

EDEBALI, Serpil. Methods of engineering of biopolymers and biocomposites. Advanced Green Materials: Fabrication, Characterization and Applications of Biopolymers and Biocomposites, p. 351–357, 1 jan. 2021.

EFTEKHARI, Mohammadreza; FATEMI, Ali. Tensile behavior of thermoplastic composites including temperature, moisture, and hygrothermal effects. Polymer Testing, v. 51, p. 151–164, maio 2016.

EL OMARI, Y. *et al.* Interfacial rheology for probing the in-situ chemical reaction at interfaces of molten polymer systems. Materials Today Communications, v. 35, p. 105640, jun. 2023.

ELFALEH, Issam *et al.* A comprehensive review of natural fibers and their composites: An eco-friendly alternative to conventional materials. Results in Engineering, v. 19, p. 101271, set. 2023.

EL-SABBAGH, A. Effect of coupling agent on natural fibre in natural fibre/polypropylene composites on mechanical and thermal behaviour. Composites Part B: Engineering, v. 57, p. 126–135, 1 fev. 2014.

ENG, Chern Chiet *et al.* Compositional and Morphological Changes of Chemical Modified Oil Palm Mesocarp Fiber by Alkaline Bleaching and Silane Coupling Agents. BioResources, v. 9, n. 3, 17 jul. 2014.

ESELINI, Najah *et al.* Production and characterization of poly (lactic acid)-based biocomposites filled with basalt fiber and flax fiber hybrid. Journal of Elastomers and Plastics, v. 52, n. 8, p. 701–716, 2020.

ESPINACH, F. X. *et al.* An alternative method to evaluate the micromechanics tensile strength properties of natural fiber strand reinforced polyolefin composites. The case of hemp strand-reinforced polypropylene. Composites Part B: Engineering, v. 273, p. 111211, mar. 2024.

ESTEBAN, Luis G. *et al.* Softwood Anatomy: A Review. Forests, v. 14, n. 2, p. 323, 6 fev. 2023.

FAN, Zhiqiang *et al.* Highly Enhanced Mechanical, Thermal, and Crystallization Performance of PLA/PBS Composite by Glass Fiber Coupling Agent Modification. Polymers, v. 15, n. 15, p. 3164, 26 jul. 2023.

FANG, Xiaoyang *et al.* Improved interfacial performance of bamboo fibers/polylactic acid composites enabled by a self-supplied bio-coupling agent strategy. Journal of Cleaner Production, v. 380, n. P1, p. 134719, 2022.

FARAH, Shady; ANDERSON, Daniel G.; LANGER, Robert. Physical and mechanical properties of PLA, and their functions in widespread applications — A comprehensive review. Advanced Drug Delivery Reviews, v. 107, p. 367–392, dez. 2016.

FAZELI, Mahyar *et al.* Lignin beyond the *status quo* : recent and emerging composite applications. Green Chemistry, v. 26, n. 2, p. 593–630, 2024.

FERNANDES, Célio *et al.* Modeling and Optimization of the Injection-Molding Process: A Review. Advances in Polymer Technology, v. 37, n. 2, p. 429–449, 2018.

FERNANDES, Felipe Cicaroni *et al.* Polyamide-6 composites reinforced with cellulose fibers and fabricated by extrusion: Effect of fiber bleaching on mechanical properties and stability. Polymer Composites, v. 38, n. 2, p. 299–308, 29 fev. 2017.

FERRAZ, André *et al.* Estimating the chemical composition of biodegraded pine and eucalyptus wood by DRIFT spectroscopy and multivariate analysis. Bioresource Technology, v. 74, n. 3, p. 201–212, 2000.

FERREIRA, Diana P.; CRUZ, Juliana; FANGUEIRO, Raul. Surface modification of natural fibers in polymer composites. *[S.l.]*: Elsevier Ltd, 2018.

FLAKE C CAMPBELL JR. Manufacturing Processes for Advanced Composites. *[S.l.]*: Elsevier, 2003.

FORMELA, Krzysztof. Strategies for compatibilization of polymer/waste tire rubber systems prepared via melt-blending. Advanced Industrial and Engineering Polymer Research, ago. 2023.

FOURATI, Yesmine *et al.* Cellulose nanofibrils reinforced PBAT/TPS blends: Mechanical and rheological properties. International Journal of Biological Macromolecules, v. 183, p. 267–275, jul. 2021.

FRASCA, Serena *et al.* Compatibility of Kraft Lignin and Phenol-Organosolv Lignin with PLA in 3D Printing and Assessment of Mechanical Recycling. ACS Applied Polymer Materials, v. 6, n. 22, p. 13574–13584, 22 nov. 2024.

FREDI, Giulia; DORIGATO, Andrea. Compatibilization of biopolymer blends: A review. Advanced Industrial and Engineering Polymer Research, v. 7, n. 4, p. 373–404, 1 out. 2024.

GARKHAIL, S. K.; HEIJENRATH, R. W. H.; PEIJS, T. Mechanical properties of natural-fibre-mat-reinforced thermoplastics based on flax fibres and polypropylene. Applied Composite Materials, v. 7, n. 5–6, p. 351–372, 2000.

GARLOTTA, Donald. A Literature Review of Poly (Lactic Acid) A Literature Review of Poly (Lactic Acid). Journal of Polymers and the Environment, v. 9, n. 2, p. 63–84, 2002.

GEORGS, Valter *et al.* A critical review on lignin structure, chemistry, and modification towards utilisation in additive manufacturing of lignin-based composites. Industrial Crops and Products, v. 233, p. 121416, 1 out. 2025.

GIRONÈS, J. *et al.* Biocomposites from Musa textilis and polypropylene: Evaluation of flexural properties and impact strength. Composites Science and Technology, v. 71, n. 2, p. 122–128, jan. 2011.

GONÇALVES, R. M.; MARTINHO, Alberto; OLIVEIRA, J. P. Recycling of Reinforced Glass Fibers Waste: Current Status. Materials, v. 15, n. 4, p. 1596, 21 fev. 2022.

GRANDA, L. A. *et al.* Towards a good interphase between bleached kraft softwood fibers and poly(lactic) acid. Composites Part B: Engineering, v. 99, p. 514–520, 2016.

GRAUPNER, Nina *et al.* Making positive use of the fibrillation of lyocell fibres in composite materials. Composites Part C: Open Access, v. 11, p. 100359, jul. 2023.

GREB, C. *et al.* Fabrics for reinforcement of engineering composites. *In*: Engineering of High-Performance Textiles. *[S.l.]*: Elsevier, 2018. p. 489–512.

GREENE, Joseph P. Sustainable Plastics. *[S.l.]*: Wiley, 2014.

GRØNDAHL, L.; JACK, K. S.; GOONASEKERA, C. S. Composite materials for bone repair. *In*: Biomedical Composites. *[S.l.]*: Elsevier, 2017. p. 83–110.

GUO, Aofei *et al.* State-of-the-art review on the use of lignocellulosic biomass in cementitious materials. Sustainable Structures, v. 3, n. 1, 2023.

GUO, Jianbing *et al.* The Influence of Compatibility on the Structure and Properties of PLA/Lignin Biocomposites by Chemical Modification. Polymers, v. 12, n. 1, p. 56, 31 dez. 2019.

GUPTA, Anju *et al.* Rheological and thermo-mechanical properties of poly(lactic acid)/lignin-coated cellulose nanocrystal composites. ACS Sustainable Chemistry and Engineering, v. 5, n. 2, p. 1711–1720, 6 fev. 2017.

GUPTA, Ayushi; KUMAR, Narendra; SACHDEVA, Anish. Factors affecting the ageing of polymer composite: A state of art. Polymer Degradation and Stability, v. 221, n. January, p. 110670, 2024.

GUPTA, Vijai Kumar *et al.* Biobased biorefineries: Sustainable bioprocesses and bioproducts from biomass/bioresources special issue. Renewable and Sustainable Energy Reviews, v. 167, p. 112683, 1 out. 2022.

GURUNATHAN, T.; MOHANTY, Smita; NAYAK, Sanjay K. A review of the recent developments in biocomposites based on natural fibres and their application perspectives. Composites Part A: Applied Science and Manufacturing, v. 77, p. 1–25, 2015.

HADJADJ, Aomar *et al.* Effects of cellulose fiber content on physical properties of polyurethane based composites. Composite Structures, v. 135, p. 217–223, jan. 2016.

HAKIM, R. H. *et al.* PLA/SiO2 composites: Influence of the filler modifications on the morphology, crystallization behavior, and mechanical properties. Journal of Applied Polymer Science, v. 134, n. 40, 2017.

HAMAD, Kotiba *et al.* Polylactic acid blends: The future of green, light and tough. Progress in Polymer Science, v. 85, p. 83–127, out. 2018.

HASAN, Afnan; RABBI, M. S.; MARUF BILLAH, Md. Making the lignocellulosic fibers chemically compatible for composite: A comprehensive review. Cleaner Materials, v. 4, n. March, p. 100078, 2022.

HASHEM, Ali; FARAG, Sohair. Cotton bleaching: evolution, current practices, and future perspectives. The International Journal of Advanced Manufacturing Technology, 18 ago. 2025.

HASHEMI, Seyedeh-Sara *et al.* A review on application of herbals and their polymer composites in wound healing. Arabian Journal of Chemistry, v. 17, n. 7, p. 105820, jul. 2024.

HASRC, V. *et al.* Versatility of biodegradable biopolymers: Degradability and an in vivo application. Journal of Biotechnology, v. 86, n. 2, p. 135–150, 2001.

HAUSSER, Nicolas; MARINKOVIC, Sinisa; ESTRINE, Boris. Improved sulfuric acid decrystallization of wheat straw to obtain high yield carbohydrates. Cellulose, v. 18, n. 6, p. 1521–1525, 2 dez. 2011.

HE, Lili *et al.* Enhanced Antioxidation and UV-Absorption Ability of Industrial Lignin via Promoting Phenolic Contents and Hydrophilicity. ACS Omega, v. 10, n. 7, p. 6745–6752, 25 fev. 2025.

HERBST, Giulia *et al.* Silane-modified high-yield lignocellulosic fibers as reinforcement of polylactic acid: Enhancement of interfacial adhesion for high-performance biocomposites. Industrial Crops and Products, v. 218, p. 119027, 15 out. 2024.

HIETALA, Maiju *et al.* Extrusion processing of green biocomposites: Compounding, fibrillation efficiency, and fiber dispersion. Journal of Applied Polymer Science, v. 131, n. 6, 15 mar. 2014.

HINTZ, H. L.; LAWAL, Sunday A. Paper: Pulping and Bleaching. Reference Module in Materials Science and Materials Engineering, 1 jan. 2018.

HOSSEINAEI, Omid *et al.* Effects of hemicellulose extraction on properties of wood flour and wood–plastic composites. Composites Part A: Applied Science and Manufacturing, v. 43, n. 4, p. 686–694, 1 abr. 2012.

HRISTOV, Velichko; VLACHOPOULOS, John. Influence of Coupling Agents on Melt Flow Behavior of Natural Fiber Composites. Macromolecular Materials and Engineering, v. 292, n. 5, p. 608–619, 14 maio 2007.

HSISSOU, Rachid *et al.* Polymer composite materials: A comprehensive review. Composite Structures, v. 262, n. December 2020, p. 0–3, 2021.

HUBBELL, Christopher A.; RAGAUSKAS, Arthur J. Effect of acid-chlorite delignification on cellulose degree of polymerization. Bioresource Technology, v. 101, n. 19, p. 7410–7415, 1 out. 2010.

HUO, Dan *et al.* Modified nano-lignocellulose preparation by azolidinone and its application in polylactic acid composite film and paper coating. Industrial Crops and Products, v. 223, p. 120151, 1 jan. 2025.

ILYAS, R. A. *et al.* Natural Fiber-Reinforced Polylactic Acid , Polylactic Acid. Polymers, v. 14, n. 202, 2022.

ISLAM, Mohammad S.; PICKERING, Kim L.; FOREMAN, Nic J. Influence of alkali fiber treatment and fiber processing on the mechanical properties of hemp/epoxy composites. Journal of Applied Polymer Science, v. 119, n. 6, p. 3696–3707, 15 mar. 2011.

ISLAM, Monjurul *et al.* Impact of bioplastics on environment from its production to end-of-life. Process Safety and Environmental Protection, v. 188, p. 151–166, 1 ago. 2024.

JALAEE, Adel; FOSTER, E. Johan. Improvement in the Thermomechanical Properties and Adhesion of Wood Fibers to the Polyamide 6 Matrix by Sequential Ball Milling Technique. ACS Sustainable Chemistry & Engineering, v. 12, n. 1, p. 490–500, 8 jan. 2024.

JANDAS, P. J. *et al.* Effect of surface treatments of banana fiber on mechanical, thermal, and biodegradability properties of PLA/banana fiber biocomposites. Polymer Composites, v. 32, n. 11, p. 1689–1700, 13 nov. 2011.

JAVIER-ASTETE, Rosario; JIMENEZ-DAVALOS, Jorge; ZOLLA, Gaston. Determination of hemicellulose, cellulose, holocellulose and lignin content using FTIR in Calycophyllum spruceanum (Benth.) K. Schum. And Guazuma crinita Lam. PLoS ONE, v. 16, n. 10 October, p. 1–12, 2021.

JAYAKUMAR, Sangeetha; SARAVANAN, T.; PHILIP, John. A review on polymer nanocomposites as lead-free materials for diagnostic X-ray shielding: Recent advances, challenges and future perspectives. Hybrid Advances, v. 4, p. 100100, dez. 2023.

JEM, K. Jim; POL, Johan F. van der; VOS, Sicco de. Microbial Lactic Acid, Its Polymer Poly(lactic acid), and Their Industrial Applications. *In*: G. Chen (Ed.), Plastics From Bacteria Natural Functions And Applications. *[S.l.: S.n.]*. v. 14 p. 121–132.

JEM, K. Jim; TAN, Bowen. The development and challenges of poly (lactic acid) and poly (glycolic acid). Advanced Industrial and Engineering Polymer Research, v. 3, n. 2, p. 60–70, 2020.

JEONG, Euichul *et al.* Innovative Injection Molding Process for the Fabrication of Woven Fabric Reinforced Thermoplastic Composites. Polymers, v. 14, n. 8, p. 1577, 13 abr. 2022.

JIJU, Poulose Sarojam *et al.* Sustainability through lignin valorization: recent innovations and applications driving industrial transformation. Bioresources and Bioprocessing, v. 12, n. 1, p. 88, 22 ago. 2025.

JOHANSSON, Matilda *et al.* Effect of lignin acetylation on the mechanical properties of lignin-poly-lactic acid biocomposites for advanced applications. Industrial Crops and Products, v. 202, p. 117049, 15 out. 2023.

JOHN, Maya Jacob; THOMAS, Sabu. Biofibres and biocomposites. Carbohydrate Polymers, v. 71, n. 3, p. 343–364, 2008.

JOSE, Josmin P. *et al.* Part One Introduction to Polymer Composites. Polymer Composites, Biocomposites, v. 1, p. 1–16, 2012.

JOSHI, S. V. *et al.* Are natural fiber composites environmentally superior to glass fiber reinforced composites? Composites Part A: Applied Science and Manufacturing, v. 35, n. 3, p. 371–376, mar. 2004.

JU, Zehui *et al.* Thermal and mechanical properties of polyethylene glycol (PEG)-modified lignin/polylactic acid (PLA) biocomposites. International Journal of Biological Macromolecules, v. 262, p. 129997, 1 mar. 2024.

JULIAN, Fernando *et al.* Bio-based composites from stone groundwood applied to new product development. BioResources, v. 7, n. 4, p. 5829–5842, 2012.

KABIR, M. M. *et al.* Chemical treatments on plant-based natural fibre reinforced polymer composites: An overview. Composites Part B: Engineering, v. 43, n. 7, p. 2883–2892, 1 out. 2012.

KAMARUDIN, Siti Hasnah *et al.* A Review on Natural Fiber Reinforced Polymer Composites (NFRPC) for Sustainable Industrial Applications. Polymers, v. 14, n. 17, p. 3698, 5 set. 2022.

KAMDEM TAMO, Arnaud *et al.* Lignocellulosic biomass and its main structural polymers as sustainable materials for (bio)sensing applications. Journal of Materials Chemistry A, v. 13, n. 30, p. 24185–24253, 2025.

KAPUGE DONA, Nawoda L.; SMITH, Rhett C. Tailoring Polymer Properties Through Lignin Addition: A Recent Perspective on Lignin-Derived Polymer Modifications. Molecules, v. 30, n. 11, p. 2455, 3 jun. 2025.

KARTHIK, A. *et al.* A Review on Surface Modification of Plant Fibers for Enhancing Properties of Biocomposites. ChemistrySelect, v. 9, n. 21, 4 jun. 2024.

KAUR, Ramandeep; SHARMA, Minaxi. Cereal polysaccharides as sources of functional ingredient for reformulation of meat products: A review. Journal of Functional Foods, v. 62, p. 103527, nov. 2019.

KHAKALO, Alexey *et al.* All-Wood Composite Material by Partial Fiber Surface Dissolution with an Ionic Liquid. ACS Sustainable Chemistry & Engineering, v. 7, n. 3, p. 3195–3202, 4 fev. 2019.

KHAN, Mohammad Z. R.; SRIVASTAVA, Sunil Kumar; GUPTA, M. K. A state-of-the-art review on particulate wood polymer composites: Processing, properties and applications. Polymer Testing, v. 89, p. 106721, set. 2020.

KHOATHANE, Moshibudi C.; SADIKU, Emmanuel R.; AGWUNCHA, Chinenyeze S. Surface Modification of Natural Fiber Composites and their Potential Applications. *In*: Surface Modification of Biopolymers. *[S.l.]*: Wiley, 2015. p. 370–400.

KHOSRAVANI, Mohammad Reza; NASIRI, Sara. Injection molding manufacturing process: review of case-based reasoning applications. Journal of Intelligent Manufacturing, v. 31, n. 4, p. 847–864, 2020.

KHOUAJA, Asma; KOUBAA, Ahmed; BEN DALY, Hachmi. Mechanical and morphological properties of cellulose biocomposites. Chemosphere, v. 379, p. 144415, 1 jun. 2025.

KILIÇ, Eylem *et al.* Circularity of new composites from recycled high density polyethylene and leather waste for automotive bumpers. Testing performance and environmental impact. Science of The Total Environment, v. 919, p. 170413, abr. 2024.

KIM, Sundol; CHUNG, Hoyong. Biodegradable polymers: from synthesis methods to applications of lignin- *graft* -polyester. Green Chemistry, v. 26, n. 21, p. 10774–10803, 2024.

KLUNKLIN, Warinporn *et al.* Effect of Bleaching Processes on Physicochemical and Functional Properties of Cellulose and Carboxymethyl Cellulose from Young and Mature Coconut Coir. Polymers, v. 15, n. 16, p. 3376, 11 ago. 2023.

KOSSENTINI KALLEL, Tasnim *et al.* Mechanical and structural properties of glass fiber-reinforced polypropylene (PPGF) composites. Polymer Composites, v. 39, n. 10, p. 3497–3508, 6 out. 2018.

KU, H. *et al.* A review on the tensile properties of natural fiber reinforced polymer composites. Composites Part B: Engineering, v. 42, n. 4, p. 856–873, 2011.

LA MANTIA, F. P.; MORREALE, M. Green composites: A brief review. Composites Part A: Applied Science and Manufacturing, v. 42, n. 6, p. 579–588, jun. 2011.

LEE, Ching Hao; KHALINA, Abdan; LEE, Seng Hua. Importance of Interfacial Adhesion Condition on Characterization of Plant-Fiber-Reinforced Polymer Composites: A Review. Polymers, v. 13, n. 3, p. 438, 29 jan. 2021.

LI, Jing *et al.* Advances in lignin chemistry during pulping and bleaching. Industrial Crops and Products, v. 229, p. 121004, 1 jul. 2025a.

LI, Kunpeng *et al.* Lignin's effect on cellulose fiber bonding and inter-fiber interface design for enhancing densified wood. Carbohydrate Polymers, v. 359, p. 123573, 1 jul. 2025b.

LI, Liangrong *et al.* From Molecular Design to Practical Applications: Strategies for Enhancing the Optical and Thermal Performance of Polyimide Films. Polymers, v. 16, n. 16, p. 2315, 16 ago. 2024.

LI, Mi *et al.* Recent advancements of plant-based natural fiber–reinforced composites and their applications. Composites Part B: Engineering, v. 200, p. 108254, nov. 2020.

LI, Shuai *et al.* Flexural and energy absorption properties of natural-fiber reinforced composites with a novel fabrication technique. Composites Communications, v. 16, p. 124–131, dez. 2019a.

LI, Shuangyan *et al.* Effect of lignin extracted by different methods on the properties and structure of lignin/starch fiber membranes. Industrial Crops and Products, v. 224, p. 120400, 1 fev. 2025c.

LI, Xiangrui *et al.* A review of research and application of polylactic acid composites. Journal of Applied Polymer Science, v. 140, n. 7, 15 fev. 2023.

LI, Yuanyuan *et al.* Encapsulating TiO_2 in Lignin-Based Colloidal Spheres for High Sunscreen Performance and Weak Photocatalytic Activity. ACS Sustainable Chemistry & Engineering, v. 7, n. 6, p. 6234–6242, 18 mar. 2019b.

LIM, L. T.; AURAS, R.; RUBINO, M. Processing technologies for poly(lactic acid). Progress in Polymer Science (Oxford), v. 33, n. 8, p. 820–852, 2008.

LIN, Minsheng *et al.* Revealing the structure-activity relationship between lignin and anti-UV radiation. Industrial Crops and Products, v. 174, p. 114212, 15 dez. 2021.

LIU, S. J. Injection molding in polymer matrix composites. *[S.l.]*: Woodhead Publishing Limited, 2012.

LIU, Shan *et al.* Current applications of poly(lactic acid) composites in tissue engineering and drug delivery. Composites Part B: Engineering, v. 199, n. May, p. 108238, 2020.

LIU, Yucheng *et al.* Characterization of silane treated and untreated natural cellulosic fibre from corn stalk waste as potential reinforcement in polymer composites. Carbohydrate Polymers, v. 218, n. April, p. 179–187, 2019.

LONG, Haibo *et al.* Effect of polyethylene glycol on mechanical properties of bamboo fiber-reinforced polylactic acid composites. Journal of Applied Polymer Science, v. 136, n. 26, 10 jul. 2019.

LÓPEZ, J. P. *et al.* Impact and flexural properties of stone-ground wood pulp-reinforced polypropylene composites. Polymer Composites, v. 34, n. 6, p. 842–848, 25 jun. 2013.

LÓPEZ, Joan P. *et al.* Tensile strength characteristics of polypropylene composites reinforced with stone groundwood fibers from softwood. BioResources, v. 7, n. 3, p. 3188–3200, 2012.

LÓPEZ, Joan Pere *et al.* Mean intrinsic tensile properties of stone groundwood fibers from softwood. BioResources, v. 6, n. 4, p. 5037–5049, 23 out. 2011.

LOTFI, Amirhossein *et al.* Natural fiber–reinforced composites: A review on material, manufacturing, and machinability. Journal of Thermoplastic Composite Materials, v. 34, n. 2, p. 238–284, 2021.

LUCENA, Andrea *et al.* Hemicellulose/PVA-based bioactive films for food packaging: Effect of the molecular weight of avocado pruning waste-derived hemicellulose on biocomposite properties. International Journal of Biological Macromolecules, v. 309, p. 142982, 1 maio 2025.

LUO, Honglin *et al.* Effects of alkali and alkali/silane treatments of corn fibers on mechanical and thermal properties of its composites with polylactic acid. Polymer Composites, v. 37, n. 12, p. 3499–3507, dez. 2016.

LUO, Shupin; CAO, Jinzhen; MCDONALD, Armando G. Esterification of industrial lignin and its effect on the resulting poly(3-hydroxybutyrate-co-3-hydroxyvalerate) or polypropylene blends. Industrial Crops and Products, v. 97, p. 281–291, 1 mar. 2017.

MA, Qingzhi *et al.* Oxidative delignification: The roles of lignin reactivity and accessibility. Journal of Cleaner Production, v. 363, p. 132351, 20 ago. 2022.

MA, Xiao long *et al.* Inherent relationship between process parameters, crystallization and mechanical properties of continuous carbon fiber reinforced PEEK composites. Defence Technology, v. 24, p. 269–284, 1 jun. 2023.

MAAOUI, Assia *et al.* Assessment of pine wood biomass wastes valorization by pyrolysis with focus on fast pyrolysis biochar production. Journal of the Energy Institute, v. 108, n. November 2022, p. 101242, 2023.

MADHAVAN NAMPOOTHIRI, K.; NAIR, Nimisha Rajendran; JOHN, Rojan Pappy. An overview of the recent developments in polylactide (PLA) research. Bioresource Technology, v. 101, n. 22, p. 8493–8501, nov. 2010.

MAGDZIARZ, Aneta *et al.* Mineral phase transformation of biomass ashes – Experimental and thermochemical calculations. Renewable Energy, v. 128, p. 446–459, 1 dez. 2018.

MALLICK, P. K. 2.18 Particulate Filled and Short Fiber Reinforced Polymer Composites. Comprehensive Composite Materials II, p. 360–400, 1 jan. 2018.

MANSOURI, Nour Eddine El; SALVADÓ, Joan. Structural characterization of technical lignins for the production of adhesives: Application to lignosulfonate, kraft, soda-anthraquinone, organosolv and ethanol process lignins. Industrial Crops and Products, v. 24, n. 1, p. 8–16, 1 jul. 2006.

MANU, T. *et al.* Biocomposites: A review of materials and perception. Materials Today Communications, v. 31, p. 103308, jun. 2022.

MARIANA, Mariana *et al.* A current advancement on the role of lignin as sustainable reinforcement material in biopolymeric blends. Journal of Materials Research and Technology, v. 15, p. 2287–2316, 1 nov. 2021.

MARTÍNEZ-LANDEROS, V. H. *et al.* Studies on the influence of surface treatment type, in the effectiveness of structural adhesive bonding, for carbon fiber reinforced composites. Journal of Manufacturing Processes, v. 39, p. 160–166, mar. 2019.

MBOOWA, Drake. A review of the traditional pulping methods and the recent improvements in the pulping processes. Biomass Conversion and Biorefinery, v. 14, n. 1, p. 1–12, 3 jan. 2024.

MEI, Qingqing *et al.* Selectively transform lignin into value-added chemicals. Chinese Chemical Letters, v. 30, n. 1, p. 15–24, jan. 2019.

MÉNDEZ, J. A. *et al.* Evaluation of the reinforcing effect of ground wood pulp in the preparation of polypropylene-based composites coupled with maleic anhydride grafted polypropylene. Journal of Applied Polymer Science, v. 105, n. 6, p. 3588–3596, 15 set. 2007.

MLHEM, Amal; ABU-JDAYIL, Basim; IQBAL, Muhammad Z. High-performance, renewable thermal insulators based on silylated date palm fiber–reinforced poly(β-hydroxybutyrate) composites. Developments in the Built Environment, v. 16, p. 100240, 1 dez. 2023.

MOFOKENG, J. P. *et al.* Comparison of injection moulded, natural fibre-reinforced composites with PP and PLA as matrices. Journal of Thermoplastic Composite Materials, v. 25, n. 8, p. 927–948, 2 dez. 2012.

MOHAMMADI, Majid; ISHAK, Mohamad Ridzwan; SULTAN, Mohamed Thariq Hameed. Exploring Chemical and Physical Advancements in Surface Modification Techniques of Natural Fiber Reinforced Composite: A Comprehensive Review. Journal of Natural Fibers, v. 21, n. 1, 31 dez. 2024.

MOHAMMED, Mohammed *et al.* Interfacial bonding mechanisms of natural fibre-matrix composites: An overview. BioResources, v. 17, n. 4, 10 ago. 2022a.

MOHAMMED, Mohammed *et al.* Surface treatment to improve water repellence and compatibility of natural fiber with polymer matrix: Recent advancement. Polymer Testing, v. 115, p. 107707, 1 nov. 2022b.

MOHAMMED, Mohammed *et al.* Challenges and advancement in water absorption of natural fiber-reinforced polymer composites. Polymer Testing, v. 124, p. 108083, jul. 2023.

MOKHENA, Teboho Clement *et al.* Mechanical properties of cellulose nanofibril papers and their bionanocomposites: A review. Carbohydrate Polymers, v. 273, p. 118507, dez. 2021.

MUJTABA, Muhammad *et al.* Lignocellulosic biomass from agricultural waste to the circular economy: a review with focus on biofuels, biocomposites and bioplastics. Journal of Cleaner Production, v. 402, p. 136815, maio 2023.

MUTJÉ, P. *et al.* Effect of maleated polypropylene as coupling agent for polypropylene composites reinforced with hemp strands. Journal of Applied Polymer Science, v. 102, n. 1, p. 833–840, 5 out. 2006.

NAIK, Rudresh; ALLU, Sai Gowtham; PURNIMA, D. PP/Jute Fiber Composites: Effect of Biological Route of Surface Treatment and Content of Jute on Composites. Applied Biochemistry and Biotechnology, v. 196, n. 5, p. 2869–2880, 19 maio 2024.

NAJAHI, Amira *et al.* High-Lignin-Containing Cellulose Nanofibrils from Date Palm Waste Produced by Hydrothermal Treatment in the Presence of Maleic Acid. Biomacromolecules, v. 24, n. 8, p. 3872–3886, 14 ago. 2023.

NANDI, Parna; DAS, Dipayan. Mechanical, thermo-mechanical and biodegradation behaviour of surface-silanized nettle fabric-reinforced poly(lactic acid) composites. Materials Chemistry and Physics, v. 297, n. January, p. 127381, 2023.

NASER, Ahmed Z.; DEIAB, I.; DARRAS, Basil M. Poly(lactic acid) (PLA) and polyhydroxyalkanoates (PHAs), green alternatives to petroleum-based plastics: a review. RSC Advances, v. 11, n. 28, p. 17151–17196, 2021.

NISHIMURA, Hiroshi *et al.* Direct evidence for α ether linkage between lignin and carbohydrates in wood cell walls. Scientific Reports, v. 8, n. 1, p. 6538, 25 abr. 2018.

NUTHONG, Wiphawee *et al.* Impact Property of Flexible Epoxy Treated Natural Fiber Reinforced PLA Composites. Energy Procedia, v. 34, p. 839–847, 2013.

OA, Ogah. Rheological Properties of Natural Fiber Polymer Composites. MOJ Polymer Science, v. 1, n. 4, 6 set. 2017.

OLADZADABBASABADI, Nazila *et al.* Leveraging lignin as mussel-bioinspired adhesives and fillers for sustainable food-packaging applications: A review. International Journal of Biological Macromolecules, v. 318, p. 145029, 1 jul. 2025.

OLEKSY, Małgorzata; DYNAROWICZ, Klaudia; AEBISHER, David. Advances in Biodegradable Polymers and Biomaterials for Medical Applications—A Review. Molecules, v. 28, n. 17, p. 6213, 24 ago. 2023.

OLIVER-ORTEGA, H. *et al.* Tensile properties and micromechanical analysis of stone groundwood from softwood reinforced bio-based polyamide11 composites. Composites Science and Technology, v. 132, p. 123–130, ago. 2016.

OLIVER-ORTEGA, Helena *et al.* Impact Strength and Water Uptake Behavior of Bleached Kraft Softwood-Reinforced PLA Composites as Alternative to PP-Based Materials. Polymers, v. 12, n. 9, p. 2144, 20 set. 2020.

OO, Hay Mon *et al.* Physicochemical characterization of forest and sugarcane leaf combustion's particulate matters using electron microscopy, EDS, XRD and TGA. Journal of Environmental Sciences, v. 99, p. 296–310, 1 jan. 2021.

ÖSTERBERG, Monika *et al.* Biobased Nanomaterials─The Role of Interfacial Interactions for Advanced Materials. Chemical Reviews, v. 123, n. 5, p. 2200–2241, 8 mar. 2023.

OUSHABI, Abdessamad. The pull-out behavior of chemically treated lignocellulosic fibers/polymeric matrix interface (LF/PM): A review. Composites Part B: Engineering, v. 174, p. 107059, 1 out. 2019.

OZYHAR, T.; BARADEL, F.; ZOPPE, J. Effect of functional mineral additive on processability and material properties of wood-fiber reinforced poly(lactic acid) (PLA)

composites. Composites Part A: Applied Science and Manufacturing, v. 132, n. November 2019, p. 105827, 2020.

PANG, Xuan *et al.* Polylactic acid (PLA): Research, development and industrialization. Biotechnology Journal, v. 5, n. 11, p. 1125–1136, 5 nov. 2010.

PAPADOPOULOU, Evie L. *et al.* Green Composites of Poly(3-hydroxybutyrate) Containing Graphene Nanoplatelets with Desirable Electrical Conductivity and Oxygen Barrier Properties. ACS Omega, v. 4, n. 22, p. 19746–19755, 26 nov. 2019.

PAPE, Peter G. Adhesion Promoters: Silane Coupling Agents. *[S.l.]*: Elsevier, 2011. v. 3

PARK, Chan-Woo *et al.* Effect of Lignin Plasticization on Physico-Mechanical Properties of Lignin/Poly(Lactic Acid) Composites. Polymers, v. 11, n. 12, p. 2089, 13 dez. 2019.

PARTANEN, Asta; CARUS, Michael. Biocomposites, find the real alternative to plastic – An examination of biocomposites in the market. Reinforced Plastics, v. 63, n. 6, p. 317–321, 2019.

PELTOLA, Heidi *et al.* Wood based PLA and PP composites: Effect of fibre type and matrix polymer on fibre morphology, dispersion and composite properties. Composites Part A: Applied Science and Manufacturing, v. 61, p. 13–22, jun. 2014.

PELTOLA, Heidi *et al.* Influence of pulp bleaching and compatibilizer selection on performance of pulp fiber reinforced PLA biocomposites. Journal of Applied Polymer Science, v. 136, n. 37, 5 out. 2019.

PENJUMRAS, P. *et al.* Effect of silanecoupling agent on properties of biocomposites based on poly(lactic acid)and durian rind cellulose. IOP Conference Series: Materials Science and Engineering, v. 137, p. 012006, jul. 2016.

PHIRI, Resego *et al.* Development of sustainable biopolymer-based composites for lightweight applications from agricultural waste biomass: A review. Advanced Industrial and Engineering Polymer Research, v. 6, n. 4, p. 436–450, out. 2023.

PICKERING, K. L.; EFENDY, M. G. Aruan; LE, T. M. A review of recent developments in natural fibre composites and their mechanical performance. Composites Part A: Applied Science and Manufacturing, v. 83, p. 98–112, 1 abr. 2016.

PINTO, Emmanuel *et al.* Cellulose processing from biomass and its derivatization into carboxymethylcellulose: A review. Scientific African, v. 15, p. e01078, 1 mar. 2022.

PLASTICS EUROPE. Plastics – the Facts 2022: An analysis of European plastics production, demand, conversion and end-of-life management. *[S.d.]*.

POLAK-KRAŚNA, Katarzyna *et al.* Physical and mechanical degradation behaviour of semi-crystalline PLLA for bioresorbable stent applications. Journal of the Mechanical Behavior of Biomedical Materials, v. 118, p. 104409, jun. 2021.

PROME, Farah Samsi *et al.* Different chemical treatments of natural fiber composites and their impact on water absorption behavior and mechanical strength. Hybrid Advances, v. 8, p. 100379, 1 mar. 2025.

QAISS, Abouelkacem; BOUHFID, Rachid; ESSABIR, Hamid. Effect of Processing Conditions on the Mechanical and Morphological Properties of Composites Reinforced by Natural Fibres. *In*: Manufacturing of Natural Fibre Reinforced Polymer Composites. Cham: Springer International Publishing, 2015. p. 177–197.

QIAO, Yao *et al.* A review of the fabrication methods and mechanical behavior of continuous thermoplastic polymer fiber–thermoplastic polymer matrix composites. Polymer Composites, v. 44, n. 2, p. 694–733, 18 fev. 2023.

QIAO, Yuhui *et al.* In-situ microfibrillated Poly(ε-caprolactone)/ Poly(lactic acid) composites with enhanced rheological properties, crystallization kinetics and foaming ability. Composites Part B: Engineering, v. 208, p. 108594, 1 mar. 2021.

RAHMAN, Rozyanty; PUTRA, Syed Zhafer Firdaus Syed. Tensile properties of natural and synthetic fiber-reinforced polymer composites. *[S.l.]*: Elsevier Ltd, 2018.

RAJESHKUMAR, G. *et al.* Environment friendly, renewable and sustainable poly lactic acid (PLA) based natural fiber reinforced composites – A comprehensive review. Journal of Cleaner Production, v. 310, n. April, p. 127483, 2021.

RAMACHANDRAN, Arun Ramnath *et al.* Modification of Fibers and Matrices in Natural Fiber Reinforced Polymer Composites: A Comprehensive Review. Macromolecular Rapid Communications, v. 43, n. 17, p. 1–38, 2022.

RANAKOTI, Lalit *et al.* Promising Role of Polylactic Acid as an Ingenious Biomaterial in Scaffolds, Drug Delivery, Tissue Engineering, and Medical Implants: Research Developments, and Prospective Applications. Molecules, v. 28, n. 2, p. 485, 4 jan. 2023.

RAO, G. Surya; DEBNATH, K.; MAHAPATRA, R. N. Recycling and degradation behaviour of the bamboo fibre reinforced green composite fabricated by injection moulding. Sustainable Materials and Technologies, v. 39, p. e00865, abr. 2024.

RASHID, Tazien; KAIT, Chong Fai; MURUGESAN, Thanabalan. A “Fourier Transformed Infrared” Compound Study of Lignin Recovered from a Formic Acid Process. Procedia Engineering, v. 148, p. 1312–1319, 1 jan. 2016.

RAY, Suprakas Sinha; BOUSMINA, Mosto. Biodegradable polymer/layered silicate nanocomposites. Polymer Nanocomposites, p. 57–129, 2006.

RAYUNG, Marwah *et al.* The Effect of Fiber Bleaching Treatment on the Properties of Poly(lactic acid)/Oil Palm Empty Fruit Bunch Fiber Composites. International Journal of Molecular Sciences, v. 15, n. 8, p. 14728–14742, 22 ago. 2014.

RENCORET, Jorge *et al.* Variations in the composition and structure of the lignins of oat (Avena sativa L.) straws according to variety and planting season. International Journal of Biological Macromolecules, v. 242, p. 124811, 1 jul. 2023.

RESE, Morten *et al.* Detailed Characterization of the Conversion of Hardwood and Softwood Lignin by a Brown-Rot Basidiomycete. Biomacromolecules, v. 26, n. 2, p. 1063–1074, 10 fev. 2025.

REYES, Pablo *et al.* Characterization of the hemicellulosic fraction obtained after pre-hydrolysis of pinus radiata wood chips with hot-water at different initial PH. Journal of the Chilean Chemical Society, v. 58, n. 1, p. 1614–1618, 2013.

RIDHO, Muhammad Rasyidur *et al.* Lignin as Green Filler in Polymer Composites: Development Methods, Characteristics, and Potential Applications. Advances in Materials Science and Engineering, v. 2022, p. 1–33, 30 abr. 2022.

RIGHETTI, Grazia Isa C.; FAEDI, Filippo; FAMULARI, Antonino. Embracing Sustainability: The World of Bio-Based Polymers in a Mini Review. Polymers, v. 16, n. 7, p. 950, 30 mar. 2024.

RODELA, Mrittika Hasan; CHOWDHURY, Indranil; HOHNER, Amanda K. Emerging investigator series: physicochemical properties of wildfire ash and implications for particle stability in surface waters. Environmental Science: Processes & Impacts, v. 24, n. 11, p. 2129–2139, 2022.

RODRÍGUEZ, L. Joana *et al.* Life-Cycle Assessment and Life-Cycle Cost study of Banana (Musa sapientum) fiber Biocomposite materials. Procedia CIRP, v. 69, p. 585–590, 2018.

ROSADO, Mario J. *et al.* Differences in the content, composition and structure of the native-like lignins in leucaena and tagasaste shrubs for biorefinery applications. Industrial Crops and Products, v. 231, p. 121195, 1 set. 2025.

RUBIO-LÓPEZ, A. *et al.* Manufacture of compression moulded PLA based biocomposites: A parametric study. Composite Structures, v. 131, p. 995–1000, 1 nov. 2015.

RUDIN, Alfred; CHOI, Phillip. Biopolymers. *In*: The Elements of Polymer Science & Engineering. *[S.l.]*: Elsevier, 2013. p. 521–535.

SABA, N.; JAWAID, M. A review on thermomechanical properties of polymers and fibers reinforced polymer composites. Journal of Industrial and Engineering Chemistry, v. 67, p. 1–11, nov. 2018.

SABLE, Inese *et al.* COMPARISON OF THE PROPERTIES OF WOOD AND PULP FIBERS FROM LODGEPOLE PINE (Pinus contorta) AND SCOTS PINE (Pinus sylvestris). BioResources, v. 7 (2), n. 203459, p. 1771–1783, 2012.

SAEIDLOU, Sajjad *et al.* Poly(lactic acid) crystallization. Progress in Polymer Science, v. 37, n. 12, p. 1657–1677, 2012.

SAFANDOWSKA, Marta *et al.* Barrier Properties of Semicrystalline Polylactide: The Role of the Density of the Amorphous Regions. Macromolecules, v. 55, n. 22, p. 10077–10089, 22 nov. 2022.

SAFDARI, Fatemeh *et al.* Rheological, Mechanical, and thermal properties of polylactide/cellulose nanofiber biocomposites. Polymer Composites, v. 39, n. 5, p. 1752–1762, 24 maio 2018.

SAMANTH, Mahima; SUBRAHMANYA BHAT, K. Conventional and unconventional chemical treatment methods of natural fibres for sustainable biocomposites. Sustainable Chemistry for Climate Action, v. 3, p. 100034, 1 jan. 2023.

SAMIR, Aya *et al.* Recent advances in biodegradable polymers for sustainable applications. npj Materials Degradation, v. 6, n. 1, 2022.

SANDBERG, Christer; HILL, Jan; JACKSON, Michael. On the development of the refiner mechanical pulping process – a review. Nordic Pulp & Paper Research Journal, v. 35, n. 1, p. 1–17, 26 mar. 2020.

SANDQUIST, David; THUMM, Armin; DICKSON, Alan R. The influence of fines material on the mechanical performance of wood fiber polypropylene composites. BioResources, v. 15, n. 1, p. 457–468, 26 nov. 2019.

SANTOS, Camila C. O. *et al.* Lignin valorization through polymer grafting by ring-opening polymerization and its application in health, packaging, and coating. Journal of Environmental Chemical Engineering, v. 11, n. 3, p. 109691, 1 jun. 2023.

SANTOS, Caroliny M. *et al.* A bibliometric review on applications of lignocellulosic fibers in polymeric and hybrid composites: Trends and perspectives. Heliyon, v. 10, n. 19, p. e38264, 15 out. 2024a.

SANTOS, Thiago F. *et al.* Towards sustainable and ecofriendly polymer composite materials from bast fibers: a systematic review. Engineering Research Express, v. 6, n. 1, p. 012501, 1 mar. 2024b.

SAYADI, Sabrine; BROUILLETTE, François. Silylation of phosphorylated cellulosic fibers with an aminosilane. Carbohydrate Polymers, v. 343, p. 122500, 1 nov. 2024.

SEKAR, Priyanka *et al.* Horizons in Coupling of Sulfur-Bearing Silanes to Hydrothermally Treated Lignin toward Sustainable Development. ACS Sustainable Chemistry & Engineering, v. 11, n. 48, p. 16882–16892, 4 dez. 2023.

SERRA-PARAREDA, Ferran *et al.* Effective Young's Modulus Estimation of Natural Fibers through Micromechanical Models: The Case of Henequen Fibers Reinforced-PP Composites. Polymers, v. 13, n. 22, p. 3947, 15 nov. 2021.

SHAKER, Khubab; ALI, Azam; MILITKY, Jiri. Treatment of Natural Fibers. *In*: *[S.l.: S.n.]*. p. 19–39.

SHANMUGAM, Vigneshwaran *et al.* Circular economy in biocomposite development: State-of-the-art, challenges and emerging trends. Composites Part C: Open Access, v. 5, p. 100138, jul. 2021.

SHOREY, Rohan; GUPTA, Arvind; MEKONNEN, Tizazu H. Hydrophobic modification of lignin for rubber composites. Industrial Crops and Products, v. 174, p. 114189, 15 dez. 2021.

SHU, Fan *et al.* Biological Activities and Emerging Roles of Lignin and Lignin-Based Products─A Review. Biomacromolecules, v. 22, n. 12, p. 4905–4918, 13 dez. 2021.

SIAKENG, Ramengmawii *et al.* Natural fiber reinforced polylactic acid composites: A review. Polymer Composites, v. 40, n. 2, p. 446–463, 26 fev. 2019.

SIKORSKA, Wanda *et al.* End-of-Life Options for (Bio)degradable Polymers in the Circular Economy. Advances in Polymer Technology, v. 2021, p. 1–18, 10 abr. 2021.

SIVA, R. *et al.* Comparison of Mechanical Properties and Water Absorption Test on Injection Molding and Extrusion - Injection Molding Thermoplastic Hemp Fiber Composite. Materials Today: Proceedings, v. 47, p. 4382–4386, 2021.

SLUITER, Amie *et al.* Determination of Structural Carbohydrates and Lignin in Biomass. Biomass Analysis Technology Team Laboratory Analytical Procedure, n. August, p. 1–14, 2004.

SPIRIDON, Iuliana *et al.* Evaluation of PLA–lignin bioplastics properties before and after accelerated weathering. Composites Part B: Engineering, v. 69, p. 342–349, 1 fev. 2015.

SPIRIDON, Iuliana; DARIE, Raluca Nicoleta; KANGAS, Heli. Influence of fiber modifications on PLA/fiber composites. Behavior to accelerated weathering. Composites Part B: Engineering, v. 92, p. 19–27, 1 maio 2016.

SREEKALA, M. S. *et al.* Oil palm fibre reinforced phenol formaldehyde composites: influence of fibre surface modifications on the mechanical performance. Applied Composite Materials, v. 7, n. 5–6, p. 295–329, 2000.

SULIS, Daniel B. *et al.* Advances in lignocellulosic feedstocks for bioenergy and bioproducts. Nature Communications, v. 16, n. 1, p. 1244, 1 fev. 2025.

SUOTA, Maria Juliane *et al.* Lignin Functionalization Strategies and the Potential Applications of Its Derivatives-A Review. *[S.l.: S.n.]*.

SUOTA, Maria Juliane *et al.* Chemical and structural characterization of hardwood and softwood LignoForce^{TM} lignins. Industrial Crops and Products, v. 173, 1 dez. 2021b.

SURENDREN, Aarsha *et al.* A review of biodegradable thermoplastic starches, their blends and composites: recent developments and opportunities for single-use plastic packaging alternatives. Green Chemistry, v. 24, n. 22, p. 8606–8636, 2022.

TÁBI, T.; HAJBA, S.; KOVÁCS, J. G. Effect of crystalline forms (α′ and α) of poly(lactic acid) on its mechanical, thermo-mechanical, heat deflection temperature and creep properties. European Polymer Journal, v. 82, p. 232–243, set. 2016.

TAN, Zhenrong *et al.* Journal of Colloid and Interface Science Lignin : Excellent hydrogel swelling promoter used in cellulose aerogel for efficient oil / water separation. Journal of Colloid And Interface Science, v. 629, p. 422–433, 2023.

TANAHASHI, Mitsuru. Development of Fabrication Methods of Filler/Polymer Nanocomposites: With Focus on Simple Melt-Compounding-Based Approach without Surface Modification of Nanofillers. Materials, v. 3, n. 3, p. 1593–1619, 4 mar. 2010.

TAPPI. T211 Ash in wood, pulp, paper and paperboard: combustion at 525 °C. TAPPI standard test methods, v. T211 om-02, p. 7, 2007.

TAPPI. Lignin in Wood and Pulp. T222 Om-02, p. 1–7, 2011.

TARRÉS, Q. *et al.* Bio-polyethylene reinforced with thermomechanical pulp fibers: Mechanical and micromechanical characterization and its application in 3D-printing by fused deposition modelling. Composites Part B: Engineering, v. 153, p. 70–77, nov. 2018.

TARRÉS, Quim *et al.* Lignocellulosic nanofibers from triticale straw: The influence of hemicelluloses and lignin in their production and properties. Carbohydrate Polymers, v. 163, p. 20–27, maio 2017.

TARRÉS, Quim *et al.* Determination of Mean Intrinsic Flexural Strength and Coupling Factor of Natural Fiber Reinforcement in Polylactic Acid Biocomposites. Polymers, v. 11, n. 11, p. 1736, 23 out. 2019.

TAZWAR, Hassan Tawsif; ANTORA, Maisha Farzana; RAHMAN, Md Zillur. Functionalization strategies for sustainable plant fiber composites: A comprehensive review of techniques, performance and future directions. Journal of Materials Research and Technology, v. 38, p. 1083–1102, 1 set. 2025.

TERZOPOULOU, Paschalina; VOUVOUDI, Evangelia C.; ACHILIAS, Dimitris S. Delignification as a Key Strategy for Advanced Wood-Based Materials: Chemistry, Delignification Parameters, and Emerging Applications. Forests, v. 16, n. 6, p. 993, 12 jun. 2025.

TERZOPOULOU, Zoi *et al.* Unravelling the impact of lignin particle size and content on enhanced value in plastic composites. Sustainable Chemistry for the Environment, v. 9, p. 100194, 1 mar. 2025.

THAKUR, Vijay Kumar *et al.* Progress in Green Polymer Composites from Lignin for Multifunctional Applications: A Review. ACS Sustainable Chemistry & Engineering, v. 2, n. 5, p. 1072–1092, 5 maio 2014.

THAM, Mun Wai *et al.* Biocomposites based on poly(lactic acid) matrix and reinforced with natural fiber fabrics: The effect of fiber type and compatibilizer content. Polymer Composites, v. 43, n. 7, p. 4191–4209, 29 jul. 2022.

THOMASON, J. L. *et al.* Influence of fibre length and concentration on the properties of glass fibre-reinforced polypropylene: Part 3. Strength and strain at failure. Composites Part A: Applied Science and Manufacturing, v. 27, n. 11, p. 1075–1084, jan. 1996.

TOCCO, Davide *et al.* Recent Developments in the Delignification and Exploitation of Grass Lignocellulosic Biomass. ACS Sustainable Chemistry & Engineering, v. 9, n. 6, p. 2412–2432, 15 fev. 2021.

TREJO-CÁCERES, M.; MARTÍN-ALFONSO, J. E.; FRANCO, J. M. Silylation of wheat straw cellulose pulp for its valorization as rheology modifier of industrial hydrophobic fluids: Cases of castor oil and bitumen. Carbohydrate Polymers, v. 364, p. 123778, 15 set. 2025.

TRENTIN, Lucas N. *et al.* Unraveling the Mechanical Behavior of Softwood Secondary Cell Walls through Atomistic Simulations. Biomacromolecules, v. 26, n. 6, p. 3395–3409, 9 jun. 2025.

TRIPATHI, Neelima; MISRA, Manjusri; MOHANTY, Amar K. Durable Polylactic Acid (PLA)-Based Sustainable Engineered Blends and Biocomposites: Recent Developments, Challenges, and Opportunities. ACS Engineering Au, v. 1, n. 1, p. 7–38, 20 out. 2021.

TRIVEDI, Alok Kumar; GUPTA, M. K.; SINGH, Harinder. PLA based biocomposites for sustainable products: A review. Advanced Industrial and Engineering Polymer Research, v. 6, n. 4, p. 382–395, out. 2023.

TSENG, Huan-Chang; CHANG, Rong-Yeu; HSU, Chia-Hsiang. Improved fiber orientation predictions for injection molded fiber composites. Composites Part A: Applied Science and Manufacturing, v. 99, p. 65–75, ago. 2017.

TSUJI, Hideto. Poly(Lactic Acid). *In*: STEVENS, Christian V.; KABASCI, Stephan (Orgs.). Bio-Based Plastics: Materials and Applications. First Edit ed. *[S.l.]*: Wiley, 2013. p. 171–239.

TÜMER, Eda Hazal; ERBIL, Husnu Yildirim. Extrusion-Based 3D Printing Applications of PLA Composites: A Review. Coatings, v. 11, n. 4, p. 390, 29 mar. 2021.

UPPAL, Neha *et al.* Cellulosic fibres-based epoxy composites: From bioresources to a circular economy. Industrial Crops and Products, v. 182, p. 114895, ago. 2022.

URDANETA, Fernando *et al.* Evaluating chemi-mechanical pulping processes of agricultural residues: High-yield pulps from wheat straw for fiber-based bioproducts. Industrial Crops and Products, v. 221, p. 119379, 1 dez. 2024.

VANHOLME, Ruben *et al.* Lignin biosynthesis and its integration into metabolism. Current Opinion in Biotechnology, v. 56, p. 230–239, 1 abr. 2019.

VERMA, Deepak; GOH, Kheng Lim. Functionalized Graphene-Based Nanocomposites for Energy Applications. *[S.l.]*: Elsevier Inc., 2019.

VIGNESHWARAN, S. *et al.* Recent advancement in the natural fiber polymer composites: A comprehensive review. Journal of Cleaner Production, v. 277, p. 124109, 2020.

WAN, Han *et al.* Synergistic reinforcement of polylactic acid/wood fiber composites by cellulase and reactive extrusion. Journal of Cleaner Production, v. 434, p. 140207, jan. 2024.

WANG, Han-Min *et al.* Advanced and versatile lignin-derived biodegradable composite film materials toward a sustainable world. Green Chemistry, v. 23, n. 11, p. 3790–3817, 2021.

WANG, Jianchuan *et al.* Shear induced fiber orientation, fiber breakage and matrix molecular orientation in long glass fiber reinforced polypropylene composites. Materials Science and Engineering: A, v. 528, n. 7–8, p. 3169–3176, mar. 2011.

WANG, Ningning *et al.* Improving interfacial adhesion of pla/lignin composites by one-step solvent-free modification method. Journal of Renewable Materials, v. 8, n. 9, p. 1139–1149, 2020.

WANG, Ru-Min; ZHENG, Shui-Rong; ZHENG, Yujun George. Polymer Matrix Composites and Technology. *[S.l.]*: Elsevier, 2011, 2011.

WASTI, Sanjita *et al.* Influence of plasticizers on thermal and mechanical properties of biocomposite filaments made from lignin and polylactic acid for 3D printing. Composites Part B: Engineering, v. 205, p. 108483, 15 jan. 2021.

WATANABE, Yoshimi. Evaluation of Fiber Orientation in Ferromagnetic Short-Fiber Reinforced Composites by Magnetic Anisotropy. Journal of Composite Materials, v. 36, n. 8, p. 915–923, 27 abr. 2002.

WEI, Yun *et al.* “Toolbox” for the Processing of Functional Polymer Composites. Nano-Micro Letters, v. 14, n. 1, p. 35, 16 dez. 2022.

WERKELIN, Johan; SKRIFVARS, Bengt Johan; HUPA, Mikko. Ash-forming elements in four Scandinavian wood species. Part 1: Summer harvest. Biomass and Bioenergy, v. 29, n. 6, p. 451–466, 1 dez. 2005.

WILDE, Kerstin; HERMANS, Frans. Transition towards a bioeconomy: Comparison of conditions and institutional work in selected industries. Environmental Innovation and Societal Transitions, v. 50, p. 100814, 1 mar. 2024.

WITZLER, Markus *et al.* Lignin-Derived Biomaterials for Drug Release and Tissue Engineering. Molecules, v. 23, n. 8, p. 1885, 27 jul. 2018.

WU, Chenchen *et al.* Manufacturing Technologies of Polymer Composites—A Review. Polymers, v. 15, n. 3, 2023.

WU, Feng; MISRA, Manjusri; MOHANTY, Amar K. Challenges and new opportunities on barrier performance of biodegradable polymers for sustainable packaging. Progress in Polymer Science, v. 117, p. 101395, 1 jun. 2021.

WU, Tingting *et al.* From 3D to 4D printing of lignin towards green materials and sustainable manufacturing. Materials Horizons, v. 12, n. 9, p. 2789–2819, 2025.

WU, Xinyu *et al.* Mechanistic insights and applications of lignin-based ultraviolet shielding composites: A comprehensive review. International Journal of Biological Macromolecules, v. 280, p. 135477, 1 nov. 2024.

WU, Yajie; RESTREPO-FLÓREZ, Juan Manuel; VASCO-CORREA, Juliana. A Superstructure-Based Lignin Valorization Process Optimization Model for Lignocellulosic Biorefineries through Biological Upgrading. ACS Sustainable Chemistry & Engineering, v. 12, n. 18, p. 6913–6926, 6 maio 2024.

XIE, Yanjun *et al.* Silane coupling agents used for natural fiber/polymer composites: A review. Composites Part A: Applied Science and Manufacturing, v. 41, n. 7, p. 806–819, 2010.

YADAV, Vivek *et al.* Lignin removal from pulp and paper industry waste streams and its application. Nanotechnology in Paper and Wood Engineering: Fundamentals, Challenges and Applications, p. 265–283, 1 jan. 2022.

YANG, Haitang *et al.* Molecularly Engineered Lignin-Derived Additives Enable Fire-Retardant, UV-Shielding, and Mechanically Strong Polylactide Biocomposites. Biomacromolecules, v. 22, n. 4, p. 1432–1444, 12 abr. 2021.

YANG, Jianlei; CHING, Yern Chee; CHUAH, Cheng Hock. Applications of lignocellulosic fibers and lignin in bioplastics: A review. Polymers, v. 11, n. 5, p. 1–26, 2019.

YANG, Mannan *et al.* Effect of Different Silane Coupling Agents on Properties of Waste Corrugated Paper Fiber/Polylactic Acid Composites. Polymers, v. 15, n. 17, p. 1–15, 2023.

YANG, Weijun *et al.* Poly(lactic acid)/lignin films with enhanced toughness and anti-oxidation performance for active food packaging. International Journal of Biological Macromolecules, v. 144, p. 102–110, 1 fev. 2020a.

YANG, Zhaozhe *et al.* Properties of Poplar Fiber/PLA Composites: Comparison on the Effect of Maleic Anhydride and KH550 Modification of Poplar Fiber. Polymers, v. 12, n. 3, p. 729, 24 mar. 2020b.

YATIGALA, Nikushi S.; BAJWA, Dilpreet S.; BAJWA, Sreekala G. Compatibilization improves physico-mechanical properties of biodegradable biobased polymer composites. Composites Part A: Applied Science and Manufacturing, v. 107, p. 315–325, abr. 2018.

YE, Haichuan *et al.* 3D-Printed Polylactic Acid/Lignin Films with Great Mechanical Properties and Tunable Functionalities towards Superior UV-Shielding, Haze, and Antioxidant Properties. Polymers, v. 15, n. 13, p. 2806, 24 jun. 2023.

YEMELE, Martin Claude Ngueho *et al.* Effect of bark fiber content and size on the mechanical properties of bark/HDPE composites. Composites Part A: Applied Science and Manufacturing, v. 41, n. 1, p. 131–137, 1 jan. 2010.

YEO, Jun-Seok; LEE, Ji-Hoon; HWANG, Seok-Ho. Effects of lignin on the volume shrinkage and mechanical properties of a styrene/unsaturated polyester/lignin ternary composite system. Composites Part B: Engineering, v. 130, p. 167–173, dez. 2017.

YU, Tao *et al.* Effect of fiber surface-treatments on the properties of poly(lactic acid)/ramie composites. Composites Part A: Applied Science and Manufacturing, v. 41, n. 4, p. 499–505, abr. 2010.

YUE, Yiying *et al.* Cellulose fibers isolated from energycane bagasse using alkaline and sodium chlorite treatments: Structural, chemical and thermal properties. Industrial Crops and Products, v. 76, p. 355–363, 15 dez. 2015.

YUSOFF, Rosni Binti; TAKAGI, Hitoshi; NAKAGAITO, Antonio Norio. Tensile and flexural properties of polylactic acid-based hybrid green composites reinforced by kenaf, bamboo and coir fibers. Industrial Crops and Products, v. 94, p. 562–573, dez. 2016.

ZANDI, M. Damous *et al.* Study of the manufacturing process effects of fused filament fabrication and injection molding on tensile properties of composite PLA-wood parts. The International Journal of Advanced Manufacturing Technology, v. 108, n. 5–6, p. 1725–1735, 30 maio 2020.

ZHANG, Da-Wei *et al.* Effect of initial fiber length on the rheological properties of sisal fiber/polylactic acid composites. Polymer Composites, v. 32, n. 8, p. 1218–1224, 11 ago. 2011.

ZHANG, Han *et al.* UV Resistance Properties of Lignin Influenced by Its Oxygen-Containing Groups Linked to Aromatic Rings. Biomacromolecules, v. 26, n. 1, p. 428–436, 13 jan. 2025.

ZHANG, Mengying *et al.* Construction of high-efficiency fixing structure of waterborne paint on silicate-modified poplar surfaces by bridging with silane coupling agents. Progress in Organic Coatings, v. 167, n. March, p. 106846, 2022.

ZHANG, Qinan *et al.* Bio-based polyesters: Recent progress and future prospects. Progress in Polymer Science, v. 120, p. 101430, set. 2021.

ZHANG, Qing *et al.* High-Value Utilization of Cellulose: Intriguing and Important Effects of Hydrogen Bonding Interactions─A Mini-Review. Biomacromolecules, v. 25, n. 10, p. 6296–6318, 14 out. 2024a.

ZHANG, Shuang-Yan *et al.* Effect of the amount of lignin on tensile properties of single wood fibers. Forest Science and Practice, v. 15, n. 1, p. 56–60, 30 mar. 2013.

ZHANG, Shuyang *et al.* 3D printed lignin/polymer composite with enhanced mechanical and anti-thermal-aging performance. Chemical Engineering Journal, v. 481, p. 148449, 1 fev. 2024b.

ZHAO, Xianhui *et al.* Sustainable bioplastics derived from renewable natural resources for food packaging. Matter, v. 6, n. 1, p. 97–127, jan. 2023.

ZHOU, Shuai *et al.* Lignin Valorization through Thermochemical Conversion: Comparison of Hardwood, Softwood and Herbaceous Lignin. ACS Sustainable Chemistry & Engineering, v. 4, n. 12, p. 6608–6617, 5 dez. 2016.

ZHOU, Yonghui; FAN, Mizi; CHEN, Lihui. Interface and bonding mechanisms of plant fibre composites: An overview. Composites Part B: Engineering, v. 101, p. 31–45, 15 set. 2016.

ZHU, Jun *et al.* Modification of Lignin with Silane Coupling Agent to Improve the Interface of Poly(L-lactic) Acid/Lignin Composites. BioResources, v. 10, n. 3, p. 4315–4325, 28 maio 2015.